On the cosmological mass function theory.

A. Del Popolo[1,2]

[1] Dipartimento di Matematica, Università Statale di Bergamo, via dei Caniana, 2 - I 24129 Bergamo, ITALY

[2] Boğaziçi University, Physics Department, 80815 Bebek, Istanbul, Turkey

Abstract

This paper provides, from one side, a review of the theory of the cosmological mass function from a theoretical point of view, starting from the seminal paper of Press & Shechter (1974) to the last developments (Del Popolo & Gambera (1998, 1999), Sheth & Tormen 1999 (ST), Sheth, Mo & Tormen 2001 (ST1), Jenkins et al. 2001 (J01), Shet & Tormen 2002 (ST2), Del Popolo 2002a, Yagi et al. 2004 (YNY)), and from another side some improvements on the multiplicity function models in literature. For what concerns this second aspect, I compare the numerical multiplicity function given in Yahagi, Nagashima & Yoshii (2004), with the theoretical multiplicity function obtained in the present paper by means of the excursion set model and an improved version of the barrier shape obtained in Del Popolo & Gambera (1998), which implicitly takes account of total angular momentum acquired by the proto-structure during evolution and of a non-zero cosmological constant. I show that the multiplicity function obtained in the present paper, is in better agreement with Yahagi, Nagashima & Yoshii (2004) simulations than other previous models (Sheth & Tormen 1999; Sheth, Mo & Tormen 2001; Sheth & Tormen 2002; Jenkins et al. 2001). The multiplicity function of the present paper gives a good fit to simulations results as the fit function proposed by Yahagi, Nagashima & Yoshii (2004), but differently from that it was obtained from a sound theoretical background. Then, I calculate the mass function evolution in a ΛCDM model by means of the previous model. I compare the result with Reed et al. (2003) (R03), who used a high resolution ΛCDM numerical simulation to calculate the mass function of dark matter haloes down to the scale of dwarf galaxies, back to a redshift of fifteen. I show that the mass function obtained in the present paper, gives similar predictions to the Sheth & Tormen mass function but it does not show the overprediction of extremely rare objects shown by the Sheth and Tormen mass function. The results confirm previous findings that the simulated halo mass function can be described solely by the variance of the mass distribution, and thus has no explicit redshift dependence. I moreover show that the PS-like approach together with the ellipsoidal model introduced in Del Popolo (2002b) gives a better description of the theoretical mass function.

Subject headings: clusters of galaxies — cosmology: theory — dark matter — galaxies: clustering — large-scale structure of the universe

1. Introduction

The universe that we observe appears quite clumpy and inhomogeneous on a spatial scale of $\simeq 200h^{-1}$ Mpc. Beyond that scale mass clumps appear to be homogeneously distributed. We observe massive clumps such as galaxies, groups of galaxies, clusters of galaxies, super-clusters (the most massive one among the hierarchy of structures) fill the space spanning a wide range of mass scales. The respective mass ranges characterizing these systems, approximately, are $\simeq 10^9 - 10^{10} M_\odot$, $\simeq 10^{11} M_\odot$, $\simeq 10^{12} - 10^{14} M_\odot$, and $\simeq 10^{15} M_\odot$ where $M_\odot$ is the solar mass. All these objects, combinedly, form the structure

what is known as the Large Scale Structure (LSS) in the universe. One of the most fundamental challenges in present universe is to understand the formation and evolution of the LSS. In order to understand the LSS, we need to have a theoretical framework within which predictions for structure formation can be made.

The leading idea of all structure formation theories is that structures was born from small perturbations in the otherwise uniform distribution of matter in the early Universe, which is supposed to be, in great part, dark (matter not detectable through light emission).

With the term Dark Matter cosmologists indicate an hypothetic material component of the universe which does not emit directly electromagnetic radiation (unless it decays in particles having this property (Sciama 1990, but also see Bowyer et al. 1999)).
Dark matter, cannot be revealed directly, but nevertheless it is necessary to postulate its existence in order to explain the discrepancies between the observed dynamical properties of galaxies and clusters of galaxies and the theoretical predictions based upon models of these objects assuming that the only matter present is the visible one. The original hypotheses on Dark Matter go back to measures performed by Oort (1932) of the surface density of matter in the galactic disk, which was obtained through the study of the stars motion in direction orthogonal to the galactic plane. The result obtained by Oort, which was after him named "Oort Limit", gave a value of $\rho = 0.15 M_0 pc^{-3}$ for the mass density, and a mass, in the region studied, superior to that present in stars. Nowadays, we know that the quoted discrepancy is due to the presence of HI in the solar neighborhood. Other studies (Zwicky 1933; Smith 1936) showed the existence of a noteworthy discrepancy between the virial mass of clusters (e.g. Coma Cluster) and the total mass contained in galaxies of the same clusters. These and other researches from the thirties to now, have confirmed that a great part of the mass in the universe does not emit radiation that can be directly observed.

The study of Dark Matter has as its finality the explanation of formation of galaxies and in general of cosmic structures. For this reason, in the last decades, the origin of cosmic structures has been "framed" in models in which Dark Matter constitutes the skeleton of cosmic structures and supply the most part of the mass of which the same is made.

The mass distribution of cosmic structures, i.e. the number of objects per unit volume and unit mass interval, is commonly called mass function or multiplicity function; it will be referred to as MF throughout the text. The determination of the cosmological MF is a difficult, not fully solved problem, both from the theoretical and the observational point of view. An analytical exact prediction of the MF is hampered, even in the simplest cosmological models, by the fact that highly non-linear gravitational dynamics is involved in the formation of high density objects; it is well known that the gravitational collapse problem has never been exactly solved, except in the case of simple symmetries (spherical planar). Large N-body simulations can be used to determine the MF of simulated halos; however such simulations, besides being time-expensive and limited in resolution, provide a numerical estimate of the final solution of the problem without directly shedding light on the difficult problem of gravitational collapse. Approximate analytical arguments, while being of limited validity, can provide useful and fully-understood solutions, which can then be compared to the results of N-body simulations.

There is general consensus in setting the birth date of the MF theory in 1974, when the seminal paper of Press & Schechter (hereafter PS) was published (the same PS formula can be found in Doroshkevich 1967). That paper proposed a heuristic procedure, based on linear theory, to obtain the distribution of the masses of collapsed clumps. That work inspired the fit for the galaxy luminosity function proposed by Schechter (1976), but received a limited attention for more than a decade. A real explosion of attention to the MF theory started in 1988, when the first large N-body simulations started to reveal a surprising adherence of their results with the PS formula. Many authors tried to extend the PS procedure in many directions, or proposed different, alternative or complementary procedures (Bond, Cole, Efstathiou & Kaiser (1991) (BCEK)). These last years are witnessing a new wave of interest, which has not yet been exhausted (see for example ST, Jenkins et al. 2001 (J01), ST1, ST2, Del Popolo 2002a, Yahagi et al. 2004 (YNY), Del Popolo 2005).

As mentioned before, the original PS work was developed within a model in which structures grow from small seeds, either Poisson distributed or set on a perturbed lattice. The extension of the PS work to more general and "standard" cosmological settings was due to Efstathiou, Fall & Hogan (1979), who limited their analysis to power-law spectra and an Einstein-de Sitter background. The first application of PS to a CDM spectrum was made by Schaeffer & Silk (1985). They "discovered' the PS MF (the procedure is described without any reference to the PS paper), complete with its unjustified

fudge factor 2, and criticized it in some interesting points; in particular, they tried to model, on purely geometrical grounds, objects which do not collapse spherically, like pancakes and filaments.

Starting from 1988, many authors extended the PS approach in many directions, trying to understand why it appeared to work, in spite of its heuristic and not fully satisfactory derivation. The situation in those years is reviewed in Lucchin (1989). Just one year before, Kashlinsky (1987) tried to determine the 2-point correlation function of structures, collapsed according to the PS prescription. Martinez-Gonzalez & Sanz (1988a) performed similar calculations with a different method, while Martinez-Gonzalez & Sanz (1988b) attempted to determine the luminosity function of galaxies of different morphological types by means of an approach which was intermediate between the PS and the peak one. Lucchin & Matarrese (1988) formulated a PS MF for the case of non-Gaussian perturbations. Lilje (1992) and Lahav et al. (1991) extended the PS result to open Universes and to flat Universes with a cosmological constant. Zhan (1990) changed the PS procedure by taking into account the correction to the background density given by the initial density contrast; as a matter of fact, such a correction is negligible if the initial time is small. Schaeffer & Silk (1988a) used the PS procedure to justify the presence of some small-scale power in the HDM cosmology; in fact, the use of Gaussian smoothing causes some large-scale power to be spread toward small scales. Again Schaeffer & Silk (1988a,b), and Occhionero & Scaramella (1988) applied the PS formula to get many cosmological predictions on collapsed structures. BCEK solved the cloud-in-cloud problem using the "excursion set approach". Lacey & Cole (1994), introduced the merging histories concept, which gives an important piece of information in the formation history of dark matter objects. Del Popolo & Gambera (1998), ST, ST1, ST2, Del Popolo (2002a), (2005), showed that the non-sphericity of collapse has important consequences on the MF.

Press and Schechter were the first to performed N-body simulations to test the validity of their formula. They found some encouraging agreement, but their simulations were limited to 1000 bodies, a very small number to reach any firm conclusion. Efstathiou, Fall & Hogan (1979) performed similar simulations, with the same number of point masses, obtaining the same conclusions as PS.

Later, Efstathiou et al. (1988) compared the results of larger (32^3 P3M, scale-free power spectra) N-body simulations to the PS formula: their dynamical range in mass was large enough to test the knee of the MF. The surprising result was that the PS formula nicely fitted their abundances of simulated halos (as found by means of a percolation friend-of-friend algorithm). Further comparisons with N-body simulations were performed by Efstathiou & Rees (1988), Narayan & White (1988), Carlberg & Couchman (1989), Carlberg (1990), BCEK, Brainerd & Villumsen (1992), White, Efstathiou & Frenk (1993), Ma & Bertschinger (1994), Jain & Bertschinger (1994), Gelb & Bertschinger (1994), Katz, Quinn, Bertschinger & Gelb (1994), Lacey & Cole (1994), Efstathiou (1995), Klypin & Rhee (1994), Klypin et al. (1995), Bond & Myers (1996b), Governato et al. (1998), YNY. Most authors reported the PS formula to fit well their N-body results; nonetheless, all the authors agree in stating the validity of the PS formula to be only statistical, i.e. the existence of the single halos is not well predicted by the linear overdensity criterion of PS (see in particular BCEK).

There are however some exceptions to this general agreement: Brainerd & Villumsen (1992) reported their MF, based on a CDM spectrum, to be very similar to a power-law with slope -2, different from the PS formula both at small and at large masses. Jain & Bertschinger (1994), Gelb & Bertschinger (1994) and Ma & Bertschinger (1994) noted that, to make the PS formula agree with their simulations (based on CDM or CHDM spectra), it is necessary to lower the value of the δ_c parameter as redshift increases. The same thing was found by Klypin et al. (1995), but was interpreted as an artifact of their clump-finding algorithm. More recent simulations seem to confirm this trend (Governato et al. 1999; YNY)).

Lacey & Cole (1994) extended the comparison to N-body simulations to the predictions for merging histories of dark-matter halos; they found again a good agreement between theory and simulations. This fact is noteworthy, as merging histories contain much more detailed information about hierarchical collapse.

It is opportune to comment on two important technical points about such comparisons. First, the δ_c parameters used by different authors as "best fit" values range from the 1.33 of Efstathiou & Rees (1988) to the 1.9 found (in a special case) by Lacey & Cole (1994). The precise value of the δ_c parameter is influenced by the shape of the filter used to calculate the PS, Gaussian filters requiring lower δ_c values. Recent simulations tend to give $\delta_c \simeq 1.5$ (e.g. Klypin et al. 1995) or $\delta_c = 1.69$ (e.g. Lacey & Cole 1994). If δ_c changes with time, a value 1.5 could be good at high redshifts, lowering to 1.7 at low redshifts.

Second, the numerical MF deeply depends on the way halos are picked up from simulations. Typical algorithms, such as the friend-of-friend or DENMAX, are parametric, i.e. they contain free parameters. For instance, the frequently used friends-of-friends algorithm defines as structures those clumps whose particles are separated among them by distances

smaller than a percolation parameter b times the mean interparticle distance. A heuristic argument, based on spherical collapse, suggests a value of 0.2 for b (with this percolation parameter the mean density contrast of halos is about 180, which is the expected density contrast of a virialized top-hat perturbation). Obviously, the use of different b parameters leads to different MFs. In practice, what is obtained in this case is not "the" MF, but the "friend-of-friend, b=0.2" MF. Then, the numerical MF contains some hidden parameters, which, together with the δ_c parameter (and the mass associated to the filter in the Lacey & Cole (1994) paper), makes such comparisons more similar to parametric fits, rather than to comparisons of a theory to a numerical experiment.

The present paper is organized as follows: section 2 contains some tools needed to formulate the MF theory: it is focused on simple models for structure formation (density perturbation growth, spherical collapse model, Zel'dovich approximation, ellipsoid collapse model, etc.).

Section 3 contains a review of the theoretical MF problem and describes the theoretical works (such as the excursion set model) which have tried to extend the validity of the original Press & Schechter work, or have proposed alternative procedures.

In the same section, it is reviewed the building of a MF theory, based on more realistic approximations for gravitational collapse than the spherical collapse. Finally, it is reviewed the work of Del Popolo & Gambera (1998), ST, ST1, ST2, Del Popolo (2002a), (2005), who showed that the non-sphericity f collapse has important consequences on the MF. Section 4 is devoted to prospects and conclusions.

2. Theoretical bases of MF theory

2.1. Background cosmology

The simplest cosmological model that describes, in a sufficient coherent manner, the evolution of the universe, from $10^{-2}s$ after the initial singularity to now, is the so called *Standard Cosmological Model* (or Hot Big Bang model). It is based upon the Friedmann-Robertson-Walker (FRW) metric, which is given by:

$$ds^2 = c^2dt^2 - a(t)^2\left[\frac{dr^2}{1-kr^2} + r^2(d\theta^2 + sin\theta^2 d\phi^2)\right] \tag{1}$$

where c is the light velocity, a(t) a function of time, or a scale factor called "expansion parameter", t is the time coordinate, r, θ and ϕ the comoving space coordinates. The evolution of the universe is described by the parameter a(t) and it is fundamentally connected to the value ρ of the average density.

The equations that describe the dynamics of the universe are the Friedmann's equations (Friedman, 1924) that we are going to introduce in a while. These equations can be obtained starting from the equations of the gravitational field of Einstein (Einstein, A., 1915):

$$R_{ik} - \frac{1}{2}g_{ik}R = -\frac{8\pi G}{c^4}T_{ik} \tag{2}$$

where now, R_{ik} is a symmetric tensor, also known as Ricci tensor, which describes the geometric properties of space-time, g_{ik} is the metric tensor, R is the scalar curvature, T_{ik} is the energy-momentum tensor.

These equations connect the properties of space-time to the mass-energy. In other terms they describe how space-time is modeled by mass. Combining Einstein equations to the FRW metric leads to the dynamic equations for the expansion parameter, a(t). These last are the Friedmann equations:

$$d(\rho a^3) = -pd(a^3) \tag{3}$$

$$\frac{1}{a^2}\dot{a}^2 + \frac{k}{a^2} = \frac{8\pi G}{3}\rho \tag{4}$$

$$2\frac{\ddot{a}}{a} + \frac{\dot{a}^2}{a^2} + \frac{k}{a^2} = -8\pi G\rho \tag{5}$$

where p is the pressure of the fluid of which the universe is constituted, k is the curvature parameter and a(t) is the scale factor connecting proper distances $\mathbf{r}$ to the comoving ones $\mathbf{x}$ through the relation $\mathbf{r} = a(t)\mathbf{x}$. Only two of the three Friedmann equations are independent, because the first connects density, ρ to the expansion parameter a(t). The

Fig. 1. Evolution of the scale factor.

character of the solutions of these equations depends on the value of the curvature parameter, k, which is also determined by the initial conditions by means of Eq. 3. The solution to the equations now written shows that if ρ is larger than $\rho_c = \frac{3H^2}{8\pi G} = 1.88 * 10^{-29} g/cm^3$ (critical density, which can be obtained from Friedmann equations putting $t = t_0$, $k = 0$, and $H = 100 km/sMpc$), space-time has a closed structure ($k = 1$) and equations shows that the system go through a singularity in a finite time. This means that the universe has an expansion phase until it reaches a maximum expansion after which it recollapse. If $\rho < \rho_c$, the expansion never stops and the universe is open $k = -1$ (the universe has a structure similar to that of an hyperboloid, in the two-dimensional case). If finally, $\rho = \rho_c$ the expansion is decelerated and has infinite duration in time, $k = 0$, and the universe is flat (as a plane in the two-dimensional case). The concept discussed can be expressed using the parameter $\Omega = \frac{\rho}{\rho_c}$. In this case, the condition $\Omega = 1$ corresponds to $k = 0$, $\Omega < 1$ corresponds to $k = -1$, and $\Omega > 1$ corresponds to $k = 1$. Fig. 1 plots the evolution of the expansion parameter for $k = -1, 0, 1$.

In a flat model, the FRW equation becomes:

$$\frac{\dot{a}^2}{a^2} = \frac{8}{3}\pi G\bar{\rho}, \tag{6}$$

whose solution is:

$$a(t) = (t/t_0)^{2/3}. \tag{7}$$

In the case of open models with no cosmological constant: $\Omega < 1$, $\Lambda = 0$, we can write:

$$\frac{\dot{a}^2}{a^2} = \frac{8}{3}\pi G\bar{\rho}\left(1 + \left(\Omega_0^{-1} - 1\right)a\right), \tag{8}$$

and the $a(t)$ evolution can be expressed through the following parametric representation:

$$\begin{aligned} a(\eta) &= \frac{\Omega_0}{2(1-\Omega_0)}(\cosh\eta - 1) \\ t(\eta) &= \frac{\Omega_0}{2H_0(1-\Omega_0)^{3/2}}(\sinh\eta - \eta). \end{aligned} \tag{9}$$

In the case of flat models with positive cosmological constant: $\Omega < 1$, $\Lambda \neq 0$, $\Omega + \Lambda/3H_0^2 = 1$, we can write:

$$\frac{\dot{a}^2}{a^2} = \frac{8}{3}\pi G\bar{\rho}\left(1 + \left(\Omega_0^{-1} - 1\right)a^3\right), \tag{10}$$

$$a(t) = \left(\Omega_0^{-1} - 1\right)^{-1/3} \sinh^{2/3}\left(\frac{3}{2}\sqrt{\frac{\Lambda}{3}}t\right). \tag{11}$$

The value of Ω can be calculated in several ways. The most common methods are the dynamical methods, in which the effects of gravity are used, and kinematics methods sensible to the evolution of the scale factor and to the space-time geometry.

2.2. **Perturbations evolution.**

Density perturbations in the components of the universe evolve with time. In order to get the evolution equations for δ in Newtonian regime, it is possible to use several models. In our model, we assume that gravitation dominates on the other interactions and that particles (representing galaxies, etc.) move collisionless in the potential ϕ of a smooth density function (Peebles 1980).

The distribution function of particles for position and momentum is given by:

$$dN = f(\mathbf{x}, \mathbf{p}, t)d^3xd^3p \tag{12}$$

and density:

$$\rho(\mathbf{x},t) = ma^{-3}\int d^3p f(\mathbf{x},\mathbf{p},t) = \rho_b\left[1+\delta(\mathbf{x},t)\right] \tag{13}$$

where m is the mass of a particle and ρ_b the background density. Applying Liouville theorem to the probability density on a limited region of phase-space of the system we have that f verifies the equation:

$$\frac{\partial f}{\partial t} + \frac{\mathbf{p}}{ma^2}\bigtriangledown f - m\bigtriangledown\phi\frac{\partial f}{\partial \mathbf{p}} = 0 \tag{14}$$

The distribution function f that appears in the previous equations cannot be obtained from observations. It is possible to measure moments of f (density, average velocity, etc.). We want now to obtain the evolution equations for δ. For this reason, we start integrating Eq. (14) on $\mathbf{p}$ and after using Eq. (13), we get:

$$a^3\rho_b\frac{\partial\delta}{\partial t} + \frac{1}{a^2}\bigtriangledown\int \mathbf{p} f d^3p = 0 \tag{15}$$

If we define velocity as:

$$\mathbf{v} = \frac{\int \frac{\mathbf{p}}{ma} f d^3p}{\int f d^3p} \tag{16}$$

and introduce it in Eq. (15) we get:

$$\rho_b\frac{\partial\delta}{\partial t} + \frac{1}{a}\bigtriangledown(\rho\mathbf{v}) = 0 \tag{17}$$

We can now multiply Eq. (14) for $\mathbf{p}$ and integrate it on the momentum:

$$\frac{\partial}{\partial t}\int p_\alpha f d^3p + \frac{1}{ma^2}\partial_\beta\int p_\alpha p_\beta f d^3p + a^3\rho(\mathbf{x},t)\phi_{,\alpha} = 0 \tag{18}$$

this last in Eq. (15) leaves us with:

$$\frac{\partial^2\delta}{\partial t^2} + 2\frac{\dot{a}}{a}\frac{\partial\delta}{\partial t} = \frac{1}{a^2}\bigtriangledown\left[(1+\delta)\bigtriangledown\phi\right] + \frac{1}{\rho_b m a^7}\partial_\alpha\partial_\beta\int p_\alpha p_\beta\phi d^3p \tag{19}$$

and finally using

$$< v_\alpha v_\beta >= \frac{\int f p_\alpha p_\beta d^3p}{ma^2\int f d^3p} \tag{20}$$

the equation for the evolution of overdensity becomes:

$$\frac{\partial^2\delta}{\partial t^2} + 2\frac{\dot{a}}{a}\frac{\partial\delta}{\partial t} = \frac{1}{a^2}\bigtriangledown\left[(1+\delta)\bigtriangledown\phi\right] + \frac{1}{a^2}\partial_\alpha\partial_\beta\left[(1+\delta) < v^\alpha v^\beta >\right] \tag{21}$$

(Peebles 1980). The term $< v_\alpha v_\beta >$ is the tensor of anisotropy of peculiar velocity. This is present in the gradient and then it behaves as a pressure force. If we consider an isolated and spherical perturbation, it is possible to assume that initial asymmetries does not grow up and so we can suppose, in this hypothesis that $< v_\alpha v_\beta >= 0$.

When the density contrast is much smaller than one, $\delta \ll 1$, and peculiar velocities, v, are small enough to satisfy $(vt/d)^2 \ll \delta$, where t is the cosmological time and d is the coherence length of the matter field, one can obtain a linear theory for perturbations evolution as follows.

In this case we have:

$$\frac{\partial^2\delta}{\partial t^2} + 2\frac{\dot{a}}{a}\frac{\partial\delta}{\partial t} = 4\pi G\rho_b\delta \tag{22}$$

This equation in an Einstein-de Sitter universe ($\Omega = 1$, $\Lambda = 0$) has the solutions:

$$\delta_+ = A_+(\mathbf{x})t^{\frac{2}{3}} \qquad \delta_-(\mathbf{x},t) = A_-(\mathbf{x})t^{-1} \tag{23}$$

The perturbation is then done of two parts: a growing one (which shall be denoted with $b(t)$), becoming more and more important with time, and a decaying one becoming negligible with increasing time, with respect to the growing one.

The solutions for the growing modes, relative to the three background models, are reported:

$\Omega = 1$:

$$b(t) = a(t). \tag{24}$$

$\Omega < 1$, $\Lambda = 0$: it is useful to use the time variable

$$\tau = (1 - \Omega(t))^{-1/2} = \sqrt{(a(\Omega_0^{-1} - 1))^{-1} + 1}. \tag{25}$$

Then:

$$b(\tau) = \frac{5}{2(\Omega_0^{-1} - 1)} \left(1 + 3(\tau^2 - 1)\left(1 + \frac{\tau}{2}\ln\left(\frac{\tau - 1}{\tau + 1}\right)\right)\right). \tag{26}$$

Note that this $b(t)$ function saturates to the value $5/2(\Omega_0^{-1} - 1)$ at large times.

$\Omega < 1$, $\Lambda \neq 0$, flat: it is useful to use the time variable

$$h = \coth(3t\sqrt{\Lambda/3}/2). \tag{27}$$

Then,

$$b(\tau) = h \int_h^\infty (x^2(x^2 - 1)^{1/3})^{-1} dx. \tag{28}$$

Growing modes are normalized so as to give $b(t) \simeq a(t)$ at early times, and $a(t_0) = 1$.

In the MF theory, collapse time estimates are often based on an extrapolations of the linear regime to density contrasts of order one. It is then convenient to define the quantity:

$$\delta_l \equiv \delta(t_i)/b(t_i). \tag{29}$$

This is the initial density contrast linearly extrapolated to the time at which $b(t) = 1$, which, in an Einstein-de Sitter background, is the present time; it will be used in the next sections.

Before concluding this section, we want to find an expression for the velocity field in the linear regime. Using the equation of motion $\mathbf{p} = ma^2\dot{\mathbf{x}}$, $\frac{d\mathbf{p}}{dt} = -m \bigtriangledown \phi$ and the proper velocity of a particle, $v = a\dot{\mathbf{x}}$, verify the equation:

$$\frac{d\mathbf{v}}{dt} + \mathbf{v}\frac{\dot{a}}{a} = -\frac{\bigtriangledown\phi}{a} = G\rho_b a \int d^3x \delta(\mathbf{x}, t)\frac{\mathbf{x} - \mathbf{x}'}{|\mathbf{x} - \mathbf{x}'|} \tag{30}$$

Supposing that $\mathbf{v}$ is a similar solution for the density, $\mathbf{v} = \mathbf{V}_+(\mathbf{x}, \mathbf{t})t^p$, we get:

$$v^\alpha = \frac{Ha}{4\pi}\frac{\partial}{\partial x^\alpha}\int d^3x' \frac{\delta(\mathbf{x}', t)}{|\mathbf{x}' - \mathbf{x}|} \tag{31}$$

(Peebles 1980). This solution is valid just as that for δ in the linear regime. At time $t = t_0$ this regime is valid on scales larger than $8h^{-1}Mpc$.

2.3. The spectrum of density perturbation.

In order to study the distribution of matter density in the universe it is generally assumed that this distribution is given by the superposition of plane waves independently evolving, at least until they are in the linear regime (this means till the overdensity $\delta = \frac{\rho - \overline{\rho}}{\overline{\rho}} << 1$). Let we divide universe in cells of volume V_u and let we impose periodic conditions on the surfaces. If we indicate with $\overline{\rho}$ the average density in the volume and with $\rho(\mathbf{r})$ the density in $\mathbf{r}$, it is possible to define the density contrast as:

$$\delta(\mathbf{r}) = \frac{\rho(\mathbf{r}) - \overline{\rho}}{\overline{\rho}} \tag{32}$$

This quantity can be developed in Fourier series:

$$\delta(\mathbf{r}) = \sum_{\mathbf{k}} \delta_{\mathbf{k}} exp(i\mathbf{kr}) = \sum_{\mathbf{k}} \delta_{\mathbf{k}} exp(-i\mathbf{kr}) \tag{33}$$

(Kolb e Turner 1990), where $k_x = \frac{2\pi n_x}{l}$ (and similar conditions for the other components) and for the periodicity condition $\delta(x, y, L) = \delta(x, y, 0)$ (and similar conditions for the other components). Fourier coefficients $\delta_{\mathbf{k}}$ are complex quantities given by:

$$\delta_{\mathbf{k}} = \frac{1}{V_u} \int_{V_u} \delta(\mathbf{r}) exp(-i\mathbf{kr}) d\mathbf{r} \tag{34}$$

For mass conservation in V_u we have also $\delta_{\mathbf{k}=0} = 0$ while for reality of $\delta(\mathbf{r})$, $\delta^*_{\mathbf{k}} = \delta_{-\mathbf{k}}$. If we consider n volumes, V_u, we have the problem of determining the distribution of Fourier coefficients $\delta_{\mathbf{k}}$ and that of $|\delta|$. We know that the coefficients are complex quantities and then $\delta_{\mathbf{k}} = |\delta_{\mathbf{k}}| \, exp(i\theta_{\mathbf{k}})$. If we suppose that phases are random, in the limit $V_u \to \infty$ it is possible to show that we get $|\delta|^2 = \sum_{\mathbf{k}} |\delta_{\mathbf{k}}|^2$. The Central limit theorem leads us to conclude that the distribution for δ is Gaussian:

$$P(\delta) \propto exp(\frac{-\delta^2}{\sigma^2}) \tag{35}$$

(Efstathiou 1990). The quantity σ that is present in Eq. (35) is the variance of the density field and is defined as:

$$\sigma^2 =< \delta^2 >= \sum_{\mathbf{k}} < |\delta_{\mathbf{k}}|^2 >= \frac{1}{V_u} \sum_{\mathbf{k}} \delta_k^2 \tag{36}$$

This quantity characterizes the amplitude of the inhomogeneity of the density field. If $V_u \to \infty$, we obtain the more usual relation:

$$\sigma^2 = \frac{1}{(2\pi)^3} \int P(k) d^3k = \frac{1}{2\pi^2} \int P(k) k^2 dk \tag{37}$$

The term $P(k) =< |\delta|^2 >$ is called "Spectrum of perturbations". It is function only of k because the ensemble average in an isotropic universe depends only on r. A choice often made for the primordial spectrum is $P(k) = Ak^n$ which in the case $n = 1$ gives the scale invariant spectrum of Harrison-Zeldovich. An important quantity connected with the spectrum is the two-points correlation function $\xi(\mathbf{r}, t)$. It can be defined as the joint probability of finding an overdensity δ in two distinct points of space:

$$\xi(\mathbf{r}, t) =< \delta(\mathbf{r}, t)\delta(\mathbf{r} + \mathbf{x}, t) > \tag{38}$$

(Peebles 1980), where averages are averages on an ensemble obtained from several realizations of universe. Correlation function can be expressed as the joint probability of finding a galaxy in a volume δV_1 and another in a volume δV_2 separated by a distance r_{12}:

$$\delta^2 P = n_V^2 [1 + \xi(r_{12})] \delta V_1 \delta V_2 \tag{39}$$

where n_V is the average number of galaxies per unit volume. The concept of correlation function, given in this terms, can be enlarged to the case of three or more points.

Correlation functions have a fundamental role in the study of clustering of matter. If we want to use this function for a complete description of clustering, one needs to know the correlation functions of order larger than two (Fry 1982). By means of correlation functions it is possible to study the evolution of clustering. The correlation functions are, in fact, connected one another by means of an infinite system of equations obtained from moments of Boltzmann equation which constitutes the BBGKY (Bogolyubov-Green-Kirkwood-Yvon) hierarchy (Davis e Peebles 1978). This hierarchy can be transformed into a closed system of equation using closure conditions. Solving the system one gets information on correlation functions.

In order to show the relation between perturbation spectrum and two-points correlation function, we introduce in Eq. (38), Eq. (33), recalling that $\delta^*_{\mathbf{k}} = \delta(-\mathbf{k})$ and taking the limit $V_u \to \infty$, the average in the Eq. (38) can be expressed in terms of the integral:

$$\xi(\mathbf{r}) = \frac{1}{(2\pi)^3} \int |\delta(\mathbf{k})|^2 exp(-i\mathbf{kr}) d^3k \tag{40}$$

This result shows that the two-point correlation function is the Fourier transform of the spectrum. In an isotropic universe, it is $|\mathbf{r}| = r$ and then $|\mathbf{k}| = k$ and the spectrum can be obtained from an integral on $|\mathbf{k}| = k$. Then correlation function may be written as:

$$\xi(r) = \frac{1}{2\pi^2} \int k^2 P(k) \frac{sin(kr)}{kr} dk \tag{41}$$

During the evolution of the universe and after perturbations enter the horizon, the spectrum is subject to modulations because of physical processes characteristic of the model itself (Silk damping (Silk 1968) for acollisional components, free streaming for collisional particles, etc.). These effects are taken into account by means of the transfer function $T(k;t)$ which connects the primordial spectrum $P(k;t_p)$ at time t_p to the final time t_f:

$$P(k;t_f) = \left[\frac{b(t_f)}{b(t_p)}\right]^2 T^2(k;t_f)P(k;t_p) \tag{42}$$

where b(t) is the law of grow of perturbations, in the linear regime. In the case of CDM models the transfer function is:

$$T(k) = \left\{1 + \left[ak + (bk)^{1.5} + (ck)^2\right]^\nu\right\}^{\frac{-1}{\nu}} \tag{43}$$

(Bond e Efstathiou 1984), where $a = 6.4(\Omega h^2)^{-1}Mpc$; $b = 3.0(\Omega h^2)^{-1}Mpc$; $c = 1.7(\Omega h^2)^{-1}Mpc$; $\nu = 1.13$. It is interesting to note that Eq. (35) is valid only if $\sigma << 1$, since $|\delta| \leq 1$. This implies than non-linear perturbations, $\sigma >> 1$, must be non-Gaussian. In fact when the amplitudes of fluctuations grow up, at a certain point modes are no longer independent and start to couple giving rise to non-linear effects that change the spectrum and correlation function (Juskiweicz et al 1984). There are also some theories (e.g., cosmic strings (Kibble & Turok 1986)) in which even in the linear regime perturbations are not Gaussian.

2.4. Spherical Collapse

Linear evolution is valid only if $\delta << 1$ or similarly, if the mass variance, σ, is much less than unity. When this condition is no longer verified (e.g., if we consider scales smaller than $8h^{-1}$ Mpc), it is necessary to develope a non-linear theory. In regions smaller than $8h^{-1}$ Mpc galaxies are not a Poisson distribution but they tend to cluster. If one wants to study the properties of galactic structures or clusters of galaxies, it is necessary to introduce a non-linear theory of clustering. A theory of this last item is too complicated to be developed in a purely theoretical fashion. The problem can be faced, by using N-Body simulations of the interesting system, assuming certain approximations that simplifies it, Spherical Collapse Model, Zel'dovich approximation (Zel'dovich 1970). This last gives a solution to the problem of the grow of perturbations in an universe with $p = 0$ not only in the linear regime but even in the mildly non-linear regime.

Spherical symmetry is one of the few cases in which gravitational collapse can be solved exactly (Gunn & Gott 1972; Peebles 1980). In fact, as a consequence of Birkhoff's theorem, a spherical perturbation evolves as a FRW Universe with density equal to the mean density inside the perturbation.

The simplest spherical perturbation is the top-hat one, i.e. a constant overdensity δ inside a sphere of radius R; to avoid a feedback reaction on the background model, the overdensity has to be surrounded by a spherical underdense shell, such to make the total perturbation vanish. The evolution of the radius of the perturbation is then given by a Friedmann equation.

The evolution of a spherical perturbation depends only on its initial overdensity. In an Einstein-de Sitter background, any spherical overdensity reaches a singularity (collapse) at a final time:

$$t_c = \frac{3\pi}{2}\left(\frac{5}{3}\delta(t_i)\right)^{-3/2} t_i. \tag{44}$$

By that time its linear density contrast reaches the value:

$$\delta_l(t_c) = \delta_c = \frac{3}{5}\left(\frac{3\pi}{2}\right)^{3/2} \simeq 1.69. \tag{45}$$

In an open Universe not any overdensity is going to collapse: the initial density contrast has to be such that the total density inside the perturbation overcomes the critical density. So, a perturbation ought to satisfy $\delta_l > 1.69 \cdot 2(\Omega_0^{-1} - 1)/5$ to be able collapse.

Of course, collapse to a singularity is not what really happens in reality. It is typically supposed that the structure reaches virial equilibrium at that time. In this case, arguments based on the virial theorem and on energy conservation show that the structure reaches a radius equal to half its maximum expansion radius, and a density contrast of about 178. In the subsequent evolution the radius and the physical density of the virialized structure remains constant, and its

density contrast grows with time, as the background density decays. Similarly, structures which collapse before are denser than the ones which collapse later.

Spherical collapse is not a realistic description of the formation of real structures; however, it has been shown (see Bernardeau 1994 for a rigorous proof or Valageas 2002a,b) that high peaks ($> 2\sigma$) follow spherical collapse, at least in the first phases of their evolution. However, a small systematic departure from spherical collapse can change the statistical properties of collapse times.

Spherical collapse can describe the evolution of underdensities. A spherical underdensity is not able to collapse (unless the Universe is closed!), but behaves as an open Universe, always expanding unless its borders collide with neighboring regions. At variance with overdensities, underdensities tend to be more spherical as they evolve, so that the spherical model provides a very good approximation for their evolution.

2.5. **Zel'dovich approximation.**

Most MF theories proposed in the literature are based at best on spherical collapse, which neglects tides which are the relevant dynamical interaction. Spherical top-hat collapse is a truly local dynamical approximation: the fate of a spherical perturbation is determined just by its initial overdensity. In other words, the dynamical role of the whole Universe outside the perturbation (according to Birkhoff's theorem) is assumed to be negligible. It is possible to construct a mixed Eulerian-Lagrangian system from the evolution equations of fluid elements by decomposing the tensor of (Eulerian) space derivatives of the peculiar velocity $\mathbf{u}$ into an expansion scalar θ, a shear tensor σ_{ab} and a vorticity tensor ω_{ab}. In this way, the following evolution equation for the density contrast can be obtained (see, e.g., Ellis 1971; here the growing mode $b(t)$ is used as time variable):

$$\frac{d^2\delta}{db^2} + 4\pi G\bar{\rho}\frac{b}{\dot{b}^2}\frac{d\delta}{db} = \frac{4}{3}\left(\frac{d\delta}{db}\right)^2\frac{1}{(1+\delta)} + (1+\delta)\left(4\pi G\bar{\rho}\frac{b}{\dot{b}^2}\delta + 2\sigma^2 - 2\omega^2\right) \tag{46}$$

Here $\sigma^2 = \sigma_{ab}\sigma_{ab}/2$ and $\omega^2 = \omega_{ab}\omega_{ab}/2$ (note that σ^2 in this context is not the mass variance). According to linear theory, any vortical mode is severely damped in the early gravitational evolution, and this remains true during the mildly non-linear regime, up to "orbit crossing OC [1] (at OC vorticity couples with the growing mode; see Buchert 1992). Then it is reasonable to assume vanishing vorticity in the present framework. On the other hand, the shear does not vanish in general: it provides the link between the mass element and the rest of the Universe.

The evolution equation for the shear reads as follows:

$$\frac{d\sigma_{ab}}{db} + \frac{2}{3}\vartheta\sigma_{ab} + \sigma_{ac}\sigma_{cb} + 4\pi G\bar{\rho}\frac{b}{\dot{b}^2}\sigma_{ab} - \frac{2}{3}\sigma^2\delta_{ab} = -4\pi G\bar{\rho}\frac{b}{\dot{b}^2}E_{ab}. \tag{47}$$

The tensor E_{ab}, represents the tidal interactions between the mass element and the rest of the Universe. Then, tides are the relevant dynamical interaction neglected by spherical collapse.

It is useful to find which is the simplest way to introduce tides in the evolution of a mass element. The simplest, realistic approximation of gravitational evolution in the (mildly) non-linear regime is the Zel'dovich approximation, that I am going to summarize.

In this approximation, one supposes to have particles with initial position given in Lagrangian coordinates $\mathbf{q}$. The positions of particles, at a given time t, the Lagrangian-to-Eulerian mapping is written as follows:

$$\mathbf{x} = \mathbf{q} + b(t)\mathbf{p}(\mathbf{q}) \tag{48}$$

where $\mathbf{x}$ indicates the Eulerian coordinates, $\mathbf{p}(\mathbf{q})$ describes the initial density fluctuations and $b(t)$ describes their grow in the linear phase and it satisfies the equation:

$$\frac{d^2b}{dt^2} + 2a^{-1}\frac{db}{dt}\frac{da}{dt} = 4\pi G\rho b \tag{49}$$

The equation of motion of particles, according to the quoted approximation, is given by:

$$\mathbf{v} = \dot{a}\mathbf{q} + \dot{b}\mathbf{p}(\mathbf{q}) \tag{50}$$

[1] In the dynamical evolution of cold matter, it can happen that two mass elements get to the same point. This event is called "orbit crossing"

The peculiar velocity of particles is given by:

$$\mathbf{u} = \frac{d\mathbf{x}}{dt} = \frac{db}{dt}\mathbf{p}(\mathbf{q}) \tag{51}$$

while the density of the perturbed system is given by:

$$\rho(\mathbf{q},t) = \overline{\rho}\left|\frac{\partial q_j}{\partial x_k}\right| = \overline{\rho}\left|\delta_{jk} + b(t)\frac{\partial p_k}{\partial q_j}\right|^{-1} \tag{52}$$

Developing the Jacobian present in Eq. (52) at first order in $b(t)\mathbf{p}(\mathbf{q})$, one obtains:

$$\frac{\delta\rho}{\overline{\rho}} \approx -b(t)\bigtriangledown_{\mathbf{q}}\mathbf{p}(\mathbf{q}) \tag{53}$$

This equation can be re-written, separating the space and time dependence, as in the equation for $\mathbf{u}$, and writing:

$$b(t) = t^{\frac{2}{3}} \qquad \mathbf{p}(\mathbf{q}) = \sum_{\mathbf{k}} i\frac{\mathbf{k}}{|\mathbf{k}|^2}A_{\mathbf{k}}exp(i\mathbf{kq}) \tag{54}$$

in the form:

$$\frac{\delta\rho}{\overline{\rho}} = \sum_{\mathbf{k}} A_{\mathbf{k}}t^{\frac{2}{3}}exp(i\mathbf{kq}) \tag{55}$$

(Efstathiou 1990), that leads us back to the linear theory. In other words, Ze'ldovich approximation is able to reproduce the linear theory, and is also able to give a good approximation in regions with $\frac{\delta\rho}{\overline{\rho}} >> 1$. Using the expression for $p(q)$, the Jacobian in Eq. (52) is a real matrix and symmetric that can be diagonalized. With this $p(q)$ the perturbed density can be written as:

$$\rho(\mathbf{q},t) = \frac{\overline{\rho}}{(1-b(t)\lambda_1(q))(1-b(t)\lambda_2(q))(1-b(t)\lambda_3(q))} \tag{56}$$

where λ_1, λ_2, λ_3 are the three eigenvalues of the Jacobian, describing the expansion and contraction of mass along the principal axes. From the structure of the last equation, we notice that in regions of high density Eq. (56) becomes infinite and the structure of collapse in a pancake, in a filamentary structure or in a node, according to values of eigenvalues. Some N-body simulations (Efstathiou e Silk, 1983) tried to verify the prediction of Ze'ldovich approximation, using initial conditions generated using a spectrum with a cut-off at low frequencies. The results showed a good agreement between theory and simulations, for the initial phases of the evolution ($a(t) = 3.6$). Going on, the approximation is no more valid starting from the time of shell-crossing. After shell-crossing, particles does not oscillate any longer around the structure but they pass through it making it vanish. This problem has been partly solved supposing that particles, before reaching the singularity they sticks the one on the other, due to a dissipative term that simulates gravity and then collects on the forming structure. This model is known as "adesion-model" (Gurbatov et al. 1985).
Summarizing, Zel'dovich approximation gives a description of the transition between linear and non-linear phase. It is expecially used to get the initial conditions for N-body simulations. The main problem with Zel'dovich and perturbative Lagrangian approximations is that they break down after OC. Many authors have then tried to develop approximations which avoid OC or make particles oscillate around pancakes (see Sahni & Coles 1996 for a complete review). It is interesting to note that the Zel'dovich approximation is the first term of a perturbative series; the perturbed quantity is not the density, as in Eulerian perturbation theory, but the displacement of the particles from the initial position.

2.5.1. Collapse time in Zel'dovich approximation

In the Ze'ldovich approximation, the density contrast δ, the expansion θ and the shear σ_{ab} evolve as follows:

$$\begin{aligned}
J(\mathbf{q},t) &= (1-b(t)\lambda_1)(1-b(t)\lambda_2)(1-b(t)\lambda_3) \\
\theta(\mathbf{q},t) &= -\frac{\lambda_1}{1-b(t)\lambda_1} - \frac{\lambda_2}{1-b(t)\lambda_2} - \frac{\lambda_3}{1-b(t)\lambda_3} \\
\sigma_{ab}(\mathbf{q},t) &= \mathrm{diag}\left(\frac{\lambda_1}{1-b(t)\lambda_1} - \frac{\theta}{3}, \frac{\lambda_2}{1-b(t)\lambda_2} - \frac{\theta}{3}, \frac{\lambda_3}{1-b(t)\lambda_3} - \frac{\theta}{3}\right) \\
\delta(\mathbf{q},t) &= ((1-b(t)\lambda_1)(1-b(t)\lambda_2)(1-b(t)\lambda_3))^{-1} - 1.
\end{aligned} \tag{57}$$

When $b(t) = 1/\lambda_1$, caustic formation takes place: the Jacobian determinant vanishes, and all the other quantities go to infinity. It is then quite reasonable, from the point of view of the mass element, to define such instant as the collapse time. Hereafter collapse will always be defined as the OC event. Note also that, after OC, the Zel'dovich evolution along the second and third axes is not really meaningful, as Zel'dovich does not work after OC. It is then possible to give collapse time estimates for any mass element. Initial conditions are "locally" given by the three λ eigenvalues, but the evolution is not physically local, as initial conditions contain non-local information about tides

It is useful to define the following variables (M98):

$$\begin{aligned} x &= \lambda_1 - \lambda_2 \\ y &= \lambda_2 - \lambda_3, \end{aligned} \tag{58}$$

and to use the growing mode $b(t)$ as time variable. Moreover, it is possible to consider regions with linear initial density contrast $\delta_l = 1$ or -1, as all the other cases can be obtained by a simple rescaling of b. The Zel'dovich collapse time is finally given by:

$$b_c^{Zel'dovich} = \frac{3}{\delta_l + 2x + y} \tag{59}$$

Fig. 2 shows the collapse time curves $b_c(x, y)$ for $\delta_l = 1$ and -1. A problem is soon apparent: in the spherical case, when $x = y = 0$, the collapse time is $3/\delta_l$, instead of the exact $1.69/\delta_l$ value. This discrepancy is due to the fact that the Zel'dovich approximation is an exact solution (before OC of course) in one dimension (see, e.g., Shandarin & Zel'dovich 1989), and is then able to describe the collapse of pancake-like structures, while it severely underestimates the collapse rate in spherical symmetry.

A way to overcome this problem is to try some simple *ansatze* for the "true" shape of the collapse time curve. In practice, a truly realistic collapse time curve will depend not only on the λ eigenvalues, but also on the values of the density (or potential) field in all the points of (Lagrangian) space.

A first way to change the Zel'dovich prediction is to force it not to assume values larger than the spherical one (M98):

$$b_c^{an1} = \min\{b_c^{Zel'dovich}, 1.69/\delta_l\}. \tag{60}$$

This b_c curve is shown in Fig. 3a for $\delta_l = 1$; it has a plateau, of height 1.69, at small x and y values. On the other hand, it is unlikely that all quasi-spherical collapses have exactly the same b_c value; a systematic trend of lower b_c values at nonvanishing x and y values is more realistic. Such a b_c curve can be modeled as the intersection of the Zel'dovich prediction with a slightly inclined plane which reaches 1.69 at $x = y = 0$ (M98):

$$b_c^{an2} = \min\{b_c^{Zel'dovich}, 1.69/\delta_l - \epsilon(2x + y)\}. \tag{61}$$

This curve, with $\epsilon = 0.2$, is shown in Fig. 3b. Monaco (1995) contains a more complete discussion of such *ansatze*. A further possibility, examined in Monaco (1995), is to insert "by hand" in Eq. (46) the shear as given by Zel'dovich (Eq. 57), and then solve the equation numerically; the resulting collapse time is very similar to that of Fig. 3a, but the transition from spherical to Zel'dovich regime is smooth.

An interesting conclusion, is that the reasonable systematic trend shown in Fig. 3b does influence the large-mass part of the mass function, moving it toward large masses, even though spherical collapse is recovered for very large overdensities (which are characterized by small x and y values). In other words, the fact that large, rare fluctuations asymptotically follow spherical collapse does not guarantee that the "spherical" PS MF (with $\delta_c = 1.69$) is recovered at large masses.

2.6. Ellipsoidal collapse

The convenience in using the homogeneous ellipsoid collapse model resides in the fact that it can easily be solved by means of a numerical integration of a system of three second-order ordinary differential equations. One of the advantages of spherical symmetry is that, because of Birkhoff's theorem, it is possible to introduce in a background metric a perturbation without influence the rest of the Universe, provided any positive perturbation is compensated for by an (outer) negative one, such to make the total mass perturbation vanish. This is necessary to ensure the self-consistency of the problem:

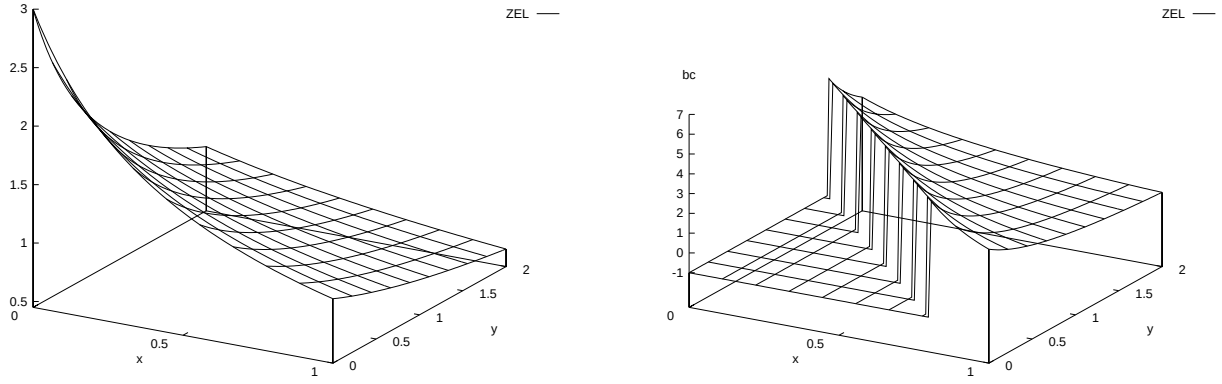

Fig. 2. Collapse times with Zel'dovich approximation. Figures taken by M98.

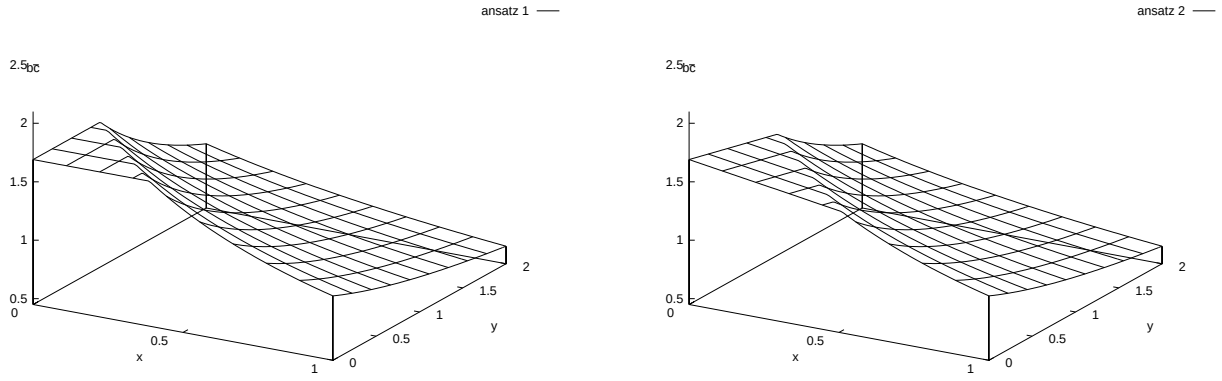

Fig. 3. Collapse times with the two *ansatze*. Figures taken by M98

the background has to evolve as if it were unperturbed. This reasoning is not valid any more when introducing a triaxial perturbation in an unperturbed background: this is going to influence the background, through non-linear feedback effects. To use ellipsoidal collapse in a cosmological context, the correct strategy is not to try to insert an ellipsoid in a uniform background, but to extract an ellipsoid from a perturbed FRW Universe.

In the following, we shall describe the ellipsoidal model and how to find solutions to the equations, both numerically and analytically.

The dynamical variables of ellipsoidal collapse are the three axes $a_i(t)$ of the ellipsoid; they are normalized as the scale factor: $a_i(t) = a(t)$ if the ellipsoid is a sphere with null density contrast. Their evolution equations are:

$$\frac{d^2a_i}{da^2} - (2a(1+(\Omega_0^{-1}-1)a))^{-1}\frac{da_i}{da} + (2a^2(1+(\Omega_0^{-1}-1)a))^{-1}a_i$$
$$\times\left[\frac{1}{3}+\frac{\delta}{3}+\frac{b_i'}{2}\delta+\lambda_{vi}'\right]=0 \tag{62}$$

in the open case (the Einstein-de Sitter case can be obtained by setting $\Omega_0 = 1$), while in the flat case with cosmological constant they are:

$$\frac{d^2a_i}{da^2} - \frac{1-2(\Omega_0^{-1}-1)a^3}{2a(1+(\Omega_0^{-1}-1)a^3)}\frac{da_i}{da} + (2a^2(1+(\Omega_0^{-1}-1)a))^{-1}a_i$$
$$\times\left[\frac{1}{3}+\frac{\delta}{3}+\frac{b_i'}{2}\delta+\lambda_{vi}'\right]=0. \tag{63}$$

Note that this time the scale factor $a(t)$ has been used as time variable. The density contrast δ is:

$$\delta = \frac{a^3}{a_1 a_2 a_3} - 1, \tag{64}$$

while the quantities b'_i and λ'_{vi} are defined as:

$$b'_i = \frac{2}{3}[a_i a_j a_k R_D(a_i^2, a_j^2, a_k^2) - 1] \quad i \neq j \neq k \tag{65}$$

(where the R_D is the Carlson's elliptical integral

$$R_D(x,y,z) = \frac{3}{2}\int_0^\infty \frac{d\tau}{(\tau+x)^{1/2}(\tau+y)^{1/2}(\tau+z)^{3/2}}, \tag{66}$$

which can be calculated by means of the routine given by Press & Teukolsky (1990)) and

$$\lambda'_{vi} = -\frac{a}{a_0}\left(\frac{\delta}{3} - a_0\lambda_i\right). \tag{67}$$

Initial conditions can be set by imposing that the a_i evolve according to Zel'dovich approximation at early times:

$$a_i \simeq a(1 - a\lambda_i) \tag{68}$$

$$\frac{da_i}{da} \simeq \frac{1}{a}(a_i(a) - a^2\lambda_i)\ . \tag{69}$$

These three coupled second-order ordinary differential equations, Eqs. (62) or (63), can be integrated by means of standard routines, as the Runge-Kutta one given in Press et al. (1992). The numerical integration has to be pushed to the singularity, when at least one axis vanishes (and the density diverges). To do this, it is useful to use logarithmic variables, to have more controlled variations from quasi-homogeneity to collapse. Moreover, the integration can be divided into two parts: the first is stopped at decoupling, defined as the instant at which the density starts to increase, while in the second part the density is used as time variable, and the integration is pushed up to large density values (Monaco 1997a). The overall precision of the numerical integration is better than 1% for the spherical collapse, but becomes about 8% for pancake-like collapses. It is to be noted that, in any case, the first collapsing axis is that corresponding to λ_1, the largest λ eigenvalue.

Fig. 4 shows the collapse "times" b_c of initially overdense (δ_l=1) and underdense (δ_l=−1) ellipsoids in an Einstein-de Sitter Universe (in this case $b_c = a_c$). Spherical collapse is obviously recovered at $x = y = 0$, while quasi-spherical collapses reasonably show a systematic departure from spherical collapse, as in Fig. 3a. The large-shear behavior is similar but not identical to that predicted by Ze'ldovich approximation (ZEL); at variance with what happens with quasi-spherical collapses, in this range ZEL tends to underestimate the collapse time. Fig. 5 shows the b_c curve for ellipsoids in an open Universe; this time δ_l=3 has been chosen, to allow all the ellipsoids to collapse. As expected, this curve is nearly identical to the one shown in Fig. 3a, apart from an obvious rescaling. Notably, numerical calculations of collapsing ellipsoids in open Universes are affected by larger errors than that quoted above if the ellipsoid takes a long time to collapse.

An analytic solution to the collapse model equations can be obtained as follows. For the unisolated ellipsoid, the evolution equations reduces to three equations for the three semiaxes of the ellipsoid and are given by (Watanabe 1993; van de Weygaert 1996):

$$\begin{aligned}\frac{d^2 a_{\rm i}}{dt^2} \ &= \ -2\pi G\left\{\rho_{\rm e}(\alpha_{\rm i} - \gamma b_{\rm i}) + \left[\frac{2}{3} - (\alpha_{\rm i} - \gamma b_{\rm i})\right]\rho_{\rm b}\right\} a_{\rm i} = \\ & -2\pi G\left[\rho_{\rm e}\alpha_{\rm i} + \left(\frac{2}{3} - \alpha_{\rm i}\right)\rho_{\rm b}\right] a_{\rm i} - \\ & 2\pi G\gamma\left(-b_{\rm i}\right)\left(\rho_{\rm e} - \rho_{\rm b}\right) a_{\rm i}\end{aligned} \tag{70}$$

where:

$$\gamma = \frac{3}{2\pi}\frac{Q}{\delta}, \qquad \mathbf{b} = (-\beta, \beta - 1, 1) \tag{71}$$

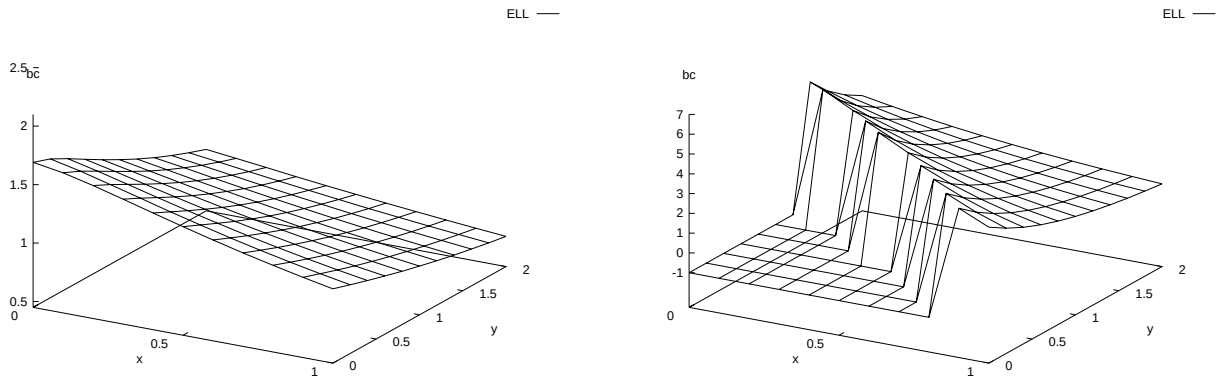

Fig. 4. Collapse times with Ellipsoidal model. Figures taken by M98.

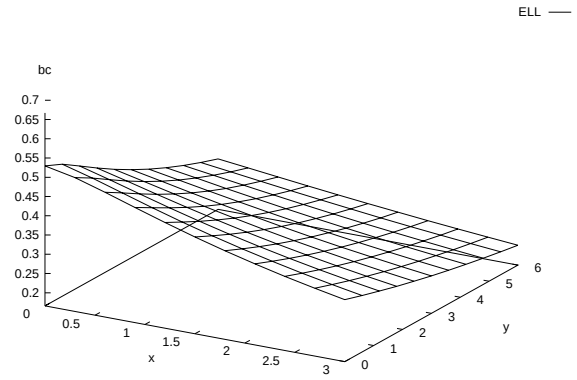

Fig. 5. Collapse times with Ellipsoidal model, open Universe. Figures taken by M98.

and where $\rho_{\rm b}$ is the density of the background universe, and $\rho_{\rm e}$ the density within the ellipsoid. The coefficients $\alpha_{\rm i}$ are given by:

$$\alpha_{\rm i} = a_1 a_2 a_3 \int_0^\infty \frac{d\lambda}{(a_{\rm i}^2+\lambda)\left[(a_1^2+\lambda)(a_2^2+\lambda)(a_3^2+\lambda)\right]^{\frac{1}{2}}} \tag{72}$$

Assuming that the external structures, giving rise to the tidal field, are at a large distance from the ellipsoid (see Eisenstein & Loeb 1995), the amplitude of the external quadrupole force is assumed to increase with the linear growth rate (Ryden 1988; Watanabe 1993; Eisenstein & Loeb 1995), $D(t)$ (this last quantity is given in Peebles 1980):

$$Q(t) = Q_0 \frac{D(t)}{D_0} \tag{73}$$

Here the subscript "0" means that the corresponding quantity is calculated at the present epoch and $D(t) = R_{\rm b}(t)$, for an Einstein-de Sitter (hereafter EdS) universe. In an Einstein-de Sitter universe, Eq. (73), $Q(t) = Q_0 \frac{R_{\rm b}(t_0)(t/t_0)^{2/3}}{R_{\rm b}(t_0)}$ reduces to $Q(t_0) = Q_0$ at time t_0.

In order to have an estimate of the value of Q_0, for a cluster interacting with a neighboring one, one can use the simple model in Watanabe (1993), considering a cluster which has a neighboring cluster with a mean density contrast $< \delta > \simeq 3$, a comoving separation $(0, 0, x_3)$, and a comoving size $\Delta x_3 = x_3/3$, the Q_{33} quadrupole component is given by:

$$Q_{33} \simeq \frac{8}{9}\pi < \delta > \left(\frac{\Delta x_3}{x_3}\right)^3 \simeq 0.3 \tag{74}$$

The previous estimate corresponds to a cluster interacting with a neighbor having a mass excess comparable to that of the Virgo cluster, and a separation three times its size.

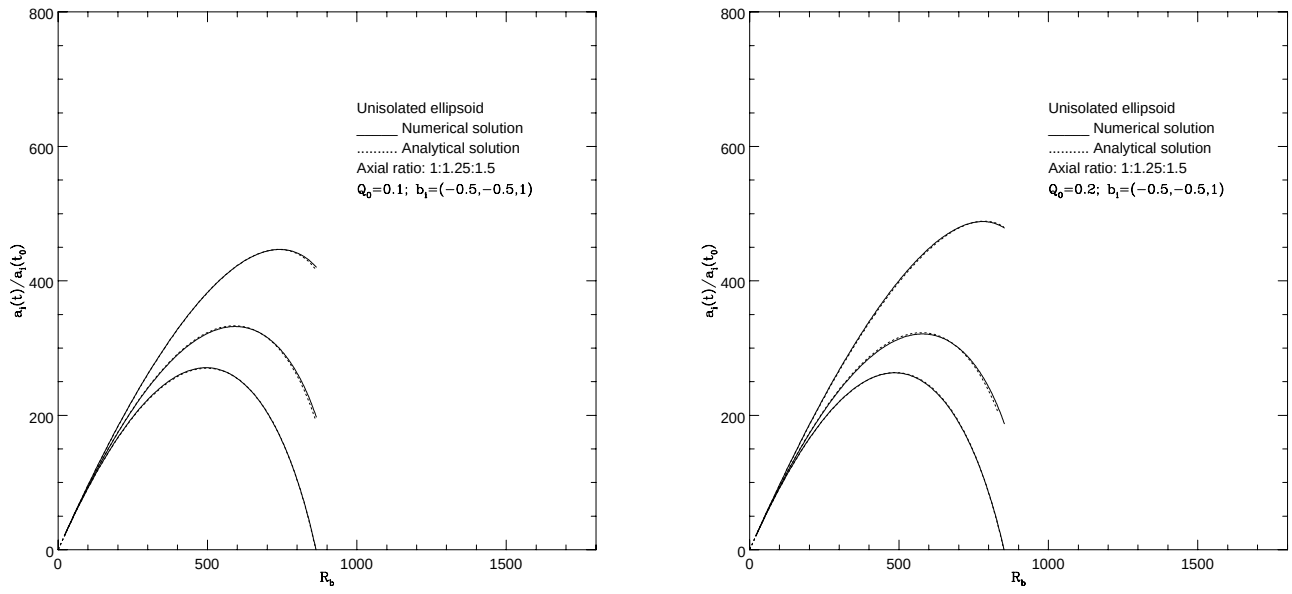

(a)

(b)

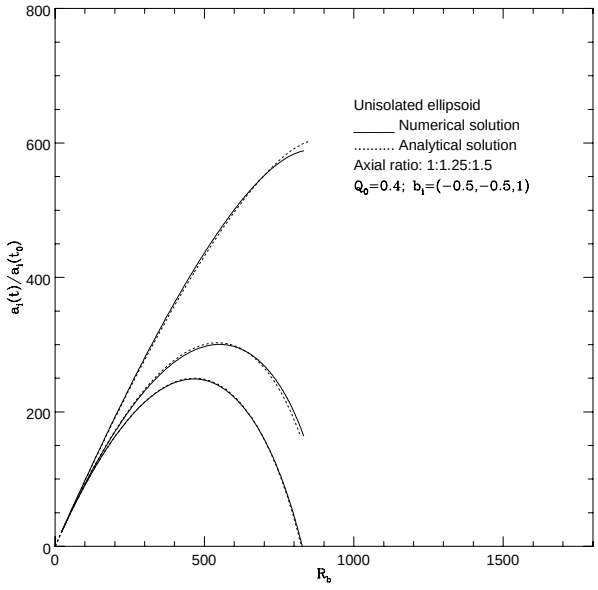

(c)

Fig. 6. Evolution of *unisolated* homogeneous ellipsoidal perturbations in an EdS universe with $H_0 = 50$km/s/Mpc, $\rho_{\rm e}/\rho_{\rm b} = 1.003$, axial ratio is $1 : 1.25 : 1.5$, $b_{\rm i} = (-0.5, -0.5, 1)$, and $Q_0 = 0.1$ (a), $Q_0 = 0.2$ (b), $Q_0 = 0.4$ (c). Figures taken from Del Popolo (2002b).

Another way of estimating Q_0 is by using the anisotropy of the velocity field in the LSC from data of Lilje, Yahil & Jones (1986). If we indicate with $Q_{\rm v0}$ the component of the largest absolute value of the anisotropic velocity, one gets: $Q_0\Omega_0^{0.6} = \frac{4\pi}{3}Q_{\rm v0}$ (Watanabe 1993). Since Lilje, Yahil & Jones (1986) deduced a value of $Q_{\rm v0} \sim 0.1 - 0.2$ at the distance of the Local Group from Virgo, we have that $Q_0\Omega_0^{0.6} \sim 0.4 - 0.8$.

It is possible to obtain an analytical solution of Eq. (70), describing the evolution of an *unisolated* ellipsoid as shown in Del Popolo (2002b) In this case the solution can be written in the form:

$$\frac{a_1(t)}{a_1(t_i)} = R_{\rm b} - \frac{3}{2}\tilde{\alpha}_1 \left(R_{\rm b} - R_{\rm e}\right) - d \times R_{\rm b}^{\left(\frac{2+3c_1}{2}\right)} \left(1 - \frac{3\tilde{\alpha}_1}{2}\right) \tag{75}$$

$$\frac{a_2(t)}{a_2(t_i)} = R_{\rm b} - \frac{3}{2}\tilde{\alpha}_2 \left(R_{\rm b} - R_{\rm e}\right) \tag{76}$$

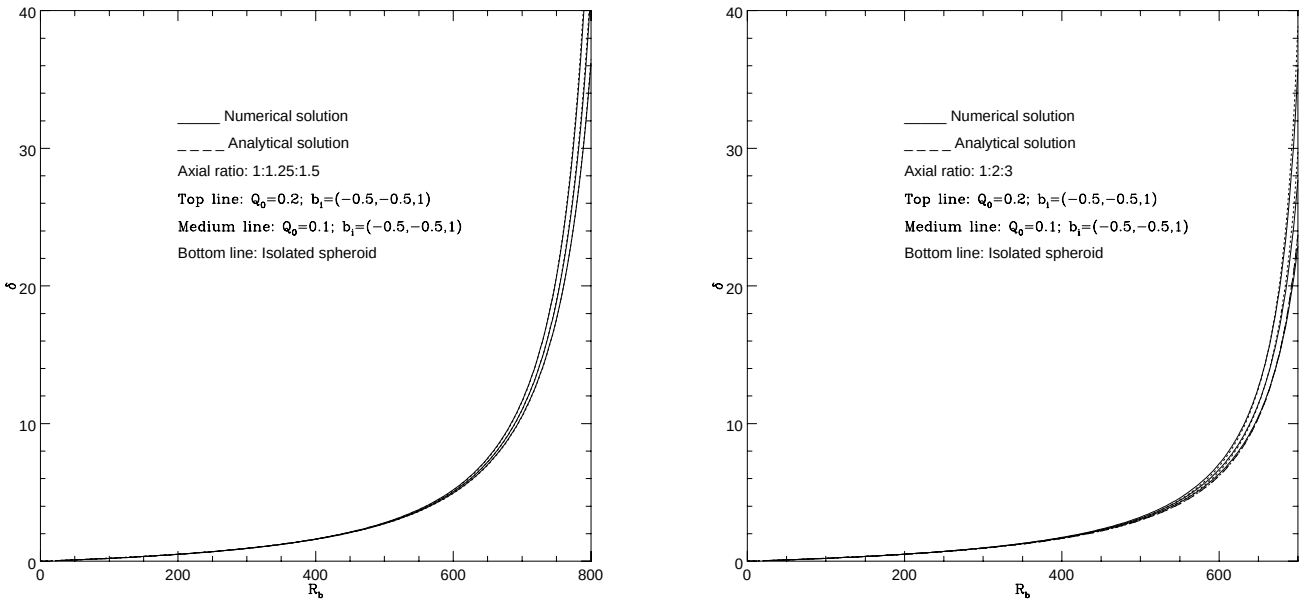

(a) (b)

Fig. 7. The evolution of the density contrast. The axial ratio of the ellipsoid is $1:1.25:1.5$ (a) and $1:2:3$ (b), the lines from bottom to top represent the case of an *isolated* ellipsoid ($b_{\rm i}=(0,0,0)$), $Q_0=0.1$, $b_{\rm i}=(-0.5,-0.5,1)$, and $Q_0=0.2$, $b_{\rm i}=(-0.5,-0.5,1)$, respectively. Figure taken from Del Popolo (2002b).

$$\frac{a_3(t)}{a_3(t_i)}=R_{\rm b}-\frac{3}{2}\tilde{\alpha}_3\left(R_{\rm b}-R_{\rm e}\right) \tag{77}$$

where $R_{\rm b}$ is the scale factor of the background universe, and $R_{\rm e}$ that of the ellipsoid.

For ellipsoids having the initial axial ratio $1:a_2:a_3$, with $a_1\geq 1.25$ and $a_2\geq 1.5$, we now have that $c_1=1.23$, $d=6\times 10^{-7}$ and:

$$\tilde{\alpha}_1=\alpha_1+0.0672\left(\frac{b_1}{b_2}\right)^{0.15}b_3^{0.6} \tag{78}$$

$$\tilde{\alpha}_2=a_{10}^{0.07}a_{20}^{-0.06}a_{30}^{-0.01}\left[\alpha_2+0.031\left(\frac{b_2}{b_1}\right)^{0.5}b_3^{0.95}\right] \tag{79}$$

$$\tilde{\alpha}_3=1.002a_{10}^{0.1}a_{20}^{-0.035}a_{30}^{-0.065}\left(\alpha_3-0.063a_{30}^{0.09}b_3^{0.95}\right) \tag{80}$$

where $b_{\rm i}$ was defined in Eq. (71).

In the case of prolate spheroids, with axial ratio $1:1:a_3$ and $1\leq a_3\leq 5$, a better approximation to the $\alpha_{\rm i}$ is:

$$\tilde{\alpha}_1=\alpha_1+0.037\left(\frac{a_{30}}{a_{10}}\right)^{0.35}\left(\frac{b_1}{b_2}\right)^{0.15}b_3^{0.6} \tag{81}$$

$$\tilde{\alpha}_2=\left(\frac{a_{10}}{a_{30}}\right)^{0.01}\left[\alpha_2+0.031\left(\frac{a_{10}}{a_{30}}\right)\left(\frac{b_2}{b_1}\right)^{0.5}b_3^{0.95}\right] \tag{82}$$

$$\tilde{\alpha}_3=1.002\left(\frac{a_{20}}{a_{30}}\right)^{0.065}\left(\alpha_3-0.063a_{30}^{0.09}b_3^{0.95}\right) \tag{83}$$

In the case of an *unisolated* ellipsoid the length of the uncollapsed axes at collapse can be obtained by means of Eq. (76)-(77):

$$\frac{a_3(t_{\rm c})}{a_2(t_{\rm c})}=\frac{a_3(t_{\rm i})}{a_2(t_{\rm i})}\frac{R_{\rm b}-\frac{3}{2}\tilde{\alpha}_3\left(R_{\rm b}-R_{\rm e}\right)}{R_{\rm b}-\frac{3}{2}\tilde{\alpha}_2\left(R_{\rm b}-R_{\rm e}\right)} \tag{84}$$

The evolution of the density contrast can be calculated using the usual definition:

$$\delta=\frac{\rho_{\rm e}-\rho_{\rm b}}{\rho_{\rm b}}=\frac{\rho_{\rm e0}}{\rho_{\rm b0}}\frac{a_{10}}{a_1}\frac{a_{20}}{a_2}\frac{a_{30}}{a_3}\left(\frac{R_{\rm b}}{R_{\rm b0}}\right)^3-1 \tag{85}$$

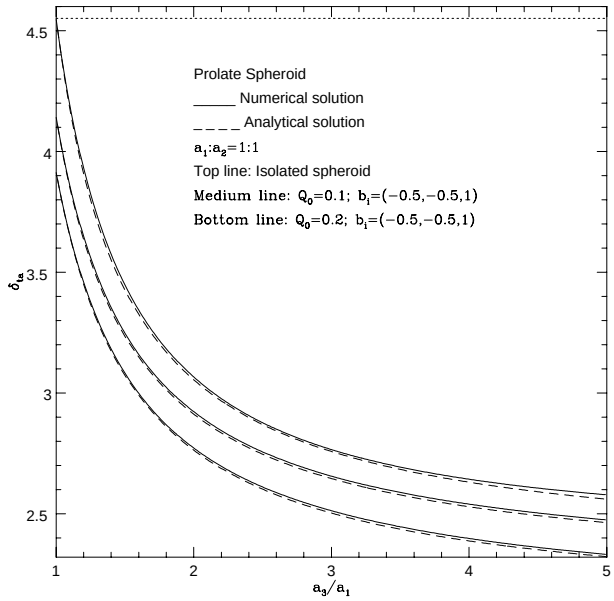

Fig. 8. The density contrast at turnaround for a prolate spheroid for several values of the longest axis, a_3, (the other two axes have fixed value $a_1 : a_2 = 1 : 1$). The solid lines, from top to bottom, represent numerical results for the density contrast for an *isolated* spheroid ($b_{\rm i} = (0, 0, 0)$), and for *unisolated* spheroids with $Q_0 = 0.1$, $b_{\rm i} = (-0.5, -0.5, 1)$ and $Q_0 = 0.2$, $(-0.5, -0.5, 1)$, respectively. The dashed lines represent the approximate solution (Eq. (37)). The upper dotted line represents the value of the density contrast at turnaround for a spherical perturbation. Figure taken from Del Popolo (2002b).

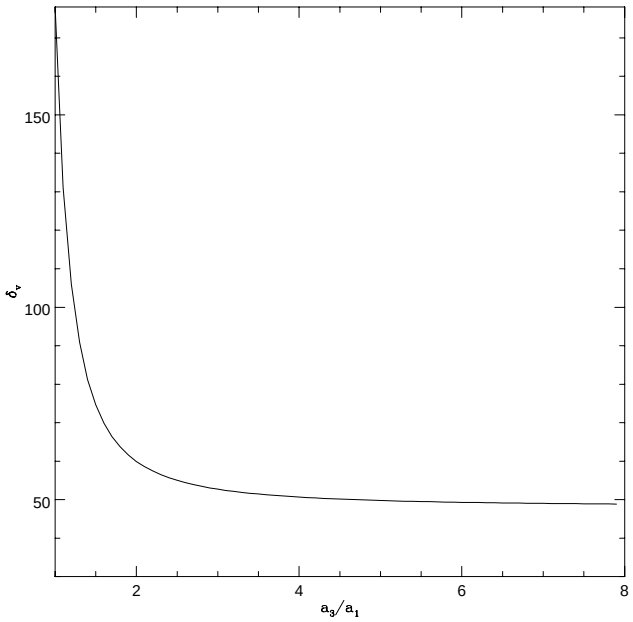

Fig. 9. Density contrast at virialization. The solid line refers to an *isolated* prolate spheroid. Figure taken from Del Popolo (2002b).

If $x(t) = x_{\rm o}X(t)$, $y(t) = y_{\rm o}Y(t)$ and $z(t) = z_{\rm o}Z(t)$, are the principal axes ($x_{\rm o}$, $y_{\rm o}$ and $z_{\rm o}$ are the initial values of the axes), the overdensity of the ellipsoid is the same used previously, the initial conditions are $X = Y = Z = R_{\rm b} = R_{\rm e} = 1$ at

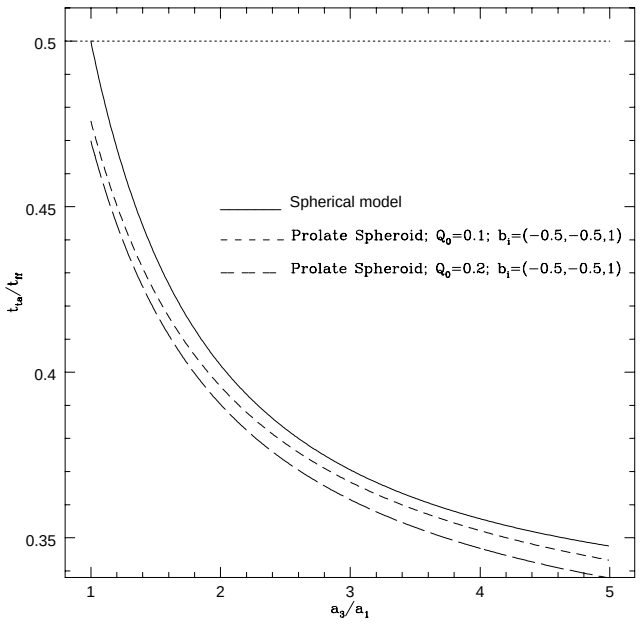

Fig. 10. Turnaround epoch for a prolate spheroid. The solid, short-dashed and long-dashed lines, represent respectively the time of turnaround for an *isolated* spheroid and for spheroids having $Q_0 = 0.1$, $b_{\rm i} = (-0.5, -0.5, 1)$ and $Q_0 = 0.2$, $(-0.5, -0.5, 1)$. The upper dotted line represents the value of the density contrast at turnaround for a spherical perturbation. Figure taken from Del Popolo (2002b).

$t = t_0$ and as before the initial velocity is equal to the Hubble velocity at t_0 (representing the initial time). The parametric equations satisfied by $R_{\rm e}(t)$ are:

$$R_{\rm e} = \frac{1}{2\delta}\left(1-\cos(\vartheta)\right), \qquad \frac{t}{t_0} = \frac{3}{4\delta^{3/2}}\left(\vartheta - \sin(\vartheta)\right) \tag{86}$$

while, since our background is an EdS universe, $R_{\rm b}(t) \propto t^{2/3}$.

It is easy to find that the density contrast is given by:

$$\begin{aligned}
\delta_{\rm i} \; = \; & \frac{R_{\rm b}^3}{XYZ} - 1 = f_1^2\left(\vartheta\right) \\
& [\left(1-\frac{3\tilde{\alpha}_1}{2}\right) f_1^{\frac{2}{3}}\left(\vartheta\right) + \frac{3}{4}\tilde{\alpha}_1 f_2\left(\vartheta\right) \\
& -d\left(1-\frac{3\tilde{\alpha}_1}{2}\right)\frac{f_1^{\frac{2f}{3}}\left(\vartheta\right)}{\delta^{f-1}}]^{-1} \times \\
& \left[\left(1-\frac{3\tilde{\alpha}_2}{2}\right) f_1^{\frac{2}{3}}\left(\vartheta\right) + \frac{3}{4}\tilde{\alpha}_2 f_2\left(\vartheta\right)\right]^{-1} \\
& \left[\left(1-\frac{3\tilde{\alpha}_3}{2}\right) f_1^{\frac{2}{3}}\left(\vartheta\right) + \frac{3}{4}\tilde{\alpha}_3 f_2\left(\vartheta\right)\right]^{-1} - 1
\end{aligned} \tag{87}$$

where $f = \frac{2+3c_1}{2}$, $f_1(\vartheta) = \frac{3}{4}\left(\vartheta - \sin(\vartheta)\right)$ and $f_2(\vartheta) = 1 - \cos(\vartheta)$. The density contrast at turn-around is obtained by calculating $\delta_{\rm i}(\vartheta_{\rm ta})$, where the parameter $\vartheta_{\rm ta}$ at the turnaround epoch is given solving the equation:

$$\frac{2}{3\tilde{\alpha}_1} = \frac{df R_{\rm b}^{f-1} + \frac{\sin(\vartheta_{\rm ta})}{f_2(\vartheta_{\rm ta})} f_1^{\frac{1}{3}} - 1}{df R_{\rm b}^{f-1} - 1} \tag{88}$$

Eq. (87) yields the familiar value $\delta = \left(3\pi/4\right)^2$ in the spherical case, ($d = 0$, $\tilde{\alpha}_1 = \alpha_1 = \tilde{\alpha}_2 = \alpha_2 = \tilde{\alpha}_3 = \alpha_3 = 2/3$). In general, in order to obtain the density contrast at turnaround, one has first to solve Eq. (88) for ϑ for an arbitrary axial ratio and substitute the value in Eq. (87). The time of turn-around can be calculated by:

$$t = \frac{3t_0}{4\delta^{3/2}}\left(\vartheta - \sin(\vartheta)\right) = \frac{t_{\rm ff}}{2\pi}\left(\vartheta - \sin(\vartheta)\right) \tag{89}$$

where $t_{\rm ff}$ is the free-fall time:

$$t_{\rm ff} = \frac{3\pi}{2\delta^{3/2}} t_0 \tag{90}$$

Similarly it is possible to calculate the density contrast at collapse and collapse time.

Figs. 6-10 plots the comparison of the analytical model with numerical simulations for several interesting quantities.

Fig. 6 shows the evolution of *unisolated* homogeneous ellipsoidal perturbations in an EdS universe with $H_0 = 50$km/s/Mpc, $\rho_{\rm e}/\rho_{\rm b} = 1.003$, axial ratio is $1:1.25:1.5$, $b_{\rm i} = (-0.5, -0.5, 1)$, and $Q_0 = 0.1$ (a), $Q_0 = 0.2$ (b), $Q_0 = 0.4$ (c).

Fig. 7, plots the evolution of the density contrast. The axial ratio of the ellipsoid is $1:1.25:1.5$ (a) and $1:2:3$ (b), the lines from bottom to top represent the case of an *isolated* ellipsoid ($b_{\rm i} = (0,0,0)$), $Q_0 = 0.1$, $b_{\rm i} = (-0.5, -0.5, 1)$, and $Q_0 = 0.2$, $b_{\rm i} = (-0.5, -0.5, 1)$, respectively.

Fig. 8, shows the density contrast at turnaround for a prolate spheroid for several values of the longest axis, a_3, (the other two axes have fixed value $a_1 : a_2 = 1:1$). The solid lines, from top to bottom, represent numerical results for the density contrast for an *isolated* spheroid ($b_{\rm i} = (0,0,0)$), and for *unisolated* spheroids with $Q_0 = 0.1$, $b_{\rm i} = (-0.5, -0.5, 1)$ and $Q_0 = 0.2$, $(-0.5, -0.5, 1)$, respectively. The dashed lines represent the approximate solution. The upper dotted line represents the value of the density contrast at turnaround for a spherical perturbation.

Fig. 9, is the density contrast at virialization, while Fig. 10 represents the turnaround epoch for a prolate spheroid. The solid, short-dashed and long-dashed lines, represent respectively the time of turnaround for an *isolated* spheroid and for spheroids having $Q_0 = 0.1$, $b_{\rm i} = (-0.5, -0.5, 1)$ and $Q_0 = 0.2$, $(-0.5, -0.5, 1)$. The upper dotted line represents the value of the density contrast at turnaround for a spherical perturbation.

2.7. Collapse time and the MF

In the previous subsections, we have studied the evolution of different mass elements and the calculation of collapse time. In fact, the problem of finding an expression for the MF is strictly connected to that of finding realistic estimates of collapse times of generic mass elements. Knowing this last, by means of statistical methods (as we shall see later) it is possible to obtain an expression for the MF. In the case of the spherical model (SPH), Zel'dovich approximation and ellipsoidal model, collapse times can be calculated analytically: in the case of spherical collapse (SPH) is simply $1.69/\delta_l$, in the case of Ze'ldovich approximation (ZEL) is $1/\lambda_3$, while the ellipsoidal collapse (ELL) can be calculated by finding the smallest positive root of Eq. (3.24) of M98 and by correcting for quasi spherical collapses as in Eq. (3.27) of M98 or using the analytical model of section 2.6. Second (2ND) and third (3ND) order [2] collapse times have been found by looking for the first instant at which $J < 0$, then using conventional root-finding algorithms to find the accurate value.

Collapse times present the disadvantage that the passage from collapse to non-collapse takes place through infinity. It is more convenient to define the quantity $F(\mathbf{q}; \Lambda)$ as the inverse collapse time of the point $\mathbf{q}$, when the initial field is smoothed at a resolution (mass variance) Λ:

$$F(\mathbf{q}; \Lambda) = \frac{1}{b_c(\mathbf{q}; \Lambda)} \tag{91}$$

F is the basic dynamical quantity needed to construct the MF. In the SPH case F is simply proportional to the linear density contrast, $F = \delta_l/1.69$; in the Zel'dovich (ZEL) case F is just equal to λ_1.

The quantity F is obviously a non-Gaussian process, and it is not a simple non-linear function of a Gaussian field (such as, for instance, a lognormal distribution): it is a complicated non-linear and non-local functional of the whole initial Gaussian perturbation field. Its 1-point PDF is the minimal amount of statistical information needed to construct the MF.

[2] The Zel'dovich approximation is the first term of a perturbative series; the perturbed quantity is not the density, as in Eulerian perturbation theory, but the displacement of the particles from the initial position. The problem of the evolution of a self-gravitating fluid can be reformulated in terms of equations for the displacement field. The equations for the displacement field have been found by several authors: Buchert (1989), Bouchet et al. (1995) and Catelan (1995). The Lagrangian system, (see Eqs. 1.42 and 1.43 in M98), can be perturbatively solved for small displacements. This has been done by Buchert (1989), Moutarde et al. (1991), Bouchet et al. (1992), Buchert (1992), Buchert & Ehlers (1993), Lachièze-Rey (1993a,b), Buchert (1994), Bouchet et al. (1995) and Catelan (1995); see also Bouchet (1996) and Buchert (1996) for reviews. The first order solution, for suitable initial conditions (as given by the linear growing mode), is the well-known Zel'dovich (1970) approximation. The perturbative series has been calculated up to third order (from this comes the notation 3RD).

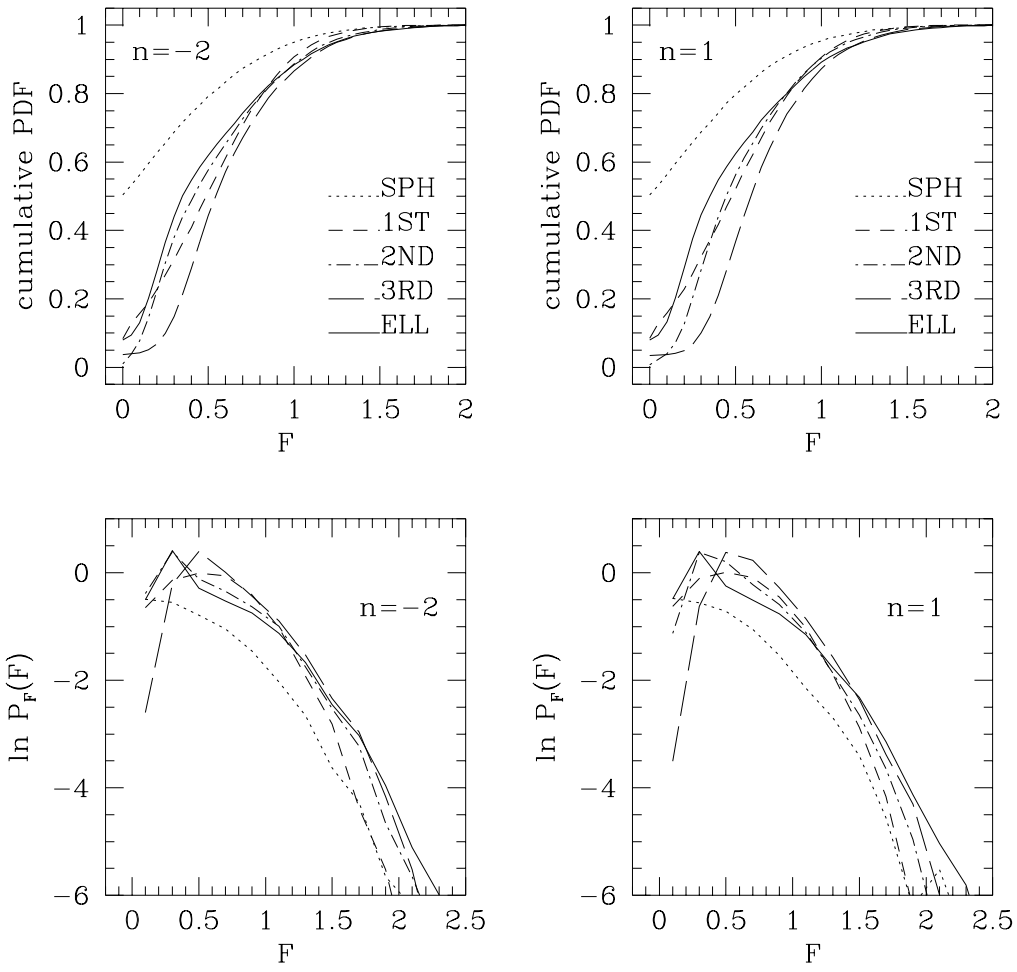

Fig. 11. Cumulative and differential PDFs of F. Figure taken from M98.

The 1-point PDFs for the F processes, relative to different dynamical predictions, can be estimated by means of the Monte Carlo realizations (see M98). Fig. 11 shows such PDFs for two different spectral indexes, namely $n = -2$ and 1. Both cumulative and differential curves (the latters in logarithm scale) are shown.

In the following, the ELL and 3RD predictions will be considered, and the PDFs will be mediated over four the spectral indexes, namely $n = -2$, -1, 0 and 1.

Summarizing, the MF problem can be formulated in terms of a non-Gaussian process F, representing the inverse collapse time of a generic mass element. If linear theory with a threshold (or spherical collapse) is considered, F is proportional to the linear density contrast, and is then Gaussian. More realistic estimates of collapse times lead to F processes which have a different statistical behavior, even in the rare event tail.

3. Mass function.

3.1. PS MF

The mass function or multiplicity function can be described by the relation:

$$dN = n(M)dM \tag{92}$$

that is the number of objects per unit volume, having a mass in the range M ed $M+dM$. The multiplicity function can also be used to define the luminosity function after having fixed the ratio $\frac{M}{L}$. Obtaining the mass function starting from that of luminosity is complicated since the ratio $\frac{M}{L}$ is known with noteworthy uncertainty and it is different for different objects

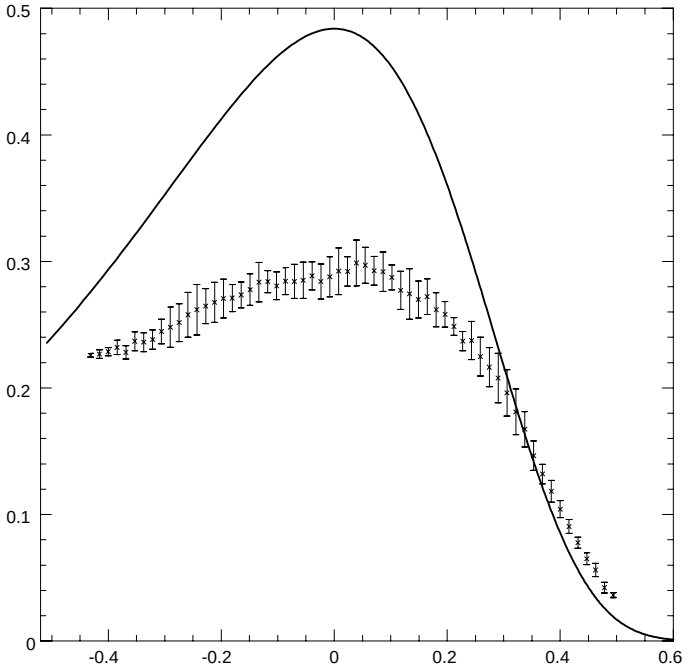

Fig. 12. Comparison of PS multiplicity function with simulations. In the plot the solid line represents the multiplicity function obtained by PS, solid line, and the numerical multiplicity function obtained by YNY. Figure taken from Del Popolo (2005).

and moreover the luminosity function for objects like galaxies depend on the morphological type (Binggeli & Tamman 1985). Finally trying to determine the luminosity function observatively is problematic (see for example G.Efstathiou, R.S.Ellis, B.A.Peterson 1988).
For the above reasons, the theoretical determination of the mass function is very important.

The theoretical derivation of the mass function of gravitationally bound objects has been pioneered by Press & Schechter (1974). To incorporate the dynamics of the structure, PS formalism adopted top-hat spherical model, according to which the collapse condition for forming massive objects is determined purely by its local average density. To make statistical predictions, however, the PS formalism assumes that initial density field is Gaussian and that massive objects form in the peaks of the density field.

This theory is based upon these hypotheses:

- The linear density field is described by a stochastic Gaussian field. The statistics of the matter distribution is Gaussian.
- The evolution of density perturbations is that described by the linear theory. Structures form in those regions where the overdensity linearly evolved and filtered with a top-hat filter exceeds a threshold δ_c ($\delta_c = 1.68$, obtained from the spherical collapse model (Gunn & Gott 1972)).
- for $\delta \geq \delta_c$ regions collapse to points. The probability that an object forms at a certain point is proportional to the probability that the point is in a region with $\delta \geq \delta_c$ given by:

$$P(\delta, \delta_c) = \int_{\delta_c}^{\infty} d\delta \frac{1}{\sigma(2\pi)^{\frac{1}{2}}} exp\left(-\frac{\delta^2}{2\sigma^2}\right) \tag{93}$$

The multiplicity function is given by:

$$\rho(M, z) = -\rho_0 \frac{\partial P}{\partial M} dM = n(M) M dM \tag{94}$$

If we add the conditions $\Omega = 1$, $|\delta_k|^2 \propto k^n$, the Press-Schechter solution is autosimilar and has the form:

$$\rho(M, z) = \frac{\rho}{\sqrt{2\pi}} \left(\frac{n+3}{3}\right) \left(\frac{M}{M_*}(z)\right)^{\frac{n+3}{6}}$$

$$\times exp\left[-\frac{1}{2}\frac{M}{M_*}(z)^{\frac{n+3}{3}}\right]\frac{dM}{M} \tag{95}$$

where $M_*(z) \propto (1+z)^{-\frac{6}{n+3}}$. Several are the problems of the theory:

- **Statistical problems:** in the limit of vanishing smoothing radii, or of infinite variance, the fraction of collapsed mass, asymptotes to 1/2. This is a signature of linear theory: only initially overdense regions, which constitute half of the mass, are able to collapse. Nonetheless, underdense regions can be included in larger overdense ones, or, more generally, non-collapsed regions have a finite probability of being included in larger collapsed ones; this is commonly called *cloud-in-cloud problem*. PS argued that the missing mass would accrete on the formed structures, doubling their mass without changing the shape of the MF; however, they did not give a true demonstration of that. Then, they multiplied their MF by a "fudge factor" 2. Other authors (see Lucchin 1989) used to multiply the MF by a factor $(1+f)$, with f denoting the fraction of mass accreted by the already formed structures.
- **Dynamical problems:** the heuristic derivation of the PS MF bypasses all the complications related to the highly non-linear dynamics of gravitational collapse. Spherical collapse helps in determining the δ_c parameter and in identifying collapsed structures with virialized halos. However, the PS procedure completely ignores important dynamical elements, such as the role of tides and the transient filamentary geometry of collapsed structures. Moreover, supposing that every structure virializes just after collapse is a crude simplification: when a region collapses, all its substructure is supposed by PS to be erased at once, while in realistic cases the erasure of substructures is connected to the two-body interaction of already collapsed clumps, an important piece of gravitational dynamics which is completely missed by the PS procedure.
- **Geometrical problems:** to estimate the mass function from the fraction of collapsed mass at a given scale it is necessary to relate the mass of the formed structure to the resolution
  In practice, the true geometry of the collapsed regions in the Lagrangian space (i.e. as mapped in the initial configuration) can be quite complex, especially at intermediate and small masses; in this case a different and more sophisticate mass assignment ought to be developed, so that geometry is taken into account. For instance, if structures are supposed to form in the peaks of the initial field, a different and more geometrical way to count collapsed structures could be based on peak abundances.

Improvements of the model are due to several authors, Heavens and Peacock (1989), Peacock & Heavens (1990), BCEK, strictly connected to the lacking factor of 2 in the theory, which has been shown to be related to the so called "cloud in cloud" problem. Heavens and Peacock (1989) took into considerations the underdense regions ($\delta < \delta_c$). Filtering a density field, $\delta(x)$ on a given scale R_f, one obtains a set of points exceding the threshold δ_c: this set is named "excursion set" (see next subsection) of the filtered field (Adler 1981). In this field is possible to identify objects using special criteria (see Apple & Jones 1990). An object who had a given value $\delta > \delta_c$, at a fixed R_f, shall have a smaller value $\delta = \delta_c$, for a larger R_f. If R_f is furtherly increased it shall disappear under the threshold. As a consequence, objects belonging to the smaller scale of clustering shall be englobed in the larger one and as a consequence half of the mass is accounted. Heavens and Peacock (1989) solved the problem taking into consideration also the underdense regions with $\delta < \delta_c$. They used, differently from PS, the relation:

$$p(>R_f) = p_G(\delta > \delta_c) + \int_{-\infty}^{\infty} \frac{dp_G}{d\delta} p_{up}(\delta_c, \delta) d\delta \tag{96}$$

where p_G is the Gaussian distribution used by PS. This relation divides the points into two classes: those going from $\delta > \delta_c$ to $\delta = \delta_c$, when R_f is increased, and they are associated to objects of radius $> R_f$, and points under the threshold having the probability p_{up} that in a following filtering, they have $\delta > \delta_c$. Using the relation for p_{up} obtained by Heavens and Peacock (1989) one gets:

$$p(>R_f) = 2p_G \tag{97}$$

which solves the problem of the fudge factor of 2 in PS.

In next subsections a wider description of the improvements to the PS theory are summarized.

Despite all of its problems, the PS procedure for a long time proved successful, as compared to N-body simulations, and a good starting point for all the subsequent works on the subject (Efstathiou et al. 1988; Efstathiou & Rees 1988,

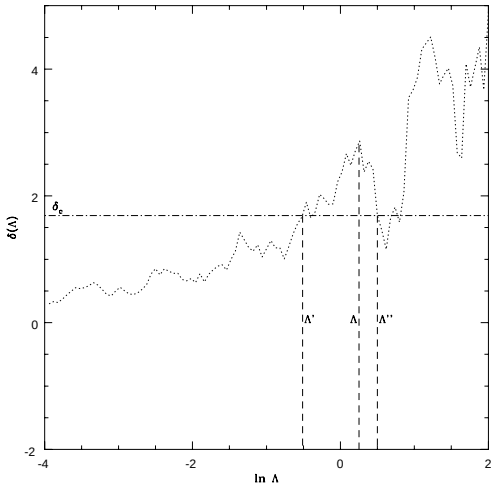

Fig. 13. The absorbing barrier problem. Figure taken by M98.

BCEK), White, Efstathiou & Frenk 1993, Jain & Bertschinger 1994, Lacey & Cole 1994, Efstathiou 1995, Bond & Myers 1996b, Governato et al. 1999).

Although the analytical framework of the PS model has been greatly refined and extended (see next subsection), more recently, it has been shown that the PS mass function, while qualitatively correct, disagrees with the results of high resolution N-body simulations. In particular, the PS formula overestimates the abundance of haloes near the characteristic mass M_* and underestimates the abundance in the high mass tail (Efstathiou et al. 1988; White, Efstathiou & Frenk 1993; Lacey & Cole 1994; Tozzi & Governato 1998; Gross et al. 1998; Governato et al. 1999; YNY). The quoted discrepancy is not surprising since the PS model, as any other analytical model, should make several assumptions to get simple analytical predictions. In Fig. 12, it is plotted a comparison of PS multiplicity function with simulations. In the plot the solid line represents the multiplicity function obtained by PS, solid line, and the numerical multiplicity function obtained by YNY. The plot shows what is well known, namely: the PS mass function, while qualitatively correct, disagrees with the results of N-body simulations. In particular, the PS formula overestimates the abundance of haloes near the characteristic mass M_* and underestimates the abundance in the high mass tail (Efstathiou et al. 1988; Lacey & Cole 1994; Tozzi & Governato 1998; Gross et al. 1998; Governato et al. 1999).

3.1.1. **The cloud-in-cloud problem**

The cloud-in-cloud problem has origin in the following inconsistency of the original PS procedure. A collapse prediction is given to any point (of the Lagrangian space) *for any resolution* Λ; in other words, a whole trajectory in the δ_l–Λ plane is given to any point, as in Fig. 13. Such trajectories start from 0 at Λ=0 (vanishing resolution implies complete smoothing, and then vanishing density contrast), then wander around the plane, eventually upcrossing or even downcrossing the threshold line $\delta_l = \delta_c$. When a trajectory lies above the threshold, the point is assumed to be part of a collapsed region of radius $R' \geq R(\Lambda)$; it is clear that the size $R'(\Lambda')$ of the formed structure is connected to the point Λ' of first upcrossing of the trajectory. On the other hand, when a trajectory downcrosses the barrier at a resolution Λ'', the point is interpreted as not included in any region of size $> R''(\Lambda'')$ (R decreases with increasing Λ), which is clearly in contradiction with what stated above.

To solve the cloud-in-cloud problem, a point whose trajectory has experienced its first upcrossing of the threshold line has to be considered as collapsed at that scale, regardless of its subsequent downcrossings. This can be done as follows: an absorbing barrier is put in correspondence with the threshold line, so as to eliminate any downcrossing event (BCEK). Alternatively, a non-collapse condition can be formulated as follows: a point is not collapsed at Λ if its density contrast *at any* $\Lambda' < \Lambda$ is below the threshold (Peacock & Heavens 1990).

The mathematical nature of the problem, and the resulting MF, strongly depend on the shape of the filter. For general filters, trajectories are strongly correlated in Λ, and then all the N-point correlations of the process at different resolutions

have to be known to solve the problem. However, if the smoothing filter sharply cuts the density field in the Fourier space, then independent modes are added as the resolution changes, and the resulting trajectories are Gaussian random walks. Such kind of filter is commonly called *sharp k-space filter*; it will be referred to as SKS filter throughout the text.

In the SKS case, the problem is suitably solved within the diffusion framework proposed by BCEK (see next subsection).

3.2. Excursion set approach

In this section, we review the formulation of the excursion set approach, mostly following the treatment given by BCEK. The terminology "excursion set approach" was introduced by BCEK, to indicate that the MF determination is based on the statistics of those regions in which the linear density contrast δ_l is larger than a threshold δ_c (such regions are called excursion sets in the theory of stochastic processes; see, e.g., Adler 1981). The PS procedure is clearly included in this approach. This section presents those works which are based on the excursion set approach.

3.2.1. Langevin equation

As previously described, the statistical properties of the Gaussian field $\delta(\mathbf{x})$ are completely specified by the two-point function in Fourier space, which is related to the power-spectrum $P(k)$ by $\langle\tilde{\delta}(\mathbf{k}_1)\,\tilde{\delta}(\mathbf{k}_2)\rangle = (2\pi)^3\delta_{_D}(\mathbf{k}_1+\mathbf{k}_2)P(k_1)$, where $\delta_{_D}$ represents the Dirac delta function, and the brackets $\langle\cdot\rangle$ denote ensemble averaging. Our Fourier transform convention is $\tilde{\delta}(\mathbf{k}) = \int d\mathbf{x}\,\delta(\mathbf{x})\,\mathrm{e}^{i\mathbf{k}\cdot\mathbf{x}}$.

We want now to study the statistical properties of the density fluctuation field at some resolution scale R_f. This is introduced by convolving $\delta(\mathbf{x})$ by some filter function $W(|\mathbf{x}'-\mathbf{x}|, R_f)$,

$$\delta(\mathbf{x},R_f) = \int d\mathbf{x}'\,W(|\mathbf{x}'-\mathbf{x}|,R_f)\,\delta(\mathbf{x}') = \frac{1}{(2\pi)^3}\int d\mathbf{k}\,\widetilde{W}(kR_f)\,\tilde{\delta}(\mathbf{k})\,\mathrm{e}^{-i\mathbf{k}\cdot\mathbf{x}}\,, \tag{98}$$

where $\widetilde{W}$ is the Fourier transform of the filter. At each point $\mathbf{x}$ the smoothed field represents the weighted average of $\delta(\mathbf{x})$ over a spherical region of characteristic dimension R_f centred in $\mathbf{x}$. The detailed properties of $\delta(\mathbf{x},R_f)$ clearly depend upon the specific choice of window function. The most commonly used smoothing kernels are the top-hat filter $W_{TH}(|\mathbf{x}|,R_f) = 3\,\Theta(R_f-|\mathbf{x}|)/4\pi R_f^3$, where $\Theta(x)$ is the Heaviside step function, and the Gaussian one $W_G(x,R_f) = (2\pi R_f^2)^{-3/2}\exp(-x^2/2R_f^2)$. Recently, for convenience of analysis, top-hat filtering has been also applied in momentum space $\widetilde{W}_{SKS}(k,R_f) = \Theta(k_f-k)$, where $k_f = 1/R_f$ and $k_f = |\mathbf{k}_f|$. This kernel is generally called sharp k-space filter. While it is easy to associate a mass to real space top-hat filtering $M_{TH}(R_f) = 4\pi\rho_b R_f^3/3$, there is always a bit of arbitrariness in assigning a mass to the other window functions. The most common procedure is to multiply the average density by the volume enclosed by the filter, obtaining $M_G(R_f) = (2\pi)^{3/2}\rho_b R_f^3$ and $M_{SKS}(R_f) = 6\pi^2\rho_b k_f^{-3}$ (Lacey & Cole 1993 (LC93)). An alternative procedure, originally introduced by Bardeen et al. (1986) (BBKS), corresponds to the choice $M_{SKS}(R_f) = 4\pi\rho_b R_{TH}^3/3$, where R_{TH} is chosen by requiring $\sigma^2_{SKS}(R_f) = \sigma^2_{TH}(R_{TH})$, and similarly for the Gaussian filter. In this way one obtains good agreement with numerical simulations of clustering growth (Lacey & Cole 1994).

In order to mimic the accretion of matter one consideres a full hierarchy of decreasing resolution scales R_f (Peacock & Heavens 1990, Cole 1991, BCEK and LC93). The effect of varying R_f can be obtained by differentiating eq. (98)

$$\frac{\partial\delta(\mathbf{x},R_f)}{\partial R_f} = \frac{1}{(2\pi)^3}\int d\mathbf{k}\,\tilde{\delta}(\mathbf{k})\,\frac{\partial\widetilde{W}(kR_f)}{\partial R_f}\,\mathrm{e}^{-i\mathbf{k}\cdot\mathbf{x}} \equiv \eta(\mathbf{x},R_f)\,. \tag{99}$$

This has the form of a Langevin equation, which shows how an infinitesimal change of the resolution scale R_f affects the value of the density fluctuation field $\delta(\mathbf{x},R_f)$ in the given position $\mathbf{x}$ through the action of the stochastic force $\eta(\mathbf{x},R_f)$. In the limit $R_f\to\infty$ one has $\delta(\mathbf{x};R_f)\to 0$, which can be adopted as initial condition for our first-order stochastic differential equation. Thus, by solving it, we can associate to each point $\mathbf{x}$ a trajectory $\delta(\mathbf{x},R_f)$ obtained by varying the resolution scale R_f. Trajectories associated to different neighbouring points will be statistically influenced by the correlation properties of the force $\eta(\mathbf{x},R_f)$, i.e. of the underlying Gaussian field $\delta(\mathbf{x})$. On the other hand the coherence of each trajectory along the R_f direction depends exclusively on the analytic form of the filter function and vanishes for the sharp k-space window (BCEK). With such a filter, by decreasing the smoothing length one adds up a new set of Fourier modes of the unsmoothed distribution to $\delta(\mathbf{x},R_f)$. For a Gaussian field this is completely independent of the previous increments, and each trajectory $\delta(\mathbf{x},R_f)$ becomes a Brownian random walk.

In the case of sharp k-space filtering the notation greatly simplifies if we use as time variable the variance of the filtered density field, $\Lambda \equiv \sigma^2(k_f) = \langle \delta(k_f)^2 \rangle = (2\pi^2)^{-1} \int_0^{k_f} dk\, k^2\, P(k)$. In such a case the stochastic process reduces to a Wiener one, namely

$$\frac{\partial \delta(\mathbf{x}, \Lambda)}{\partial \Lambda} = \zeta(\mathbf{x}, \Lambda) \ , \tag{100}$$

with $\langle \zeta(\mathbf{x}, \Lambda) \rangle = 0$ and

$$\langle \zeta(\mathbf{x}, \Lambda_1)\, \zeta(\mathbf{x}, \Lambda_2) \rangle = \delta_{_D}(\Lambda_1 - \Lambda_2) \tag{101}$$

[see eq. (17) for the spatial correlation]. In the following we will adopt Λ as time variable, unless explicitly stated. The solution of the Langevin equation (100) in an arbitrary point of space (the position $\mathbf{x}$ is here understood), with the initial condition $\delta(\Lambda = 0) = 0$, is simply $\delta(\Lambda) = \int_0^\Lambda d\Lambda' \zeta(\Lambda')$. By ensemble averaging this expression one obtains $\langle \delta(\Lambda) \rangle = 0$ and $\langle \delta(\Lambda_1) \delta(\Lambda_2) \rangle = \min(\Lambda_1, \Lambda_2)$, which uniquely determine the Gaussian distribution of $\delta(\Lambda)$.

As already told PS model is intrinsically flawed by the cloud-in-cloud problem, namely the fact that a fluctuation on a given scale can contain substructures of smaller scales and the same fluid elements can be assigned, according to the PS collapse criterion, to haloes of different mass. Moreover, in a hierarchical scenario, one expects to find all the mass collapsed in objects of some scale, while the PS model can account only for half of it: this problem is intimately related to the fact that in a Gaussian field only half volume is overdense. Press and Schechter faced the problem by simply multiplying their result by a fudge factor of 2. In this section we review how the Langevin equations introduced above can be used to extend the PS theory in such a way to solve both problems.

The solution of the cloud-in-cloud problem has been given by Peacock & Heavens (1990), Cole (1991) and BCEK. Their approach consists in considering at any given point the trajectory $\delta(R_f)$ as a function of the filtering radius, and then determining the *largest* R_f at which $\delta(R_f)$ upcrosses the threshold $t_f(z_f)$ corresponding to the formation redshift z_f. This determines the largest mass collapsed at that point, all sub-structures having been erased. So, the computation of the mass function is equivalent to calculating the fraction of trajectories that first upcross the threshold t_f as the scale M decreases. The solution of the problem is enormously simplified for Brownian trajectories, that is for sharp k-space filtered density fields. In such a case one only has to solve the Fokker-Planck equation for the probability density $\mathcal{W}(\delta, \Lambda)\, d\delta$ that the stochastic process at Λ assumes a value in the interval $\delta, \delta + d\delta$,

$$\frac{\partial \mathcal{W}(\delta, \Lambda)}{\partial \Lambda} = \frac{1}{2} \frac{\partial^2 \mathcal{W}(\delta, \Lambda)}{\partial \delta^2} \ , \tag{102}$$

with the absorbing boundary condition $\mathcal{W}(t_f, \Lambda) = 0$ and initial condition $\mathcal{W}(\delta, 0) = \delta_D(\delta)$. The solution is well known (Chandrasekhar 1943)

$$\mathcal{W}(\delta, \Lambda; t_f)\, d\delta = \frac{1}{\sqrt{2\pi\Lambda}} \left[\exp\left(-\frac{\delta^2}{2\Lambda} \right) - \exp\left(-\frac{(\delta - 2t_f)^2}{2\Lambda} \right) \right] d\delta \ . \tag{103}$$

Defining $S(\Lambda, t_f) = \int_{-\infty}^{t_f} d\delta\, \mathcal{W}(\delta, \Lambda, t_f)$ as survival probability of the trajectories, one obtains the density probability distribution of first-crossing variances by differentiation

$$\mathcal{P}_1(\Lambda) = -\frac{\partial S(\Lambda, t_f)}{\partial \Lambda} = -\frac{\partial}{\partial \Lambda} \int_{-\infty}^{t_f} d\delta\, \mathcal{W}(\delta, \Lambda; t_f) = \left[-\frac{1}{2} \frac{\partial \mathcal{W}(\delta, \Lambda, t_f)}{\partial \delta} \right]_{-\infty}^{t_f} = \frac{t_f}{\sqrt{2\pi\Lambda^3}} \exp\left(-\frac{t_f^2}{2\Lambda} \right) \ . \tag{104}$$

The function $\mathcal{P}_1(\Lambda)\, d\Lambda$ yields the probability that a realization of the random walk is absorbed by the barrier in the interval $(\Lambda, \Lambda + d\Lambda)$ or, by the ergodic theorem, the probability that a fluid element belongs to a structure with mass in the range $[M(\Lambda + d\Lambda), M(\Lambda)]$. Finally, the comoving number density of haloes with mass in the interval $[M, M + dM]$ collapsed at redshift z_f is

$$n(M, z_f)\, dM = \frac{\rho_b}{M}\, \mathcal{P}_1(\Lambda) \left| \frac{d\Lambda}{dM} \right| dM \ . \tag{105}$$

Inserting the expression of $\mathcal{P}_1(\Lambda)$ of eq. (104) in the latter equation one obtains the well-known PS expression for the mass function

$$n(M, z_f)\, dM = \frac{\rho_b\, t_f(z_f)}{\sqrt{2\pi}} \frac{1}{M^2 \sqrt{\Lambda(M)}} \left| \frac{d \ln \Lambda}{d \ln M} \right| \exp\left(-\frac{t_f(z_f)^2}{2\, \Lambda(M)} \right) dM \ . \tag{106}$$

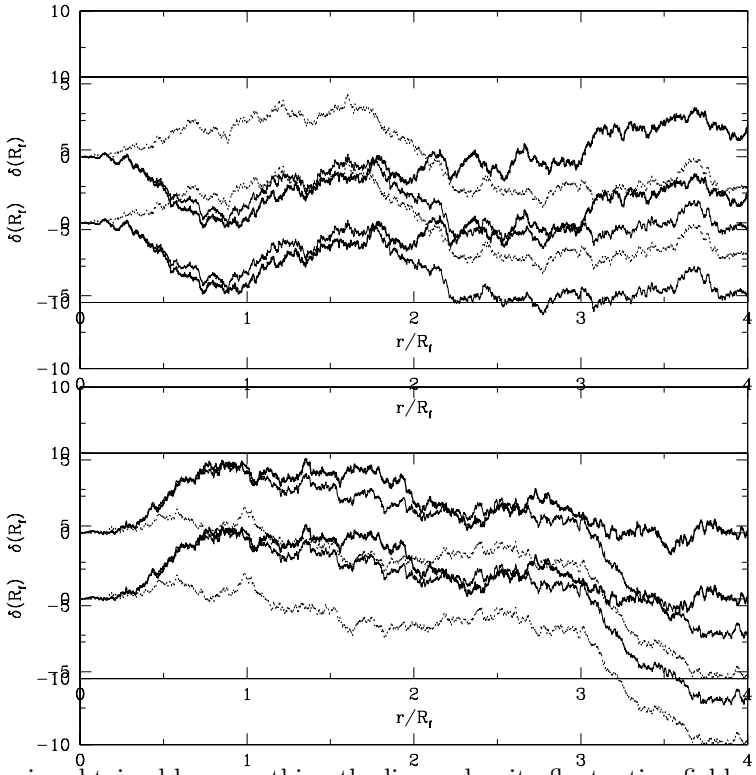

Fig. 14. Examples of trajectories obtained by smoothing the linear density fluctuation field with a series of sharp k-space filters (with decreasing resolution scales $R_f = 1/k_f$) at two points separated by the distance r. Here we consider $r = 4\,\mathrm{Mpc}$ and a CDM power spectrum (with density parameter $\Omega = 1$ and present Hubble constant $H_\circ = 50\,\mathrm{km\,s^{-1}\,Mpc^{-1}}$) linearly extrapolated to $\sigma_8 = 1$. The *heavy continuous* line represents the trajectory associated to a point $\mathbf{x}$ in Lagrangian space. The trajectory associated to the point $\mathbf{y}$ such that $|\mathbf{y} - \mathbf{x}| = r$ is plotted with a *light continuous* line. The *dotted* line is obtained by: *i*) considering the trajectory associated to $\mathbf{y}$, *ii*) artificially removing any correlation with the trajectory at $\mathbf{x}$ and *iii*) suitably rescaling the result. In practice, the dotted line represents a trajectory which is completely independent of the one associated to $\mathbf{x}$, but which has the same statistical one-point properties. This is what is generally used in building up merger trees of dark matter haloes.

The original fudge factor of 2 of the PS approach is now naturally justified.

Previous investigations (e.g. Peacock & Heavens 1990; BCEK) have shown that only for sharp k-space filtering it is possible to write an analytic formula for the mass function obtained from the excursion set approach. Numerical solutions of the cloud-in-cloud problem with physically more acceptable smoothing kernels like Gaussian and top-hat result in mass functions that are a factor of two lower in the high-mass tail and have different small-mass slopes compared with the PS formula. The standard interpretation of this result is that the excursion set method is not reliable for $M \ll M_*$, where M_*, defined by $\Lambda(M_*) = t_f^2$, is the typical mass collapsing at z_f.

3.2.2. **Merging histories**

Merging histories are an important piece of information in the formation history of dark matter objects. They are a natural outcome of MF theories: a mass point, found in an object of mass M at a given time, will be found in another, more massive object at a subsequent time; from the conditional probabilities connected with such events it is possible to construct the statistics of accretion and merging histories of collapsed structures. This was attempted first by Carlberg (1990), whose results are in contradiction with more recent works outlined in the following. Bower (1991) constructed merging histories by using the PS formalism, obtaining the same results as that obtained by means of the diffusion formalism, which are now reported.

Suppose that we have smoothed the initial density distribution on a scale R using some spherically symmetric window function $W_M(r)$, where $M(R)$ is the average mass contained within the window function. There are various possible choices for the form of the window function (c.f. LC93). We use a real-space top-hat window function, $W_M(r) = \Theta(R -$

$r)(4\pi R^3/3)^{-1}$, where Θ is the Heaviside step function. In this case $M = 4\pi\rho_0 R^3/3$, where ρ_0 is the mean mass density of the universe. The mass variance $S(M) \equiv \sigma^2(M)$ may be calculated from

$$\sigma^2(M) = \frac{1}{2\pi^2}\int P(k)W^2(kR)k^2\mathrm{d}k\,, \tag{107}$$

where $P(k)$ is the power spectrum of the matter density fluctuation, and $W(kR)$ is the Fourier transform of the real space top-hat.

The "excursion set" derivation due to BCEK leads naturally to the extended Press-Schechter formalism. The smoothed field $\delta(M)$ is a Gaussian random variable with zero mean and variance S. The value of δ executes a random walk as the smoothing scale is changed. Adopting an ansatz similar to that of the original Press-Schechter model, we associate the fraction of matter in collapsed objects in the mass interval $M, M+\mathrm{d}M$ at time t with the fraction of trajectories that make their *first upcrossing* through the threshold $\omega \equiv \delta_c(t)$ in the interval $S, S+\mathrm{d}S$. This may be translated to a mass interval through equation (107). The threshold $\delta_c(t)$ corresponds to the critical density at which a pertubation will separate from the background expansion, turn around, and collapse. It is extrapolated using linear theory, $\delta_c(t) = \delta_{c,0}/D_{\rm lin}(z)$, where $D_{\rm lin}(z)$ is the linear growth function. The halo mass function (here in the notation of LC93) is then:

$$f(S,\omega)\mathrm{d}S = \frac{1}{\sqrt{2\pi}}\frac{\omega}{S^{3/2}}\exp\left[-\frac{\omega^2}{2S}\right]\mathrm{d}S\,. \tag{108}$$

The *conditional* mass function, the fraction of the trajectories in halos with mass M_1 at z_1 that are in halos with mass M_0 at z_0 ($M_1 < M_0$, $z_0 < z_1$) is

$$f(S_1,\omega_1 \mid S_0,\omega_0)\mathrm{d}S_1 = \frac{1}{\sqrt{2\pi}}\frac{(\omega_1-\omega_0)}{(S_1-S_0)^{3/2}}\exp\left[-\frac{(\omega_1-\omega_0)^2}{2(S_1-S_0)}\right]\mathrm{d}S_1\,. \tag{109}$$

The probability that a halo of mass M_0 at redshift z_0 had a progenitor in the mass range $(M_1, M_1+\mathrm{d}M_1)$ is given by (LC93):

$$\frac{\mathrm{d}P}{\mathrm{d}M_1}(M_1,z_1 \mid M_0,z_0)\mathrm{d}M_1 = \frac{M_0}{M_1}f(S_1,\omega_1 \mid S_0,\omega_0)\left|\frac{\mathrm{d}S}{\mathrm{d}M}\right|\mathrm{d}M_1\,, \tag{110}$$

where the factor M_0/M_1 converts the counting from mass weighting to number weighting.

We can now derive two more useful quantities. Given the mass of a parent halo M_0 and the redshift step $z_0 \to z_1$, the *average* number of progenitors with mass larger than M_l is:

$$\bar{N} \equiv \langle N_p(M\,|M_0)\rangle = \int_{M_l}^{M_0}\mathrm{d}M\,\frac{M_0}{M}\,\frac{\mathrm{d}P}{\mathrm{d}M}(M,z_1|M_0,z_0)\,. \tag{111}$$

We can also readily calculate the average fraction of M_0 that dwelt in the form of progenitor halos of mass $M > M_l$:

$$\bar{f_p} = \int_{M_l}^{\infty}\mathrm{d}M\,\frac{\mathrm{d}P}{\mathrm{d}M}(M,z_1|M_0,z_0)\,, \tag{112}$$

and define the complimentary quantity for the average fraction of M_0 that came from "accreted" mass, $\bar{f}_{\rm acc} = 1 - \bar{f_p}$.

In order to describe the accretion history of an object, it suffices to lower the barrier in a continuous way, and follow the position in Λ of the first upcrossing point: if this performs a discontinuous jump (which happens when the trajectory goes down and then up again), the object containing the mass point considered suffers a discontinuous merging with a structure of comparable size, while if the point moves continuously the object is just accreting material. It is clear that, if the trajectory is a random walk, the first upcrossing point will always perform discrete jumps; continuous accretion will be recognized only if an (arbitrary) minimum resolution step is fixed.

LC93 also proposed a Monte Carlo approach to simulate ensembles of formation histories, based on realizing a large number of random walks. Their Monte Carlo method for simulating merging histories is commonly used to model the formation of virialized galactic halos, in which gas dynamical is inserted "by hand". Such Monte Carlo models of galaxy formation will be discussed in §5.1.2. As a matter of fact, they found a weak inconsistency in their formalism (a probability density going slightly negative), probably caused by the simplicistic mass assignment. The same authors (Lacey & Cole 1994) compared their results to N-body simulations, finding an overall satisfactory agreement.

Finally, Sheth (1995,1996) obtained a complete analytical description for the merging histories of objects formed from a Poisson distribution of seed masses, the problem analyzed by the original PS paper. The resulting MF has turned up to be the same as the distribution function proposed by Saslaw & Hamilton (1984).

3.3. The statistics of the collapsed regions

An idea which traces back to Doroshkevich (1970) is to suppose that structures form in the peaks of the initial density field. This idea became a standard paradigm in the framework of biased galaxy scenarios. Kaiser (1984) noted that high-level peaks show an enhanced correlation with respect to the underlying matter field, a fact which provided an explanation for the large correlation length of clusters with respect to galaxies, and gave freedom to tune the normalization of the CDM model to reproduce the large-scale distribution of galaxies. Peacock & Heavens (1985) and BBKS calculated a number of statistical expectation values for the peaks of a Gaussian random field, as the number density of peaks of given height. This quantity seemed suitable to determine a peak MF, but two important problems, recognized by BBKS hampered such a determination (see next subsection for details).

In order to get the peak MF, it is necessary to study the stochastic properties of the collapsed regions, defined as regions where the linearly evolved density contrast $\delta(M,\mathbf{x})$ exceeds a threshold δ_c. The correct choice of the threshold δ_c, insofar as it is well defined, is a matter of debate. Many authors take the value 1.69 inspired by the spherical collapse model. On the other hand, comparison of the quasi-linear estimate of $n(>M)$ (described below) with estimates from numerical simulations suggests a smaller value, Carlberg and Couchman (1989) advocating $\delta_c = 1.44$ and Efstathiou and Rees (1988) advocating $\delta_c = 1.33$ (but see also Brainerd and Villumsen (1992) and Katz, Quinn and Gelb (1992)). The collapsed regions occupy a volume fraction V given by the Gaussian distribution,

$$\frac{\mathrm{d}V}{\mathrm{d}\nu} = \frac{1}{\sqrt{2\pi}} e^{-\nu^2/2} \tag{113}$$

leading to

$$V(\nu) = \mathrm{erfc}(\nu/\sqrt{2})/2 \tag{114}$$

$$= (2\pi)^{-1/2}\nu^{-1}e^{-\nu^2/2}(1-\nu^{-2}+O(\nu^{-4})) \tag{115}$$

To say more one needs to know the shape of the spectrum of perturbations. We shall list the relevant results given by BBKS. They involve only two moments of the spectrum, defined by

$$\langle k^2(M)\rangle = \sigma^{-2}(M)\int_0^\infty k^2 \exp(-k^2R_f^2)P(k)\frac{\mathrm{d}k}{k} \tag{116}$$

$$\langle k^4(M)\rangle = \sigma^{-2}(M)\int_0^\infty k^4 \exp(-k^2R_f^2)P(k)\frac{\mathrm{d}k}{k} \tag{117}$$

The quantity $\langle k^2\rangle$ is the mean of the ∇^2 operator, ie., of the quantity $\delta^{-1}\nabla^2\delta$. Similarly, $\langle k^4\rangle$ is the mean of ∇^4.

A relevant length scale is defined by $R_*^2 = 3\langle k^2\rangle/\langle k^4\rangle$. For any spectral index $n > -1$, it is easy to show that in the limit of small filtering scale R_f,

$$\frac{R_*}{R_f} = \left(\frac{6}{1+n}\right)^{1/2} \tag{118}$$

For the case of CDM with $.7 < n < 1$, the ratio is in the range 1 to 3 for the entire range of cosmologically interesting masses.

Another relevant length scale is $\langle k^2\rangle^{-1/2}$. On large filtering scales, such that $P(k)$is increasing fairly strongly at $k^{-1} \simeq R_f$, the ratio $\langle k^2\rangle^{-1/2}/R_f$ is close to 1. As the scale is reduced it increases, but is $\lesssim 10$ for $M > 10^6 M_\odot$.

Finally, it is convenient to define the dimensionless parameter

$$\gamma(M) = \langle k^2\rangle/\langle k^4\rangle^{1/2} \tag{119}$$

It falls from about .7 to about .3 as M decreases from $10^{15}M_\odot$ to $10^6 M_\odot$, for $.7 < n < 1$.

For sufficiently large ν, each collapsed region is a sphere surrounding a single peak of δ. However, the departure from sphericity is considerable in the cosmologically interesting regime. BBKS show that a quantity x^{-1}, which is roughly the fractional departure from sphericity, is well approximated by

$$x = \gamma\nu + \theta(\gamma,\gamma\nu) \tag{120}$$

where

$$\theta(\gamma,\gamma\nu)=\frac{3(1-\gamma^2)+(1.216-.9\gamma^4)\exp[-\gamma/2(\gamma\nu/2)^2]}{[3(1-\gamma^2)+.45+(\gamma\nu/2)^2]^{1/2}+\gamma\nu/2} \tag{121}$$

We emphasize that this is the asphericity seen in the linearly evolved, filtered density contrast. The asphericity in the true, unfiltered density contrast will be bigger, and will increase during collapse.

Three useful number densities are given by BBKS. First, the density n_χ of the Euler number of the surfaces bounding the collapsed regions is

$$\frac{1}{2}n_\chi(\nu,\langle k^2\rangle)=\frac{(\langle k^2\rangle/3)^{3/2}}{(2\pi)^2}(\nu^2-1)e^{-\nu^2/2} \tag{122}$$

Second, the number density of upcrossing points on these surfaces is

$$n_{\rm up}(\nu,\langle k^2\rangle,\gamma)=\frac{(\langle k^2\rangle/3)^{3/2}}{(2\pi)^2}\times$$
$$\left[\nu^2-1+\frac{4\sqrt{3}}{5\gamma^2(1-5\gamma^2/9)^{1/2}}e^{-5\gamma^2\nu^2/18}\right]e^{-\nu^2/2} \tag{123}$$

An upcrossing point on a surface of constant δ is defined as one where $\boldsymbol{\nabla}\delta$ points along some arbitrarily chosen reference direction.

The third number density is $n_{\rm peak}$, the number density of peaks which are more than ν standard deviations high. BBKS give expressions for $n_{\rm peak}$, but they point out also that in the cosmologically interesting regime it is quite well approximated by $n_{\rm up}$. We shall use this approximation in what follows. It suggests that if a collapsed region contains several peaks, they are not buried deep inside it; rather, the boundary of the region is presumably corrugated, wrapping itself partially around each peak.

3.3.1. **The number density** $n(>M)$

The main application of these results is to estimate the number density $n(>M)$ of gravitationally bound systems with mass bigger than M, at a given epoch before $z_{\rm nl}(M)$ (where nl stands for "non linear"). The systems are supposed to be identifiable by looking at the linearly evolved density contrast $\delta(M,\mathbf{x})$. Each collapsed region, defined as one in which $\delta(M,\mathbf{x})>\delta_c$, is supposed to contain one or more systems with mass bigger than M.

If each collapsed region is identified with a single system, then $n(>M)=n_{\rm coll}$. In general this recipe is useless for lack of an expression for $n_{\rm coll}$. A different prescription, which does lead to a calculable expression, is to identify each peak within a collapsed region with a different collapsed object,

$$n(>M)=n_{\rm peak}\simeq n_{\rm up} \tag{124}$$

This estimate (usually without the simplifying second equality) is widely used in the literature. It is certainly the same as the estimate $n(>M)=n_{\rm coll}$ for large ν, where we know that there is just one peak per collapsed region. To what extent the prescriptions are the same for lower ν is not known, because the number of peaks per collapsed region is not known.

By means of the previous quoted theory it seemed suitable to determine a peak MF, but two important problems, recognized by BBKS, (who did not attempt to determine an MF from the peak number density) hampered such a determination: (i) the peak number density was based on the initial field smoothed at a single scale, so the peak MF suffered from the same cloud-in-cloud problem (the *peak-in-peak* problem) as the PS one; (ii) it was not clear which mass had to be assigned to a peak.

The first (i) problem can be easily described as follows. If at some epoch the linearly evolved density contrast does have many peaks within a collapsed region, an interesting situation arises. At a somewhat earlier epoch, $\delta(M,\mathbf{x})$ was smaller, and a separate contour $\delta(M,\mathbf{x})=\delta_c$ was wrapped around each peak. In other words, each peak of the linearly evolved density contrast, filtered on scale M, was inside a single collapsed region, and presumably represented a separate gravitationally bound system. At the later epoch when the collapsed region encompasses many peaks of the linearly evolved density contrast, we have a bigger gravitationally bound system. If the original systems survive, the identification of each peak with a separate system is correct, but it misses the larger system which contains the original systems. Of course, missing this one system does not affect the total count much, so if this case is typical of collapsed regions containing

many peaks the estimate $n(>M) = n_{\rm peak}$ is better than the estimate $n(>M) = n_{\rm coll}$. If, on the other hand, the original systems have merged, that identification is wrong, and the whole of the collapsed region should be identified with just one gravitationally bound system. If this case is typical, the estimate $n(>M) = n_{\rm coll}$ would be better, if only we had a formula for it. Which case is the more likely? A clue is provided by the observation made earlier, that if there are several peaks in a collapsed region they typically seem to lie near the surface of the region, a part of the surface wrapping itself around each peak. This picture would suggest that the estimate $n(>M) = n_{\rm peak}$ is the more reasonable, the peaks of the linearly evolved density contrast in a typical collapsed region representing structures which have not existed long enough to merge.

Even if the determination of a peak MF has some problems, several authors tried to formulate it in different ways, e.g. Colafrancesco et al. (1989). Let's Using the method of the last paper, let's denote by $N_{\rm pk}(\nu, M)d\nu$ the number density of peaks of heightbetween ν and $\nu+d\nu$ and

$$n_{\rm pk} = \int_{\nu_c}^{\infty} N_{\rm pk}(\nu, M)d\nu \tag{125}$$

In order to obtain the mass multiplicity for objects belonging to a catalog of contrast δ_c, one considers peaks on a hierarchy of resolution scales, M. Following the original PS choice, the mass of different objects is identified with the filtering mass M. The mass per unit volume $n(M)MdM$, is obtained by differentiating with respect M the mass of the peaks of the filtered field with overdensity exceeding δ_c, that is:

$$n(M)MdM = (1+f)\left|\frac{d[n_{\rm pk}(\delta_c; M)M_{\rm pk}(\delta_c, M)]}{dM}\right| dM. \tag{126}$$

which s a generalization of PS Ansatz, where $1+f$ takes account of the secondary infall of matter initially in underdense regions, and $M_{\rm pk}$ is the average mass of peaks above δ_c (see Eq. 3-7 of Colafrancesco et al. 1989) calculated modelling the peak as an ellipsoid, and estimated its mass by means of the volume inside the ellipsoid surface with density larger that a given threshold.

As a matter of fact, there is not a general agreement on the actual validity of the peak paradigm. From the theoretical point of view, structures are *not* predicted to form in the peaks of the initial field; for instance, according to Zel'dovich approximation, structures form in the peaks of the largest eigenvalue of the deformation tensor. Then the peak paradigm can not be valid in general, except for the highest peaks. Some numerical simulations (Katz, Quinn & Gelb 1993; van de Weygaert & Babul 1994) have shown that galactic-size peaks often disrupt or merge with larger structures, as a result of tidal interactions with external structures. Manrique & Salvador-Solé have argued that such results are due to the lack of correction for the peak-in-peak problem. On the other hand, Bond & Myers (1996b) have found their peak-patch structures, which account for the peak-in-peak problem, to represent well N-body structures.

The excursion set and peak approaches are somewhat complementary. In fact, excursion sets are effective in determining the total fraction of collapsed mass, and then the global normalization, but are not accurate in deciding how the collapsed mass fragments into clumps, i.e. to count the number of objects formed. On the contrary, the peak approach clearly determines the number of formed objects, but does not determine the mass to be associated with the structures, and hence the global normalization.

3.3.2. **Relations between the peak model and PS formalism**

The peak model can be connected to PS formalism. As known Press and Schechter (1974) worked with the differential number density,

$$\frac{{\rm d}n}{{\rm d}M} \equiv \frac{\rm d}{{\rm d}M} n(>M) \tag{127}$$

At a given epoch, if the filtering mass M is increased by an amount ${\rm d}M$ then ν is increased by an amount ${\rm d}\nu$, and the volume fraction occupied by the collapsed regions is reduced by an amount ${\rm d}V$ given by Eq. (113). Press and Schechter suppose that the eliminated volume consists of objects with mass between M and $M + {\rm d}M$, corresponding to the idealisation that filtering the density contrast on any mass scale M cuts out precisely those objects with mass less than M while leaving

unaffected objects with mass bigger than M. Ignoring the overdensity $\simeq (1+\delta_c)$ of the collapsed regions this implies that the number density $\mathrm{d}n$ of such objects is given by

$$M\frac{\mathrm{d}n}{\mathrm{d}M}=\left[M\frac{\mathrm{d}(R_f^2)}{\mathrm{d}M}\right]\frac{\mathrm{d}(\sigma^2(M))}{\mathrm{d}(R_f^2)}\frac{\mathrm{d}\nu}{\mathrm{d}(\sigma^2(M))}\frac{\mathrm{d}V}{\mathrm{d}\nu}\frac{\mathrm{d}n}{\mathrm{d}V} \tag{128}$$

$$=\left[\frac{2R_f^2}{3}\right]\left[-\sigma^2(M)\langle k^2\rangle\right]\left[-\frac{\nu}{2\sigma^2(M)}\right]\left[\frac{1}{\sqrt{2\pi}}e^{-\nu^2/2}\right]\left[\frac{1}{V_f}\right] \tag{129}$$

$$=\frac{R_f^2\langle k^2\rangle}{3}\frac{1}{4\pi^2R_f^3}\nu e^{-\nu^2/2} \tag{130}$$

Press and Schechter multiplied this formula by a factor 2, so that when integrated over all masses it would give the total mass density of the universe, rather than just the half corresponding to the regions of space where the linearly evolved density contrast is positive. They thus arrived at the estimate

$$n(>M)\simeq n_{\rm ps}\equiv\int_M^\infty\frac{\langle k^2\rangle'}{6\pi^2R_f'}\nu' e^{-\nu'^2/2}\frac{dM'}{M'} \tag{131}$$

In this equation, $R_f'=R_f(M')$, and similarly for $\langle k^2\rangle'$ and ν'. The factor 2 inserted by Press and Schechter is not justified (as previously described) by their argument, because the linearly evolved density contrast has nothing to do with reality in the non-linear regime $\sigma(M)>1$. On the other hand, the neglected overdensity gives a factor $\simeq(1+\delta_c)=2$ to 3. Thus the factor 2 goes in the right direction, and the Press-Schechter formula is reasonably well founded theoretically. A somewhat different justification for the formula has been given by Bond *et al* (1991b).

As told before, there are two alternative estimates $n(>M)=n_{\rm ps}$ and $n(>M)=n_{\rm peak}$. A comparison of these two shows that the estimates agree to better than a factor 2 for $\nu\lesssim 2$. Presumably, this indicates that in this regime the assumptions underlying the two estimates are compatible, in that increasing M by a small amount cuts out portions of the collapsed regions which have mass of order M and are centred on peaks with height of order $\nu(M)$.

For large ν, the Press-Schechter estimate falls below $n_{\rm peak}$. This can be understood analytically, from the expression

$$\frac{\mathrm{d}n_{\rm peak}}{\mathrm{d}M}\simeq\frac{\mathrm{d}n_{\rm up}}{\mathrm{d}M}=\frac{\partial n_{\rm up}}{\partial\nu}\frac{\mathrm{d}\nu}{\mathrm{d}M}+\frac{\partial n_{\rm up}}{\partial\langle k^2\rangle}\frac{\mathrm{d}\langle k^2\rangle}{\mathrm{d}M}+\frac{\partial n_{\rm up}}{\partial\gamma}\frac{\mathrm{d}\gamma}{\mathrm{d}M} \tag{132}$$

The first term dominates for large ν, leading to the ratio

$$\frac{\mathrm{d}n_{\rm ps}/\mathrm{d}M}{\mathrm{d}n_{\rm peak}/\mathrm{d}M}=2\left(\frac{3}{R_f^2\langle k^2\rangle}\right)^{3/2}\nu^{-3} \tag{133}$$

Apart from the factor 2, this is just the filter volume divided by the average volume of a collapsed region.

As we saw earlier, the smallness of the size of the 'collapsed regions' is an artefact of the filtering. The conclusion is that for very rare fluctuations, $n_{\rm peak}$ is a better estimate that $n_{\rm PS}$, the latter being considerably too small (Thomas & Couchman 1992). However, other sources of error are likely to be more important than the difference between $n_{\rm peak}$ and n_{PS}.

3.4. Dynamics and MF

The models treated till now identifies collapsed structures as those regions whose linear density contrast exceeds some threshold. Many simplifications are used to obtain the mass function which at the end leads to neglects important elements such as the role of tides. Such simplifications could lead to oversimplified and misleading arguments. A number of authors have tried to insert elements of realistic dynamics in the theoretical MF. Such attempts are reviewed in the following.

Some authors have inserted elements of realistic dynamics in the MF problem by extending the original PS approach or the diffusion or the peak one (Lucchin & Matarrese 1988). This approach named *PS-like method* shall be analized in the next subsection. The peak-patch formalism by Bond & Myers (1996a), described above, is also characterized by a more realistic description of the dynamical evolution of peaks, even though structures are always identified through the peaks of the linear field. Other determinations of the MF were proposed by Henriksen & Lachièze-Rey (1990), where collapsed regions were identified by means of correlated velocity structures, and by Newman & Wasserman (1990) and Bernardeau & Schaeffer (1991), who related (in quite different ways) the MF to the correlation properties of the matter field. Monaco

(1995) constructed a MF in a PS-like approach, based on realistic collapse time estimates, found by means of extensions of the Zel'dovich approximation, and by the use of the homogeneous ellipsoid collapse model.

One of the problems with the PS approach, reported by Cavaliere et al. (1991), is that it supposes matter clumps to instantaneously pass from non-collapsed to collapsed, and to be immediately incorporated in a larger clump. In other words, PS seems to imply vanishing time scales for the formation and destruction of clumps. As a matter of fact, PS simply does not contain any information on such timescales: the change of the MF with time is a combination of *creation* of new clumps, *destruction* of old clumps and *accretion* of mass onto existing clumps. Such terms cannot be disentangled by means of the PS approach alone, without further assumptions: for instance, the "static" procedure proposed by LC93, which is based only on statistics, cannot provide a precise definition of formation time (it is arbitrarily, though reasonably, defined as the time taken by a clump to double its mass).

Cavaliere et al. (1991) proposed a *dynamical* procedure, based on creation and destruction time scales, to model the MF and an evolution equation for $n(M,t)$.

Blain & Longair (1993a,b) and Sasaki (1994) used a similar approach, obtaining identical results.

A completely different approach to the MF was proposed by Silk (1978) and Silk & White (1978). Aggregation (and fragmentation) of collapsed clumps of similar size can be described by means of an aggregation kinetic equation (Smoluchowski 1916; Ernst 1986). The behavior of the MF given by Smoluchowsky equation has been reviewed elsewhere (see, e.g., Lucchin 1989; Cavaliere, Colafrancesco & Menci 1991b; Cavaliere, Menci & Tozzi 1994).

More recently, Shaviv & Shaviv (1993, 1995) have analyzed the Smoluchowsky equation (always in the gravitational context) in a different way; at variance with Cavaliere and coworkers, they found their MF to depend on initial conditions. Another application of Smoluchowsky equation in a cosmological context is due to Edge et al. (1990), to explain the evolution of the X-ray luminosity function of galaxy clusters.

As a general remark, such kinetic approaches can describe those aggregation events which take place between already collapsed clumps. The direct hierarchical (first) collapse of structures remains well described by a diffusion formalism, like the one proposed by BCEK.

The first determination of a mass function, based on a self-consistent realistic dynamical approximation, is probably due to the works on the adhesion model.

Some authors compared the predictions of clump formation, as given by the adhesion model, to N-body simulations, in 1D (Doroshkevich & Kotok 1990; Williams et al. 1991) and 2D (Nusser & Dekel 1990; Kofman et al. 1992), finding satisfactory agreement.

Vergassola et al. (1994), attempted an analytical estimate of the MF with adhesion, by using and extending a number of theorems demonstrated by Sinai (see references in the cited paper). They were able to find the asymptotic dependences of the MF: it behaves exactly like PS at large masses (the exact position of the typical mass is not determined), but has a different slope at small masses. However, they could not find the exact normalization of the MF.

Lagrangian perturbations can be used to construct an MF fully based on realistic dynamics. At variance with adhesion theory, this dynamical approximation is of truncated type, i.e. small-scale power has to be filtered out to avoid small-scale multi-stream regions. Moreover, Lagrangian perturbations show interesting connections with the homogeneous ellipsoid collapse model, which can also be used to give reliable collapse time estimates, as in Monaco (1995). Such topics have been addressed in Monaco (1997a,b).

3.4.1. **PS-like approach**

In previous sections, we saw how finding realistic estimates of collapse times of generic mass elements. The problem of translating such information into an expression for the MF is of purely statistical nature. Such a statistical problem, in the simple case in which the inverse collapse time F is proportional to the initial density contrast, has received much attention in the scientific literature. Two main approaches were identified, namely the excursion set and the peak ones; the first approach was shown to be easier to manage than the second one, at the expense of a simplified treatment of the geometry of collapsed regions in Lagrangian space, while the peak approach, whose validity relies on the validity of the peak hypothesis, better takes into account geometry, at the expense of an increased complexity of the formalism, especially when trying to include a proper treatment of the peak-in-peak problem.

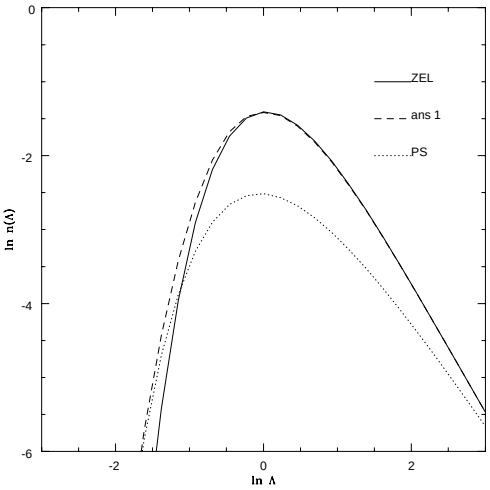

Fig. 15. PS-like $n(\Lambda)$ curves for Ze'ldovich approximation and ansätz 1, compared to the PS one. Figure taken from M98.

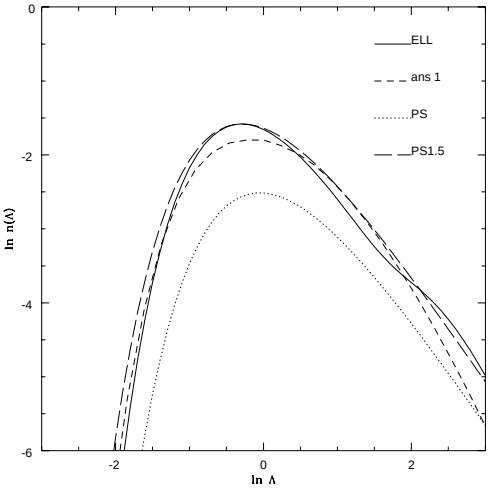

Fig. 16. PS-like $n(\Lambda)$ curves for ELL and ansätz 2, compared to the PS one and with a PS with δ_c=1.5 and the fudge factor 2; see text. Figure taken from M98.

In this section, the MF will be determined by means of a simplified PS-like, single-scale approach, which consists of estimating the probability of having initial conditions that make the mass element collapse.

A first determination of the MF can be obtained by applying the same statistical approach as in the original PS paper: the fraction of collapsed mass is obtained by integrating, at a given fixed scale, over all initial conditions which make a mass element collapse before a given time. This determination obviously suffers from the same cloud-in-cloud problem as the PS one; however, most mass is predicted to finally collapse by realistic collapse time estimates, so a PS-like MF is nearly normalized, by more than 90%. It is then natural to suspect that an MF obtained by means of the absorbing barrier formalism can be not very different from the PS-like one, as only a minor part of the mass, lying in the strongest underdensities, has to be redistributed; this mass is not expected to influence the MF in any interesting mass range. As shown by M98, that under some conditions the PS-like and the absorbing barrier MFs are very similar; the simplified PS-like approach suffices in finding the main features of the dynamical MF (M98).

Integration over initial conditions requires that initial conditions are specified, and that their joint PDF is known. In the PS case, where linear theory and spherical collapse were used, initial conditions were simply provided by the initial density contrast. In the most general case, initial conditions are given by the value of the density (or, equivalently, of the potential) at every point, so that a direct integration is hard to perform. An intermediate case is provided by the Zel'dovich

approximation, and by the other approximations which require the same initial conditions and ellipsoidal collapse. In this case, the joint PDF of initial conditions, the λ eigenvalues, is known (Doroshkevich 1970):

$$P_\lambda(\lambda_1,\lambda_2,\lambda_3)d\lambda_1 d\lambda_2 d\lambda_3 = \frac{675\sqrt{5}}{8\pi\Lambda^3}\exp\left(-\frac{3}{\Lambda}\mu_1^2+\frac{15}{2\Lambda}\mu_2\right)$$
$$\times(\lambda_1-\lambda_2)(\lambda_1-\lambda_3)(\lambda_2-\lambda_3)d\lambda_1 d\lambda_2 d\lambda_3. \quad (134)$$

Λ is again the mass variance; $\mu_1=\lambda_1+\lambda_2+\lambda_3$ and $\mu_2=\lambda_1\lambda_2+\lambda_1\lambda_3+\lambda_2\lambda_3$ are principal invariants of the Zel'dovich deformation tensor. It is convenient to express this PDF in terms of the linear density δ_l and the x and y variables defined in Eq. (58); in this case the joint PDF is factorized into a Gaussian for δ_l and a joint PDF for x and y:

$$P(\delta_l,x,y)d\delta_l dx dy = \frac{1}{\sqrt{2\pi\Lambda}}\exp\left(-\frac{\delta_l^2}{2\Lambda}\right)d\delta_l\frac{225}{4}\sqrt{\frac{5}{2\pi}}\frac{1}{\Lambda^{5/2}}\exp\left(-\frac{5}{2\Lambda}(x^2+xy+y^2)\right)$$
$$\times xy(x+y)dxdy = P_{\delta_l}(\delta_l;\Lambda)d\delta_l\times P_{x,y}(x,y;\Lambda)dxdy. \quad (135)$$

The fraction of collapsed mass can then be obtained as follows:

$$\Omega(<\Lambda)=\int_0^\infty dx\int_0^\infty dy P_{x,y}(x,y;\Lambda)\int_{\delta_c(x,y)}^\infty d\delta_l\, P_{\delta_l}(\delta_l;\Lambda), \quad (136)$$

where the function $\delta_c(x,y)$, which substitutes the δ_c parameter of PS, is defined as the solution of the equation:

$$b_c(\delta_c,x,y)=b(t_0), \quad (137)$$

where $b(t_0)$ is the instant at which the MF is wanted (it will usually be set equal to one). By writing the function δ_c as $\delta_0-f(x,y)$, where δ_0 is the spherical value 1.69 and the positive function $f(x,y)$, vanishing at the origin, gives the effect of the shear, it is possible to write the $n(\Lambda)$ function as:

$$n(\Lambda)=n_{PS}(\Lambda)\times\mathcal{I}(\Lambda), \quad (138)$$

where $n_{PS}(\Lambda)$ is the PS curve, and $\mathcal{I}(\Lambda)$ is a correction term:

$$\mathcal{I}(\Lambda)=\frac{1}{\Lambda}\int_0^\infty dx\int_0^\infty dy\, P_{x,y}(x,y)\exp\left(-\frac{1}{2\Lambda}f^2(x,y)+\frac{\delta_0}{\Lambda}f(x,y)\right)$$
$$\times\left(1-\frac{1}{\delta_0}\left(f-x\frac{\partial f}{\partial x}-y\frac{\partial f}{\partial y}\right)\right). \quad (139)$$

$n(\Lambda)$ curves have been calculated for Zel'dovich, ellipsoidal model, and for the two *ansatze* previously presented. Details of the calculations are reported by Monaco (1995). Fig. 15 presents the $n(\Lambda)$ curve for Zel'dovich and for the first *ansätz*, Eq. (60), in which spherical collapse is recovered when Zel'dovich predicts a slower collapse. The canonical PS $n(\Lambda)$curve is shown for comparison; the PS curve has not been multiplied by the fudge factor of two at this stage, in order to compare the results of the PS-like procedures in the different cases, with no guarantee of normalization (in Monaco 1995 all the curves were multiplied by two). It can be seen that the Zel'dovich curve underestimates the number of large-mass[3] objects, and gives more intermediate- and small-mass objects, also thanks to its better normalization. The *ansätz* curve reproduces the PS one at large masses, and reduces to the Zel'dovich one at small masses, as expected.

Fig. 16 shows the ellipsoidal model prediction, in comparison with the second *ansätz*, Eq. (61) (with $\epsilon=0.2$), the canonical PS curve (without the fudge factor 2, as before) and a PS curve with δ_c=1.5, representative of the typical outcome of N-body simulations (and then with the factor 2). Both the *ansätz* curve and ellipsoidal model predict an overabundance of large-mass clumps with respect to the canonical PS curve: it is again demonstrated that a systematic displacement of collapse times from the spherical value influences the large-mass tail of the MF, even though spherical collapse is asymptotically recovered. In particular, the ellipsoidal model curve is quite similar to the PS 1.5 curve (PS curve with $\delta_c=1.5$). It is however to be stressed that this similarity, while encouraging, has to be taken with care, as it is not clear how the collapsed objects predicted by this theory are related to the N-body clumps. As a technical remark, this ellipsoidal model curve has been computed by using the full b_c curves; in Monaco (1995) only the overdense curve was considered, and the Zel'dovich behavior was forced at large x and y values.

[3] I freely use the word mass in this context to indicate the large-mass (small Λ) or small-mass (large Λ) part of the MF

3.4.2. MF and $n(\Lambda)$

The passage from the resolution to the mass variable requires knowledge of how collapsed matter gathers in clumps, an element which is missing in the excursion set approach; The volume of the excursion sets as a function of resolution, and then the mass of structures, is obtained by means of the rule:

$$Mn(M)dM = \bar{\varrho} \left| \frac{d\Omega}{dM} \right| dM = \bar{\varrho} n(\Lambda) \left| \frac{d\Lambda}{dM} \right| dM. \tag{140}$$

A more realistic resolution-mass relation would predict a whole distribution of masses to form at a given resolution:

$$\Lambda \rightarrow p(M;\Lambda). \tag{141}$$

The $p(M;\Lambda)$ function gives the probability that a mass M is formed at a resolution Λ; its mean value will be of order:

$$\int_0^\infty Mp(M;\Lambda)dM \sim \bar{\varrho} R(\Lambda)^3, \tag{142}$$

as the smoothing length $R(\Lambda)$ is the relevant scale in this case; the proportionality constant, of order one, will in general depend on the shape of the filter, on the power spectrum and on the resolution. The MF would then be given by:

$$Mn(M)dM = \bar{\rho} \left(\int_0^\infty n(\Lambda) p(M,\Lambda) d\Lambda \right) dM \ , \tag{143}$$

i.e., by the $n(\Lambda)$ curve convolved with the distribution $p(M,\Lambda)$.

Such a p distribution is expected, at small resolutions, to be peaked at its mean value, while its shape at large resolutions is expected be more complex, probably influenced by the details of the prescription chosen to fragment the collapsed medium (M98). Then, with respect to using the simple golden rule, the introduction of the p distribution is expected not to influence dramatically the large mass tail of the MF, while it is likely to influence the small-mass part, which is confirmed to be a not robust prediction of this kind of MF theories. Finally, differences in the p distributions for different filter shapes could in principle at least attenuate the differences between the MFs found with SKS and Gaussian filtering.

3.4.3. Conclusions

As shown in M98, a PS-like procedure is enough to obtain the main features of the MF. If SKS filtering is used, it has been demonstrated that the diffusion formalism can be extended to the non-Gaussian F process, by considering it as a diffusion process. The problem can then be transformed to the diffusion of a Wiener process with a moving absorbing barrier. For Gaussian smoothing, the simple approximation proposed by Peacock & Heavens (1991) has been shown very successful in finding the MF.

The following conclusions can be drawn:

1. A larger number of large-mass objects is expected to form with respect to the canonical PS prediction with δ_c=1.69.
2. The fact that spherical collapse is asymptotically recovered for the strongest overdensities does not guarantee that the "spherical" canonical PS MF, with δ_c=1.69, is recovered at large masses.
3. The large-mass part of the MF is considered robust with respect to the dynamical prediction. The ELL prediction tends to give more objects than the 3RD one in the large-mass tail; this is due to the fact that 3rd-order Lagrangian theory slightly underestimates spherical collapse; thus the ELL prediction is considered more believable in that range.
4. PS-like gives fewer objects than the SKS one, by roughly a factor of 2, in the large- and intermediate-mass ranges.
5. PS-like is very similar to the PS one with a $\delta_c \simeq 1.5$ parameter (indicated as PS 1.5).

The small-mass part of the MF is not considered a robust prediction of the theory, for at least three reasons:

1. The definition of collapse, which is based on the concept of orbit crossing, is not expected to reproduce common small-mass structures like virialized halos. OC regions rather represent those large-scale collapsed environments in which the virialized halos are embedded.

2. All the dynamical predictions used are considered good as long as the inverse collapse time is not small. Thus, the small-mass part of the MF is based on non-robust dynamical predictions.
3. The p distribution of the forming masses, at a given resolution, is likely to significantly affect the small-mass part of the MF.

The prediction of more large-mass objects, caused by the improved dynamical description of collapse, confirms some previous claims, for example by Lucchin & Matarrese (1988) and Porciani et al. (1996), who introduced non-Gaussianity of dynamical origin in the PS or diffusion approaches. This increase can be seen as the effect of tides on the dynamics of the mass element (Bertschinger & Jain 1994). Besides, even spherical collapse, when the global interpretation of collapse times is assumed (§2.3.4), leads to the prediction of more large-mass objects (Blanchard et al. 1992; Yano et al. 1996; Betancort-Rijo & Lopez-Corredoira 1996).

The similarity of the (Gaussian-smoothed) dynamical MF with a PS one, with δ_c=1.5, makes the dynamical MF be consistent with many numerical simulation (§2.2), even though this agreement is not a real proof of validity as (i) OC regions are not the halos extracted from simulations, and (ii) the resolution-mass relation is still treated in a simplified way. However, the dynamical MF theory does not predict the trend of lower δ_c values at higher redshifts, observed in recent N-body simulations (see references in §2.2). An explanation of this behavior was proposed by Monaco (1995): the presence of small-scale power can effectively slow down gravitational collapse, through dynamical events of the kind of previrialization, proposed by Peebles (1990; see also Lokas et al. 1996; Bouchet 1996), or through dynamical friction with those possible particles which evaporate out of the collapsed structures (Antonuccio & Colafrancesco 1994). Such events could be effective for power spectra with $n > -1$ (Lokas et al. 1996). In CDM-like spectra, the effective spectral index at M_* is smaller than -1 at high redshifts, where δ_c=1.5 (or even less) is found, but becomes larger at lower redshifts, where δ_c starts to increase to 1.7 or even larger values. However, such a behavior could also be due to a dependence of the p distribution on the power spectrum.

3.5. More recent developments using the excursion set model: the moving barrier model and the multiplicity function

As reported in the introduction, the PS model when compared to numerical simulations gives a smaller number of high-mass halos while giving a larger number of low-mass halos. The quoted discrepancy, that lead to research new expressions for the mass function, is not surprising since the PS model, as any other analytical model, should make several assumptions to get simple analytical predictions. The main assumptions that the PS model combines are the simple physics of the spherical collapse model with the assumption that the initial fluctuations were Gaussian and small. On average, initially denser regions collapse before less dense ones, which means that, at any given epoch, there is a critical density, $\delta_c(z)$, which must be exceeded if collapse is to occur. In the spherical collapse model, this critical density does not depend on the mass of the collapsed object, while taking account of the effects of asphericity and tidal interaction with neighbors, it is possible to show that it is mass dependent (Del Popolo & Gambera 1998, SMT). In the second hand, the Gaussian nature of the fluctuation field means that a good approximation to the number density of bound objects that have mass m at time z is given by considering the barrier crossing statistics of many independent and uncorrelated random walks, where the barrier shape $B(m, z)$, is connected to the collapse threshold. Simply changing the barrier shape, SMT showed that it is possible to incorporate the "quoted effects" [4] in the excursion set approach. Moreover, using the shape of the modified barrier in the excursion set approach, it is possible to obtain a good fit to the universal halo mass function [5]. The excursion set approach allows one to calculate good approximations to several important quantities, such as the "unconditional" and "conditional" mass functions. ST1 provided formulas to calculate these last quantities starting from the shape of the barrier.

In the following, I'll use an improved version of the barrier obtained in Del Popolo & Gambera (1998) to get the multiplicity functions, which shall be compared with those obtained by PS, ST, J01, YNY, and with numerical simulations of YNY.

[4] Namely that in the case of objects collapsing at the same time, the less massive regions must initially have been denser than the more massive ones.

[5] Note that at present there is no good numerical test of analytic predictions for the low mass tail of the mass function.

In order to calculate the barrier shape, it is possible to follow Del Popolo & Gambera (1998) model. The equation governing the collapse of a density perturbation taking account angular momentum acquisition by protostructures can be obtained using a model due to Peebles (Peebles 1993) (see also Del Popolo & Gambera 1998, 1999).
Let's consider an ensemble of gravitationally growing mass concentrations and suppose that the material in each system collects within the same potential well with inward pointing acceleration given by $g(r)$ (see Del Popolo & Gambera 1998). We indicate with $dP = f(L, rv_r, t)dLdv_rdr$ the probability that a particle can be found in the proper radius range r, $r + dr$, in the radial velocity range $v_r = \dot{r}$, $v_r + dv_r$ and with angular momentum $L = rv_\theta$ in the range dL. The radial acceleration of the particle is:

$$\frac{dv_r}{dt} = \frac{L^2(r)}{M^2r^3} - g(r) = \frac{L^2(r)}{M^2r^3} - \frac{GM}{r^2} \tag{144}$$

Eq. (144) can be derived from a potential and then from Liouville's theorem it follows that the distribution function, f, satisfies the collisionless Boltzmann equation:

$$\frac{\partial f}{\partial t} + v_r\frac{\partial f}{\partial r} + \frac{\partial f}{\partial v_r}\cdot\left[\frac{L_2}{r^3} - g(r)\right] = 0 \tag{145}$$

Assuming a non-zero cosmological constant Eq. (144) becomes:

$$\frac{dv_r}{dt} = -\frac{GM}{r^2} + \frac{L^2(r)}{M^2r^3} + \frac{\Lambda}{3}r \tag{146}$$

(Peebles 1993; Bartlett & Silk 1993; Lahav 1991; Del Popolo & Gambera 1998, 1999). Integrating Eq. (146) we have:

$$\frac{1}{2}\left(\frac{dr}{dt}\right)^2 = \frac{GM}{r} + \int\frac{L^2}{M^2r^3}dr + \frac{\Lambda}{6}r^2 + \epsilon \tag{147}$$

where the value of the specific binding energy of the shell, ϵ, can be obtained using the condition for turn-around, $\frac{dr}{dt} = 0$.

In turn the binding energy of a growing mode solution is uniquely given by the linear overdensity, δ_i, at time t_i. From this overdensity, using the linear theory, we may obtain that of the turn-around epoch and then that of the collapse. We find the binding energy of the shell, C, using the relation between v and δ_i for the growing mode (Peebles 1980) in Eq. (147) and finally the linear overdensity at the time of collapse is given by:

$$\delta_{\rm c} = \delta_{\rm co}\left[1 + \int_{r_{\rm i}}^{r_{\rm ta}}\frac{r_{\rm ta}L^2\cdot{\rm d}r}{GM^3r^3} + \Lambda\frac{r_{\rm ta}r^2}{6GM}\right] \simeq \delta_{\rm co}\left[1 + \frac{\beta_1}{\nu^{\alpha_1}} + \frac{\Omega_\Lambda\beta_2}{\nu^{\alpha_2}}\right] \tag{148}$$

where $\alpha_1 = 0.585$, $\beta_1 = 0.46$, $\alpha_2 = 0.4$ and $\beta_2 = 0.02$, where $\delta_{\rm co} = 1.68$ is the critical threshold for a spherical model, $r_{\rm i}$ is the initial radius, $r_{\rm ta}$ is the turn-around radius, L the angular momentum. The angular momentum appearing in Eq. (148) is the total angular momentum acquired by the proto-structure during evolution. In order to calculate L, it is possible to use the same model as described in Del Popolo & Gambera (1998, 1999) (more hints on the model and some of the model limits can be found in Del Popolo, Ercan & Gambera 2001).

The CDM spectrum used to calculate the mass function plotted in Figs. 17-19 is that of BBKS (equation (G3)), with transfer function:

$$T(k) = \frac{[\ln(1 + 2.34q)]}{2.34q}\cdot[1 + 3.89q + (16.1q)^2 + (5.46q)^3 + (6.71)^4]^{-1/4} \tag{149}$$

(where $q = \frac{k\theta^{1/2}}{\Omega_{\rm X}h^2{\rm Mpc}^{-1}}$. Here $\theta = \rho_{\rm er}/(1.68\rho_\gamma)$ represents the ratio of the energy density in relativistic particles to that in photons ($\theta = 1$ corresponds to photons and three flavors of relativistic neutrinos). The power spectrum was normalized to reproduce the observed abundance of rich cluster of galaxies (e.g., Bahcal & Fan 1998).

In the excursion set approach, the average comoving number density of haloes of mass m the universal or "unconditional" mass function, $n(m, z)$, is given by:

$$n(m, z) = \frac{\overline{\rho}}{m^2}\frac{d\log\nu}{d\log m}\nu f(\nu) \tag{150}$$

(BCEK), where $\overline{\rho}$ is the background density, $\nu = \left(\frac{\delta_{\rm c}(z)}{\sigma(m)}\right)^2$ is the ratio between the critical overdensity required for collapse in the spherical model, $\delta_{\rm c}(z)$, to the r.m.s. density fluctuation $\sigma(m)$, on the scale r of the initial size of the object m. The function $\nu f(\nu)$ is obtained by computing the distribution of first crossings, $f(\nu)d\nu$, of a barrier $B(\nu)$, by independent, uncorrelated Brownian motion random walks. The mass function can be thus calculated once a shape for the barrier is

given and the power spectrum is known. In the case of spherical collapse, characterized by a constant barrier (for all ν), PS and BCEK obtained:

$$\nu f(\nu) = \left(\frac{\nu}{2\pi}\right)^{\frac{1}{2}} \exp(-\frac{\nu}{2}) \tag{151}$$

In the case of a nonspherical collapse, the shape of the barrier is no longer a constant and moreover it depends on mass (Del Popolo & Gambera 1998; SMT). As shown by ST1, for a given barrier shape, $B(S)$, where $S \equiv S_* \left(\frac{\sigma}{\sigma_*}\right)^2 = \frac{S_*}{\nu}$ and $\sigma_* = \sqrt{S_*} = \delta_{co}$, the first crossing distribution is well approximated by:

$$f(S)dS = |T(S)| \exp(-\frac{B(S)^2}{2S}) \frac{dS/S}{\sqrt{2\pi S}} \tag{152}$$

where $T(S)$ is the sum of the first few terms in the Taylor expansion of $B(S)$:

$$T(S) = \sum_{n=0}^{5} \frac{(-S)^n}{n!} \frac{\partial^n B(S)}{\partial S^n} \tag{153}$$

The quantity $Sf(S,t)$ is a function of the variable ν alone, where $\nu \equiv (\delta_c(t)/\sigma(M))^2$. Since δ_c and σ evolve with time in the same way, the quantity $Sf(S,t)$ is independent on time. Setting $2Sf(S,t) = \nu f(\nu)$, one obtains the so-called multiplicity function $f(\nu)$. That's why the shape of the barrier influences the form of the multiplicity function.

In the case of the ellipsoidal barrier shape given in ST:

$$B(\sigma^2, z) = \sqrt{a}\delta_c(z) \left[1 + \frac{\beta}{(a\nu)^\alpha}\right] \tag{154}$$

the Eqs. (152),(153), give, after truncating the expansion at $n = 5$ (see ST):

$$\nu f(\nu) = \sqrt{a\nu/2\pi}[1 + \beta(a\nu^2)^{-\alpha} g(\alpha)] \exp\left(-0.5a\nu^2[1 + \beta(a\nu^2)^{-\alpha}]^2\right) \tag{155}$$

where

$$g(\alpha) = \mid 1 - \alpha + \frac{\alpha(\alpha-1)}{2!} - ... - \frac{\alpha(\alpha-1)\cdots(\alpha-4)}{5!} \mid \tag{156}$$

Using the values for β and α of ST ($a = 0.707$, $\delta_c(z) = 1.686(1+z)$, $\beta \simeq 0.485$ and $\alpha \simeq 0.615$) in Eq. (155), one gets (ST1):

$$\nu f(\nu) \simeq A_1 \left(1 + \frac{0.094}{(a\nu)^{0.6}}\right) \sqrt{\frac{a\nu}{2\pi}} \exp\left\{-a\nu \left[1 + \frac{0.5}{(a\nu)^{0.6}}\right]^2 /2\right\} \tag{157}$$

with $A_1 \simeq 1$. This last result is in good agreement with the fit of the simulated first crossing distribution (ST):

$$\nu f(\nu) d\nu = A_2 \left(1 + \frac{1}{(a\nu)^p}\right) \sqrt{\frac{a\nu}{2\pi}} \exp(-a\nu/2) \tag{158}$$

where $p = 0.3$, and $a = 0.707$.

The normalizatition factor A_2 has to satisfy the constraint:

$$\int_0^\infty f(\nu) d\nu = 1 \tag{159}$$

and as a consequence it is not an independent parameter, but is expressed in the form:

$$A_2 = \left[1 + 2^{-p}\pi^{-1/2}\Gamma(1/2 - p)\right]^{-1} = 0.3222^6. \tag{160}$$

If the barrier takes account of the cosmological constant, like in Eq. (148), using the same method that lead to Eq. (155), we have that:

$$\nu f(\nu) = A_1 \left(1 + \frac{\beta_1 g(\alpha_1)}{(a\nu)^{\alpha_1}} + \frac{\beta_2 g(\alpha_2)}{(a\nu)^{\alpha_2}}\right) \sqrt{\frac{a\nu}{2\pi}} \exp\left\{-a\nu \left[1 + \frac{\beta_1}{(a\nu)^{\alpha_1}} + \frac{\beta_2}{(a\nu)^{\alpha_2}}\right]^2 /2\right\} \tag{161}$$

In the case of the barrier given in Eq. (148) with $\Lambda = 0$, the "unconditional" multiplicity function can be approximated by:

$$\nu f(\nu) \simeq A_4 \left(1 + \frac{b}{(a\nu)^{0.585}}\right) \sqrt{\frac{a\nu}{2\pi}} \exp\left\{-ac\nu \left[1 + \frac{d}{(a\nu)^{0.585}}\right]^2\right\} \tag{162}$$

where $a = 0.707$, $b = 0.1218$, $c = 0.4019$, $d = 0.5526$ and $A_4 \simeq 1.75$ is obtained from the normalization condition.

In the case of the barrier with non-zero cosmological constant, Eq. (148), a good approximation to the multiplicity function is given by:

$$\nu f(\nu) \simeq A_5 \left(1 + \frac{0.1218}{(a\nu)^{0.585}} + \frac{0.0079}{(a\nu)^{0.4}}\right) \sqrt{\frac{a\nu}{2\pi}} \exp\{-0.4019 a\nu \left[1 + \frac{0.5526}{(a\nu)^{0.585}} + \frac{0.02}{(a\nu)^{0.4}}\right]^2\} \tag{163}$$

where $A_5 = 1.75$. As previously reported, for matter of completeness, to the previous functions, namely PS, ST, Eq. (163) we have to add J01, which satisfies the equation:

$$\nu f(\nu) = 0.315 exp(- \mid 0.61 + ln[\sigma^{-1}(M)] \mid^{3.8}) \tag{164}$$

In order to express the above relation as a function of ν, one substitutes $\sigma^{-1}(M) = \nu/\delta_c$ and I assume a constant value of δ_c, that of the Einstein-de Sitter Universe namely $\delta_c = 1.686$. The above formula is valid for $0.5 \leq \nu \leq 4.8$.

YNY (Eq. 7, hereafter YNY7) proposed the following function to fit the numerical multiplicity function:

$$\nu f(\nu) = A_6[1 + (B\nu/\sqrt{2})^C]\nu^D \exp[-(B\nu/\sqrt{2})^2], \tag{165}$$

where, A_6 is a normalization factor to satisfy the unity constraint, $\int_0^\infty f(\nu)d\nu = 1$, therefore

$$A_6 = 2(B/\sqrt{2})^D\{\Gamma[D/2] + \Gamma[(C+D)/2]\}^{-1}. \tag{166}$$

The best-fit parameters are given as B=0.893, C=1.39, and D=0.408, and from these parameters, A_6 is constrained so that $A_6 = 0.298$.

This best-fit, function from Eq. (165), is shown in Figs. 17-19 and is only valid at $0.3 \leq \nu \leq 3$.

3.5.1. **Results**

The analytic multiplicity functions of PS, ST, J01, YNY7, and Eq. (163), are compared with the numerical simulations of YNY. Those simulations adopt the ΛCDM cosmological parameters of $\Omega_m = 0.3$, $\Omega_\lambda = 0.7$, $h = 0.7$, and $\sigma_8 = 1.0$, using 512^3 particles in common (see YNY for details).

The numerical multiplicity functions are shown by crosses with errorbars in five panels of Fig. 17. All the data from the initial redshift to the present $z = 0$ is compiled to draw the average curves (crosses) with error bars indicating the epoch to epoch variation. In the panel (f), all the numerical multiplicity functions are shown by thin lines.

Four analytic multiplicity functions described in the previous section are also shown in this figure, that is PS (solid line), ST (dotted line), J01 (long-dashed line), YNY7 (dashed line), and the one of the Del Popolo (2005) described by Eq. (163) (dot-dashed line). Since the data are available only in the region at $\nu \leq 3$, these functions could be erroneous at $\nu \geq 3$.

Note that the comparison of the above curves, except for the PS model, with the results of N-body simulations show a very good agreement. However, there are some discrepancies between the YNY multiplicity function and other model functions (except the one in Del Popolo 2005). First, the multiplicity function of the Del Popolo (2005), similarly to that of YNY, in the low-ν region of $\nu \leq 1$, systematically falls below the ST and the J01 functions. In this region the multiplicity function of the Del Popolo (2005) is very close to that of YNY.

As seen in Fig. 17, and in agreement with YNY, the numerical multiplicity functions reside between the ST and J01 multiplicity functions at $2 \leq \nu \leq 3$ (except for the run 35b). Additionally, the numerical multiplicity functions have an apparent peak at $\nu \sim 1$ instead of the plateau that is seen in the J01 function.

On the other hand, in the high-ν region, where ν is significantly larger than unity, the multiplicity function of the Del Popolo (2005) like YNY takes values between ST and J01 functions. These differences between numerical multiplicity functions and analytic ones, like ST, ST1 and J01, are within 1 σ error bars, and they are possibly due to the different box sizes adopted (see YNY for a discussion). To be more precise, throughout the peak range of $0.3 \leq \nu \leq 3$, the ST multiplicity function is in disagreement with the high mass resolution N-body simulations of YNY and that of Del Popolo (2005). As shown by YNY the ST functional form provides a good fit to them only choosing parameter values of $a = 0.664, p = 0.321$, and $A_2 = 0.301$. The multiplicity function obtained in the Del Popolo (2005) has a peak at $\nu \sim 1$ as in the ST function, and YNY numerical multiplicity function and YNY7, instead of a plateau as in the J01 function.

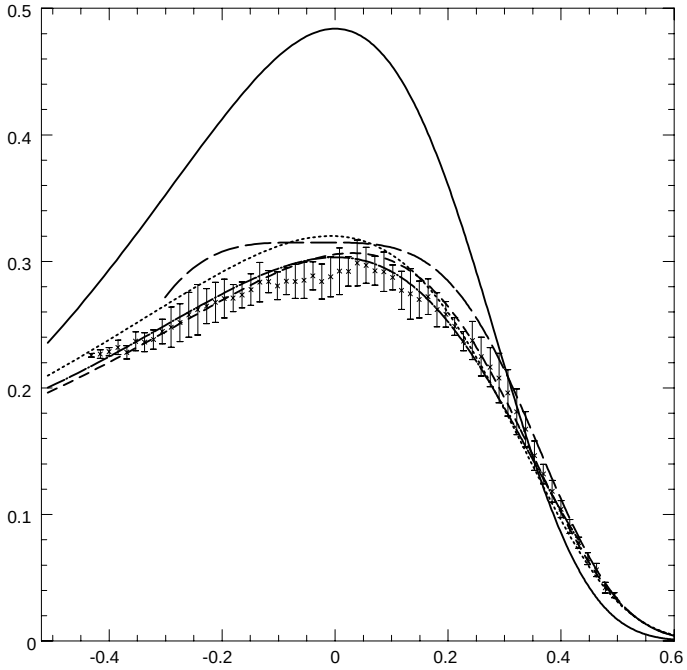

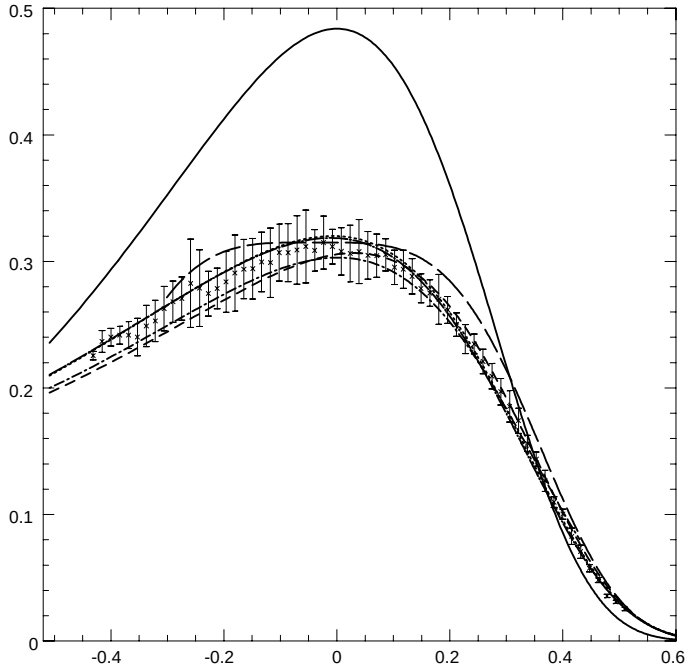

1a

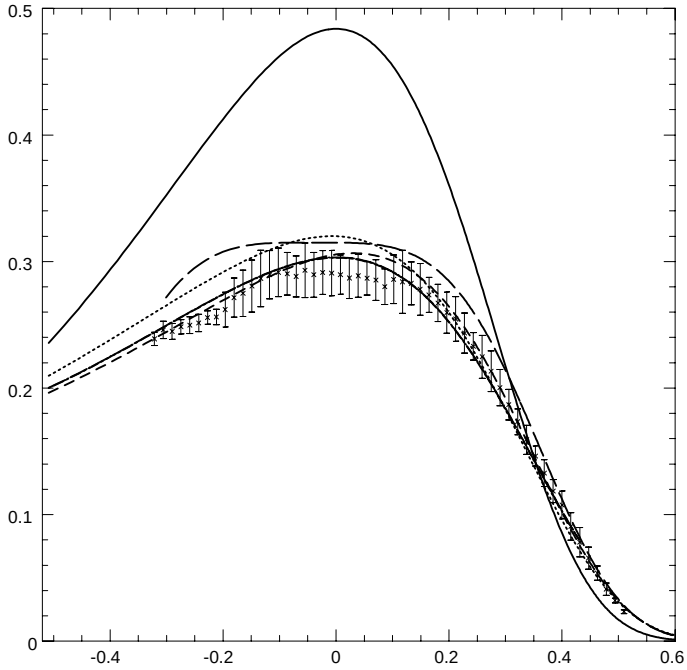

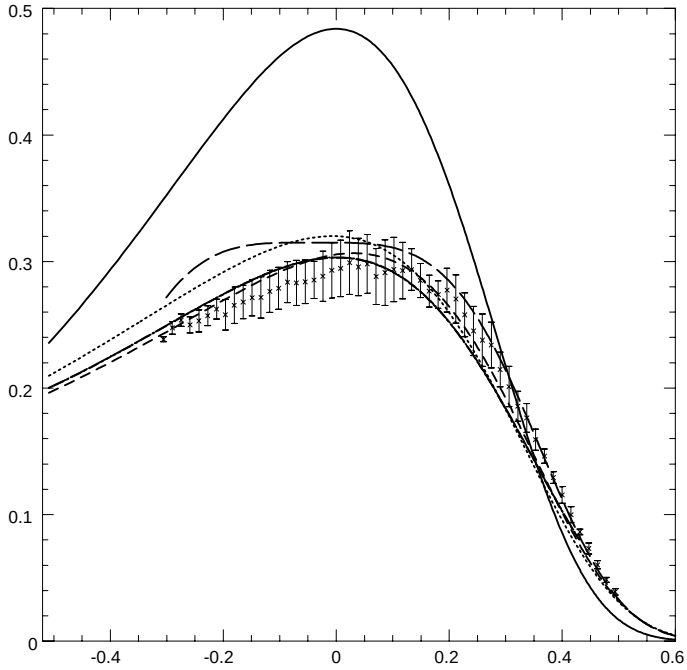

1c

Moreover, the functional form proposed in YNY, namely YNY7, provides a better fit when compared with the ST functional form but it is not based on theoretical background. The function obtained in this paper, similarly to YNY7 provides a better fit to simulations than the ST functional form, and at the same time has been obtained from solid physical, theoretical, arguments. The better agreement observed between the multiplicity function of Del Popolo (2005) and YNY simulations, when compared with the ST, is connected to the shape of the barrier (δ_c). As reported in Sec. 2, taking account of the effects of asphericity and tidal interaction with neighbors, Del Popolo & Gambera (1998), showed that the threshold is mass dependent, and in particular that of the set of objects that collapse at the same time, the less massive ones must initially have been denser than the more massive, since the less massive ones would have had to hold themselves together against stronger tidal forces.

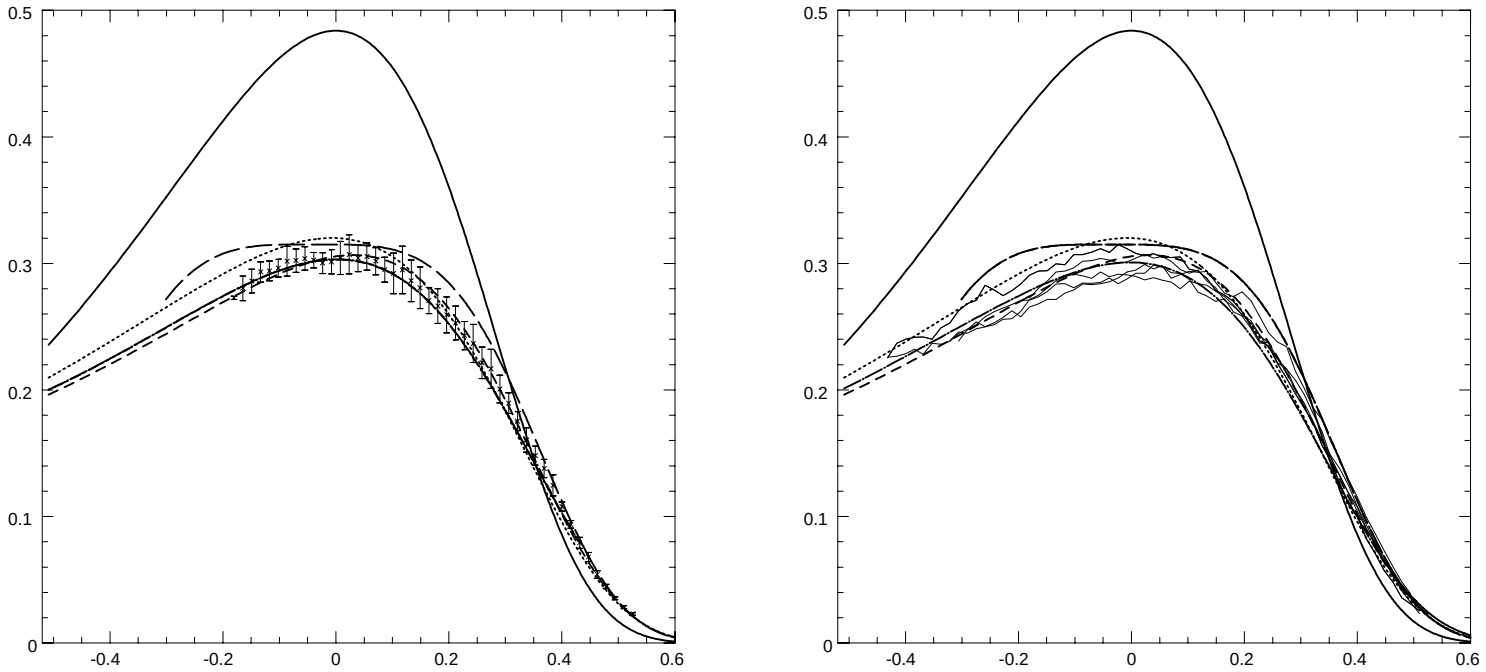

Fig. 17. The multiplicity functions from five runs of YNY simulations (crosses with error bars) are shown in the panels (*a*-*e*), except for the panel (*f*) which shows the results from all the runs (thin lines). In each panel are the solid line represents PS multiplicity function, the dotted line the ST multiplicity function, the long-dashed line the J01 multiplicity function, the short-dashed line YNY7, and the dot-dashed line the one calculated by Del Popolo (2005). Figure taken from Del Popolo (2005).

The shape of the barrier given in Eq. (148) is a direct consequence of the angular momentum acquired by the proto-structure during evolution and the effects of the cosmological constant.

Similarly to ST, the barrier increases with S (decrease with mass, M) differently from other models (see Monaco 1997a, b). It is interesting to note that the increase of the barrier with S has several important consequences and these models have a richer structure than the constant barrier model.

The decrease of the barrier with mass means that, in order to form structure, more massive peaks must cross a lower threshold, $\delta_c(\nu, z)$, with respect to under-dense ones. At the same time, since the probability to find high peaks is larger in more dense regions, this means that, statistically, in order to form structure, peaks in more dense regions may have a lower value of the threshold, $\delta_c(\nu, z)$, with respect to those of under-dense regions. This is due to the fact that less massive objects are more influenced by external tides, and consequently they must be more overdense to collapse by a given time. In fact, the angular momentum acquired by a shell centred on a peak in the CDM density distribution is anti-correlated with density: high-density peaks acquire less angular momentum than low-density peaks (Hoffman 1986; Ryden 1988). A larger amount of angular momentum acquired by low-density peaks (with respect to the high-density ones) implies that these peaks can more easily resist gravitational collapse and consequently it is more difficult for them to form structure. Therefore, on small scales, where the shear is statistically greater, structures need, on average, a higher density contrast to collapse.

It is evident that the effect of a non-zero cosmological constant adds to that of L. The effect of a non-zero cosmological constant is that of slightly changing the evolution of the multiplicity function with respect to open models with the same value of Ω_0. This is caused by the fact that in a flat universe with $\Omega_\Lambda > 0$, the density of the universe remains close to the critical value later in time, promoting perturbation growth at lower redshift. The evolution is more rapid for larger values (in absolute value) of the spectral index, n.

As previously reported, the ST model gives a better fit to simulations than PS model, but it has some discrepancies with simulations. ST model was introduced at the beginning (Sheth & Tormen 1999) as a fit to the GIF simulations and in a subsequent paper (SMT) was recognized the importance of aspherical collapse in the functional form of the mass

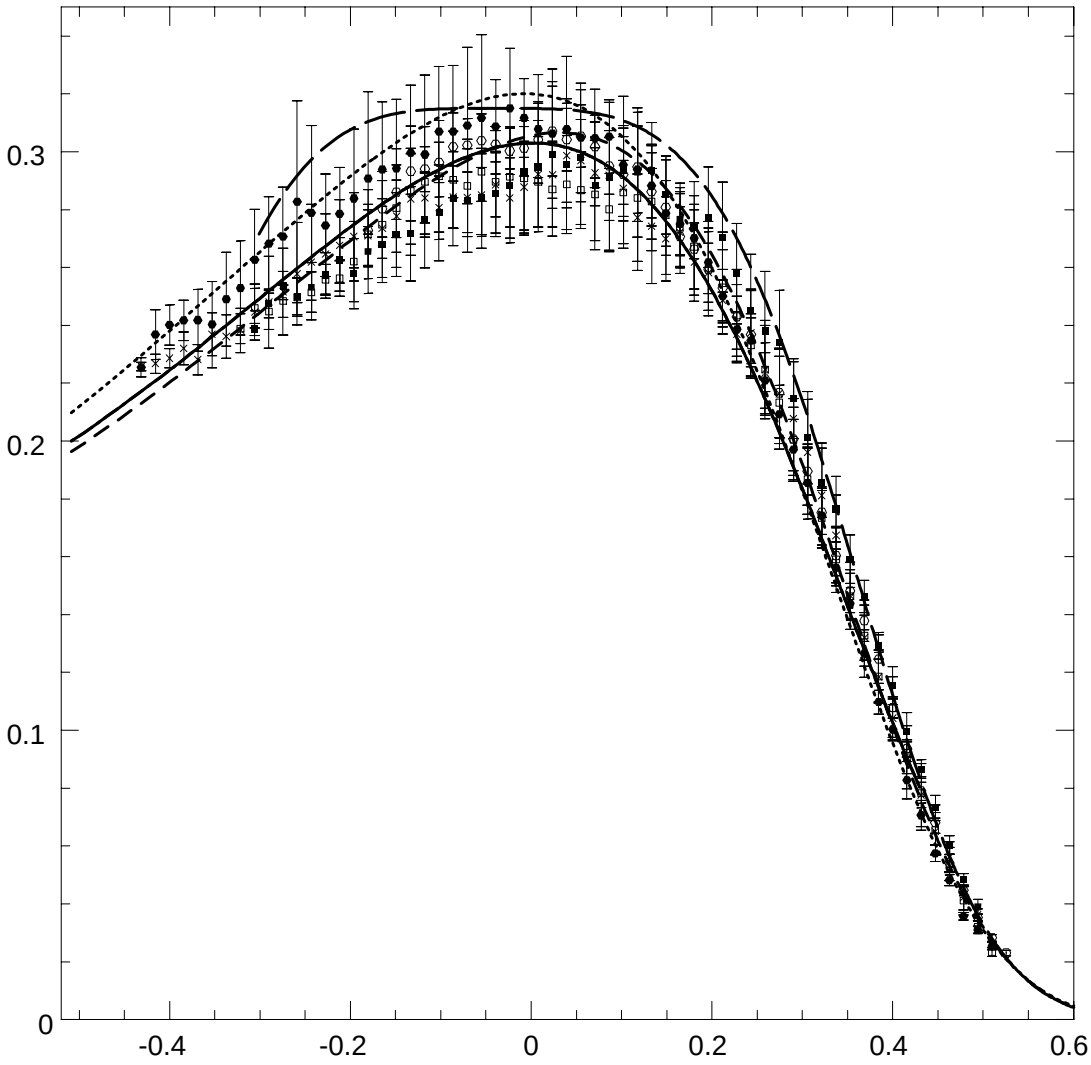

Fig. 18. The best-fit multiplicity function. In the plot the solid line represents the multiplicity function obtained in Del Popolo (2005), the short-dashed line YNY7, the dotted line the ST multiplicity function, the long-dashed line the J01 multiplicity function. The errorbars with open circles represents the run 140 of YNY, those with filled squares the case 70b, those with open squares the case 70a, those with filled circles the case 35b, those with crosses the case 35a. Figure taken by Del Popolo (2005).

function. The effects of asphericity were taken into account by changing the functional form of the critical overdensity (barrier) by means of a simple intuitive parameterization of elliptical collapse of isolated spheroids. The model proposed in Del Popolo (2005) has several similitudes with ST and ST1 models, namely it uses the excursion set approach as extended by ST1 to calculate the multiplicity function, but at the same time it differs from ST and ST1 for the way the barrier was calculated and for the fact that takes account of angular momentum acquisition, and a non-zero cosmological constant, things that are not taken into account into ST and ST1. These differences gives rise to a multiplicity function in better agreement with simulations. This shows the importance of the form of the barrier. The improvement of the multiplicity function of Del Popolo (2005) and ST with respect to PS is probably connected also to the fact that incorporating the non-spherical collapse with increasing barrier in the excursion set approach results in a model in which fragmentation and mergers may occur, effects important in structure formation.

In the case of non-spherical collapse with increasing barrier, a small fraction of the mass in the Universe remains unbound, while for the spherical dynamics, at the given time, all the mass is bound up in collapsed objects. Moreover,

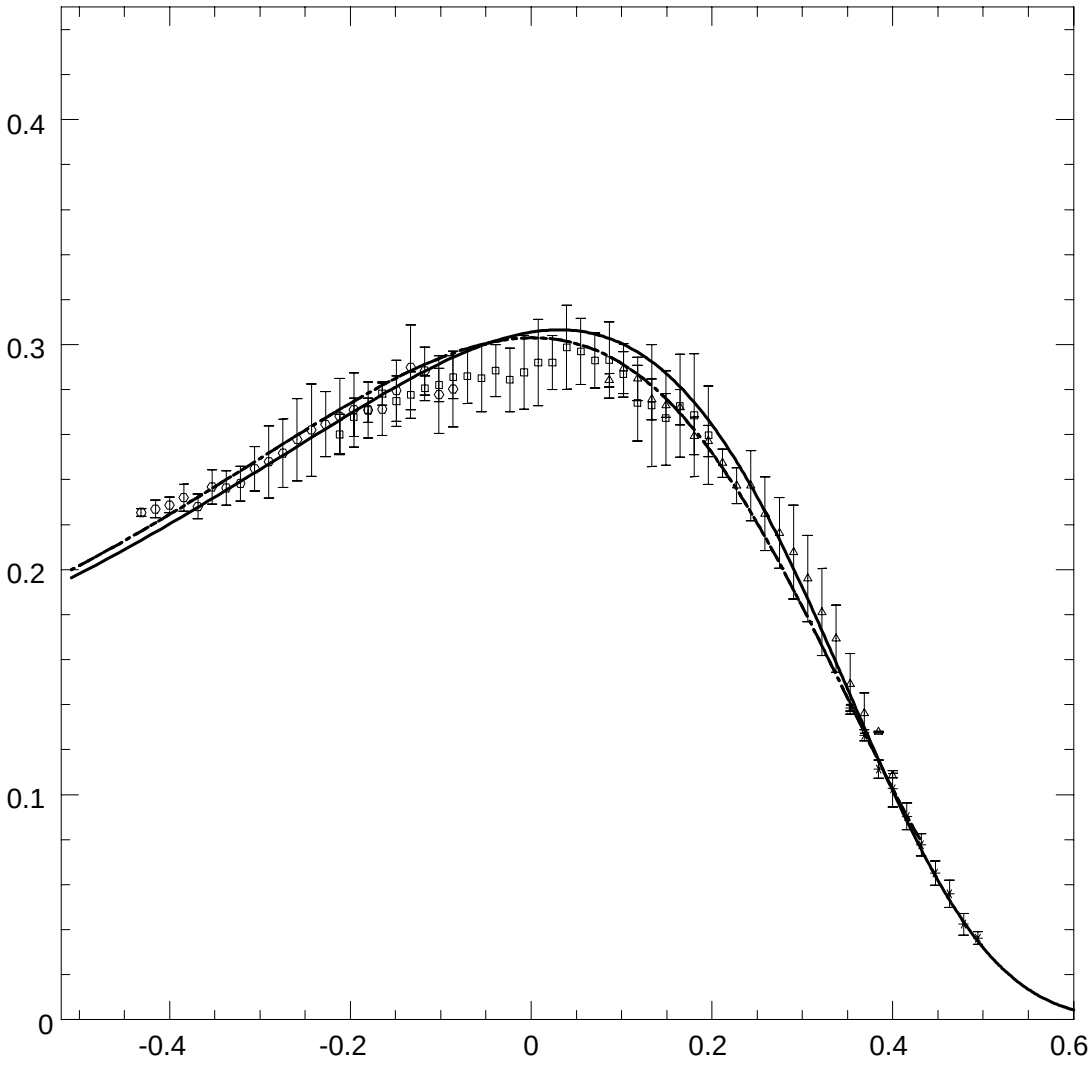

Fig. 19. Time dependence of the multiplicity function from the 35a run, for four redshift ranges of $0 \leq z < 1$ (open circles), $1 \leq z < 3$ (open squares), $3 \leq z < 6$ (open triangles), and $z \geq 6$, (crosses). Also shown are YNY7 (solid line) and the model of Del Popolo (2005) (dot-dashed line). Figure taken by Del Popolo (2005).

incorporating the non-spherical collapse with increasing barrier in the excursion set approach results in a model in which fragmentation and mergers may occur (ST). If the barrier decreases with S (Monaco 1997a,b), this implies that all walks are guaranteed to cross it and so there is no fragmentation associated with this barrier shape.

In other words, the excursion set approach with a barrier taking account effects of physics of structure formation gives rise to good approximations to the numerical multiplicity function: the approximation goodness increases with a more improved form of the barrier (taking account more and more physical effects: angular momentum acquisition, non zero cosmological constant, etc). Another important aspect of the quoted method is its noteworthy versatility: for example it is very easy to take account of the presence of a non zero cosmological constant englobing it in the barrier. I recall that the YNY numerical multiplicity function assumes a non zero cosmological constant while the theoretical models (ST,ST1, J01) does not take this into account.

Fig. 19 shows the multiplicity function from the 35a run, for four redshift ranges of $0 \leq z < 1$ (open circles), $1 \leq z < 3$ (open squares), $3 \leq z < 6$ (open triangles), and $z \geq 6$, (crosses). At high redshifts, high-ν halos in the exponential part of the YNY7 (solid line) function and Eq. (163) (dot-dashed line of Del Popolo 2005) are probed. As redshift decreases, the probe window moves to the lower-ν region. Fig. 19 shows that the multiplicity function of Del Popolo (2005), Eq. (163),

and YNY7 both gives a good fit to the numerical simulations. For small values of ν, Eq. (163) is a slightly better fit to data, and at large values of ν the two functions decays in the same way.

3.5.2 Multiplicity function evolution

In this section, I compare the analytic mass function of the present paper with that of ST, and with **?** (R03) simulation results at several redshifts. In Fig. 7, I compare the mass function of the present paper with ST, and with R03 simulation results at several redshifts. In the figure, the solid line represents the ST mass function at $z = 0, 5, 8, 15$, going from right to left, respectively. The dashed line the mass function of the present paper for the same values of the redshift, the errorbars with open squares, crosses, open triangles and solid triangles represents R03 at $z = 0, 5, 8, 15$. Fig. 7 shows that the ST function provides a good fit to R03 data, except at very high redshifts, where it significantly overpredicts the halo abundance. At all redshifts up to z=10, the difference is $\simeq 10\%$ for each of our well sampled mass bins. However, the ST function begins to overpredict the number of haloes increasingly with redshift for z>10, up to $\simeq 50\%$ by z=15. The simulation mass functions appear to be generally steeper than the ST function, especially at high redshifts. This is in agreement with the theoretical mass function calculated in the present paper which gives a better description of the R03 mass function for higher values of z for which the ST mass function overpredicts the simulation results.

In Fig. 8, I plot the mass function for all of our outputs in the $f(\sigma) - \ln(\sigma^{-1})$ plane. Large values of $\ln \sigma^{-1}$ correspond to rare haloes of high redshift and/or high mass, while small values of $\ln \sigma^{-1}$ describe haloes of low mass and redshift combinations. The solid line is the ST mass function while the dashed line the one obtained in the present paper and the dotted line represents a crude multiplicative factor to the ST function as follows, with $\delta_{\rm co} = 1.686$:

$$f(\sigma) = f(\sigma; {\rm ST}) \Big[exp[-0.7/(\sigma[\cosh(2\sigma)]^5)] \Big], \tag{167}$$

valid over the range of -1.7 $\leq \ln \sigma^{-1} \leq$ 0.9. The ST and the mass function of the present paper differs more in the high mass region, where the mass function of the present paper is steeper than ST and in better agreement with numerical simulations data than ST mass function. The ST function fits the simulated mass function to better than 10% over the range of -1.7 $\leq \ln \sigma^{-1} \leq$ 0.5 while it appears to significantly overpredict haloes for $\ln \sigma^{-1} \geq 0.5$. The magnitude of the ST overprediction at high values of $\ln\sigma^{-1}$ is consistent with being a function purely of $\ln\sigma^{-1}$ rather than redshift, a natural consequence of the fact that the mass function is self similar in time (e.g. **?**; **?**; **?**). The empirical adjustment to the ST mass function (Eq. (167)), dotted line, describes much better numerical simulations data: for -1.7 $\leq \ln \sigma^{-1} \leq$ 0.5, Eq. (167) matches R03 data to better than 10% for well-sampled bins, while for 0.5 $\leq \ln \sigma^{-1} \leq$ 0.9, where Poisson errors are larger, data is matched to roughly 20%.

YNY and **?** made a similar choice, namely they introduced an empirical mass function obtained from a fit to their simulations that gives a better fit to simulations than ST model. It is important to stress that even if the functional forms proposed in R03, YNY and **?** provide a better fit to simulations when compared with the ST functional form, they are not based on theoretical background. The function obtained in the present paper, similarly, for example, to R03 provides a better fit to simulations than the ST functional form, and at the same time has been obtained from solid physical, theoretical, arguments. The better agreement observed between the mass function of the present paper and R03 simulations, when compared with the ST, is connected to the shape of the barrier ($\delta_{\rm c}$).

In other words, the excursion set approach with a barrier taking account effects of physics of structure formation gives rise to good approximations to the numerical multiplicity function: the approximation goodness increases with a more improved form of the barrier (taking account more and more physical effects: angular momentum acquisition, non zero cosmological constant, etc). Another important aspect of the quoted method is its noteworthy versatility: for example it is very easy to take account of the presence of a non zero cosmological constant englobing it in the barrier. I recall that the YNY numerical multiplicity function assumes a non zero cosmological constant while the theoretical models (ST, **?**, **?**) does not take this into account.

4. PROSPECTS AND CONCLUSIONS

In the previous sections, we have seen that from the seminal paper of PS to last results, large progress has been made in the field of the cosmological mass function. If the PS model, explained quite well the N-body simulations of 80' and first part of 90', its limits have been shown by more recent simulations (e.g. **?**; YNY). Its theoretical limits, for example

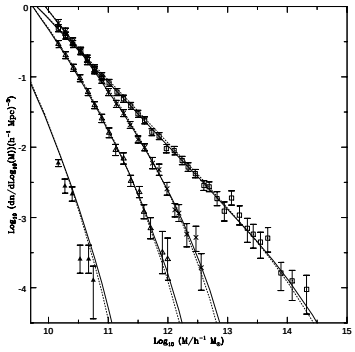

Fig. 20. Comparison of the mass function evolution calculated in the present paper with ST mass function and R03 simulations. Solid curves are the Sheth & Tormen function at z=0, 5, 8, & 15 (from right to left). The dashed line the mass function of the present paper for the same values of the redshift, the errorbars with open squares, crosses, open triangles and solid triangles represents R03 result at the same redshift.

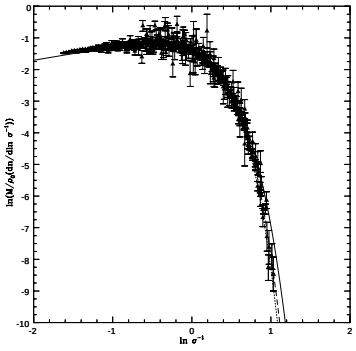

Fig. 21. Mass function plotted in redshift independent form for all of R03 outputs: redshifts used are 0, 1., 2., 3., 4., 5., 6.2, 7.8, 10., 12.1, 14.5. The solid line is ST prediction while the dashed and dotted line represent the result of the present paper and Eq. (167), respectively.

the lack of the "fudge factor of 2", has been solved in some papers (e.g. **?**). We have reviewed the excursion set model, the relation between peak model and the MF, one approach (PS-like approach) that takes into account the dynamics in the MF theory. All the previous results, give a MF in better agreement with simulations but only in more recent years several works have shown how it is possible to obtain MF functions in very good agreement with simulations (**?**, **?**, ST, **?**, **?**, **?**, YNY).

Even if the last models for the mass function gives much better results than the previous ones, it is necessary to recall which are the limits of the theory and the problems that must be attacked.

The main problems are the following:

—It is necessary to add more physics to the dynamical MF theory, to describe events such as the aggregation and fragmentation of already collapsed structures. In this way, the dynamics inside structures could be resolved; this is necessary to describe objects such as galaxies inside larger structures, as groups or clusters. The theories presented in the last subsection are somehow able to take account of some of the quoted effects, like fragmentation, angular momentum acquisition, presence of a non zero cosmological constant. Changing the shape of the barrier it is possible to take into account more physical effects to the dynamical MF theory.

—It is necessary to take in full account the geometry of collapsed regions in Lagrangian space, going beyond the usual golden rule described in previous sections. In the realistic case in which the stochastic process on which the MF is based is non Gaussian, this investigation can be performed through Monte Carlo simulations of initial fields.

—It is necessary to understand the role of filtering in the MF problem, as different kinds of filters (sharp k-space, Gaussian) lead to different and not equivalent formulations of the problem.

—It is necessary to understand in detail what is the total mass of a structure, and to find a rigorous, well-posed and easily interpretable definition for it, suitable to help in the interpretation of observations.

Another important point to remark is connected to N-body simulations. For example, as shown by YNY there is a discrepancy in the numerical multiplicity functions from various simulation runs. There are three strategies to resolve this discrepancy. The first is to run simulations having still higher mass dynamic range free from the box size effect. The second is to increase the number of realizations, because there is a scatter from the runs using the same box size. The third is to run simulations whose box size is smaller than that of the present work, although it might sound contradictorily. From simulations with smaller box size, one obtain the information on the conditional multiplicity function which coincides with the unconditional multiplicity function at $\nu << 1$. Comparing the unconditional multiplicity function from simulations with a large box size and the conditional multiplicity function from those of a small box size will offer not only the clues to resolve the above mentioned discrepancies, but also insights into the mechanism how the PS ansatz works to reproduce the numerical multiplicity function.

ACKNOWLEWDGMENTS

The author thanks the referee M. V. Sazhin for his helpful comments.

References

Abell G.O., 1958, ApJS, 3, 211
Abell G.O., Corwin H.G., Olowin R.P, 1989, ApJS, 70, 1
Adler, R., 1981, "the Geometry of Random Fields", John Wiley, New York.
Anninos P., Norman M.L., 1996, ApJ, 459, 12
Antonuccio-Delogu, V., Atrio-Barandela, F., 1992, Ap.J 392, 403
Antonuccio-Delogu, V., Colafrancesco, S., 1994, ApJ, 427, 72
Apple, L., Jones, B.J.T., 1990, MNRAS 245, 522
Applegate, J., Hogan, C., Scherrer, R.J., 1987, Phys.Rev. D 35, 1151.
Arnold L., 1973, Stochastic Differential Equations. Wiley, New York
Ashman, K.M., 1992, PASP, 104, 1109
Ashman, K.M., Salucci, P., Persic, M. 1993, MNRAS 260, 610
Audit E., Alimi J.M., 1996, A&A, 315, 11
Avila-Reese V., Firmani C., 1996, in Persic M., Salucci P. eds., Dark Matter 1996. Pasp Conf. Ser.
Bagla, J.S., Padmanabhan, T. 1994, MNRAS 266, 227
Bahcal N.A., Fan X., 1998, ApJ 504, 1
Bahcall N.A., 1988, ARA&A, 26, 631
Bahcall N.A., Cen, R. 1992, ApJ, 398, L81
Bahcall N.A., Cen, R. 1993, ApJ, 407, L49
Bajtlik S., 1995, in Meylan G. ed., QSO Absorption Lines. Springer, Berlin
Balland C., Blanchard A., 1995, A&A, 298, 323
Barbosa D., Bartlett J.G., Blanchard A., Oukbir J., 1996, A&A, 314, 13
Bardeen, J.M, Bond, J.R., Kaiser, N., Szalay, A.S., 1986, Ap.J, 304, 15
Barrow J.D., Silk J., 1981, ApJ, 250, 432
Bartlemann M., Ehlers J., Shneider P. 1993, A&A 280,351
Bartlemann M., Steinmetz M., 1996, MNRAS, 283, 431
Bartlett J.G., Silk J., 1993, ApJ, 407, L45
Bartlett J.G., Silk J., 1994, ApJ, 423, 12
Beers T.C., Flynn K., Gebhardt K., 1990, AJ, 100, 32
Bernardeau F., 1994a, A&A, 291, 697
Bernardeau F., 1994b, ApJ, 427, 51
Bernardeau F., Kofman L., 1995, ApJ, 443, 479
Bernardeau F., Schaeffer R., 1991, A&A, 250, 23
Bertola F., Pizzella A., Persic M., Salucci P., 1993, ApJ, 416, L45
Bertschinger, E., Jain, B. 1994, ApJ, 431, 486
Betancort-Rijo J., Lopez-Corredoira M., 1996, ApJ, 470, 674
Binney J., 1977, ApJ, 215, 483

Binney J., Tremaine S., 1987, Galactic Dynamics. Princeton University Press, Princeton
Binney, J., 1977, MNRAS, 181, 735
Biviano A., Girardi M., Giuricin G., Mardirossian F., Mezzetti M., 1993, ApJ, 411, L13
Blain A.W., Longair M.S., 1993a, MNRAS, 264, 509
Blain A.W., Longair M.S., 1993b, MNRAS, 265, L21
Blanchard A., Valls-Gabaud D., Mamon G.A., 1992, A&A, 264, 365
Blanford R.D., 1990, in Courvoisier T.J.L., Mayor M. eds., Active Galactic Nuclei. Springer, Berlin
Blummenthal, G.R., Faber, S.M., Primack, J.R., Rees, M.J., 1984, Nature 311, 517
Bond J.R., 1989, in Large-Scale Motions in the Universe, eds. V. Rubin, G. Coyne (Princeton: Princeton University Press)
Bond J.R., Cole, S., Efstathiou, G., Kaiser, N., 1991, ApJ, 379, 440 (BCEK)
Bond J.R., Myers S.T., 1996a, ApJS, 103, 1
Bond J.R., Myers S.T., 1996b, ApJS, 103, 41
Bond J.R., Myers S.T., 1996c, ApJS, 103, 63
Bond J.R., Szalay A.S., Silk J., 1988, ApJ, 324, 627
Bond, J.R., Efstathiou, G., 1984, Ap.J 285, L45
Borgani S., Coles P., Moscardini L., 1994, MNRAS, 271, 223
Bouchet F.R., 1996, in Bonometto S., Primack J., Provenzale A., eds., Dark Matter in the Universe. (see also preprint astro-ph/9603013)
Bouchet F.R., Colombi S., Hivon E., Juszkiewicz R., 1995, A&A, 296, 575
Bouchet F.R., Juszkiewicz R., Colombi S., Pellat R., 1992, ApJ, 394, L5
Bower R.G., 1991, MNRAS, 248, 332
Bower, R.G., Coles, P., Frenk, C.S., White, S.D.M., 1993, AP.J 405, 403
Bowyer S., et al. 1999, ApJ 526, 10
Brainerd T.G., Sherrer R., Villumsen J.V., 1993, ApJ, 418, 570
Brainerd T.G., Villumsen J.V., 1992, ApJ, 394, 409
Buchert T., 1989, A&A, 223, 9
Buchert T., 1992, MNRAS, 254, 729
Buchert T., 1994, MNRAS, 267, 811
Buchert T., 1996, in Bonometto S., Primack J., Provenzale A. eds., Dark Matter in the Universe. (see also preprint astro-ph/9603013)
Buchert T., Ehlers J., 1993, MNRAS, 264, 375
Buchert T., Melott A.L., Weiß A.G., 1994, A&A, 288, 349
Carlberg R.G., 1990, ApJ, 350, 505
Carlberg R.G., Couchman H.M.P., 1989, ApJ, 340, 47
Catelan P., 1995, MNRAS, 276, 115
Catelan P., Lucchin F. Matarrese S., Porciani C., 1998, MNRAS 297, 692 (CLMP)
Catelan P., Theuns T., 1996a, MNRAS, 282, 436
Catelan P., Theuns T., 1996b, MNRAS, 282, 455
Cavaliere A., Colafrancesco S., 1988 ApJ, 331, 660
Cavaliere A., Colafrancesco S., 1990, in Oegerle W.R., Fitchett M.J., Danly L. eds., Clusters of galaxies. Cambridge University Press, Cambridge
Cavaliere A., Colafrancesco S., Menci N., 1991a, ApJ, 376, L37
Cavaliere A., Colafrancesco S., Menci N., 1991b, in Fabian A.C. ed., Clusters and Superclusters of galaxies.Kluwer Ac. Pub., Dordrecht
Cavaliere A., Colafrancesco S., Menci N., 1992, ApJ, 392, 41
Cavaliere A., Colafrancesco S., Menci N., 1993, ApJ, 415, 50
Cavaliere A., Colafrancesco S., Scaramella R., 1991, ApJ, 380, 15
Cavaliere A., Fusco Femiano R., 1976, A&A, 49, 137
Cavaliere A., Giallongo E., Vagnetti F., Messina A., 1983, ApJ, 269, 57 et al. 1983,
Cavaliere A., Menci N., 1993, ApJ, 407, L9
Cavaliere A., Menci N., 1994, ApJ, 435, 528
Cavaliere A., Menci N., Setti G., 1991, A&A, 245, L21
Cavaliere A., Menci N., Tozzi P., 1994, in Seitter W.C., ed., Cosmological Aspects of X-ray Clusters of Galaxies. Kluwer Ac. Pub., Dordrecht
Cavaliere A., Menci N., Tozzi P., 1996, ApJ, 464, 44
Cavaliere A., Padovani P., 1988, ApJ, 333, L33

Cavaliere A., Perri F., Vittorini V., 1997, MemSAIt, 68, 27
Cavaliere, A., Colafrancesco, S., Scaramella, R., 1991, Ap.J. 380, 1
Cen R., 1997, ApJ, 479. 285
Cen R., Miralda-Escudé J., Ostriker J.P., Rauch M., 1994, ApJ, 437, L9
Centrella, J., Mellot, A.L., 1983, Nature, Lond., 305, 196
Chandrasekhar, S., 1943, Rev.Mod.Phys. 15, 1
Chandrasekhar, S., von Neumann, J., 1942, Ap.J 95, 489
Chandrasekhar, S., von Neumann, J., 1943,Ap.J 97,1
Charlton J.C., Salpeter E.E., 1991, ApJ, 375, 517
Colafrancesco S., Lucchin F., Matarrese S., 1989, ApJ, 345, 3
Colafrancesco S., Vittorio N., 1994, ApJ, 422, 443
Cole S., 1991, ApJ, 367, 45
Cole S., Aragon-Salamanca A., Frenk C.S., Navarro J.F., Zepf S.E., 1994, MNRAS, 271, 781
Cole S., Kaiser N., 1988, MNRAS, 233, 637
Cole S., Kaiser N., 1989, MNRAS, 237, 1127
Coles P., Jones B., 1991, MNRAS, 248, 1
Coles P., Lucchin F., 1995, Cosmology. Wiley, New York
Coles P., Melott A.L., Shandarin S.F., 1993, MNRAS, 260, 765
Crone M.M., Evrard A.E., Richstone D.O., 1996, ApJ, 467, 489
Danziger I.J., 1996, in Persic M., Salucci P. eds., Dark Matter 1996.
Davis M., 1996, in Turok N. ed., Critical Dialogues in Cosmology.
Davis M., Efstathiou G., Frenk C. S., & White, S. D. M. 1985, ApJ, 292, 371
Davis M., Peebles P.J.E., 1983, ApJ, 267, 465
Davis, M., Efstathiou, G., Frenk, C.S., White, S.D.M., Ap.J 292 371.
Davis, M., Peebles, P.J.E., 1977, Ap.J supplement series, 34, 425
Dejonghe H., Merritt D., 1992, ApJ, 391, 531
Dekel A., Rees M., 1987, Nature, 326, 455
Del Popolo A., Gambera M., 1998, A&A 337, 96
Del Popolo A., Gambera M., 1999, A&A 344, 17
Del Popolo A., Gambera M., 2000, A&A 357, 809
Del Popolo, A., E. N. Ercan, Z. Q. Xia, 2001, AJ 122, 487
Del Popolo A., 2002a, MNRAS 337, 529
Del Popolo A., 2002b, MNRAS 336, 81
Del Popolo A., 2005, IJMPD, in press
Dimopoulos, R., Esmailzadeh, L.J.H., Starkman, G.D., 1988, Phys.Rev.Lett. 60, 7.
Dinshaw N., Foltz C.B., Impey C.D., Weymann R.J., Morris S.L., 1995,
Doroshkevich A.G., 1967, Astrofizika, 3, 175 (Astrophysics,3, 84)
Doroshkevich A.G., 1970, Astrofizika 6, 581 (transl.: 1973, Astrophysics 6, 320)
Doroshkevich A.G., Kotok T.V., 1990, MNRAS, 246, 10
Edge A.C., Stewart G.C., Fabian A.C., Arnaud K.A., 1990, MNRAS, 245, 559
Efstathiou G., 1989, in Peacock J.A., Heavens A.F., Davies A.T. eds., Physics of the Early Universe. Edinburgh University Press, Edinburgh
Efstathiou G., 1995, MNRAS, 272, L25
Efstathiou G., Ellis R.S., Peterson B.A., 1988, MNRAS, 232, 431
Efstathiou G., Fall S.M., Hogan C., 1979, ApJ, 189, 203
Efstathiou G., Frenk C.S., White S.D.M., Davis M., 1988, MNRAS, 235, 715
Efstathiou G., Rees M.J., 1988, MNRAS, 230, 5P
Efstathiou, G., 1990, in " The physics of the early Universe",eds Heavens, A., Peacock, J., Davies, A. (SUSSP)
Efstathiou, G., Eastwood, J.W., 1981, MNRAS, 194, 503
Efstathiou, G., Frenk, C.S., White, S.D.M., Davis, M., 1988,MNRAS 235,715
Efstathiou, G., Silk, J., 1983, Fundamentals of cosmic Physics, 9, 1
Ehlers J., Buchert T., 1997, GRG, 29, 733 (astro-ph/9609036)
Einstein, A., 1915, Preuss.Akad.Wiss.Berlin, Sitzber., 844.
Eisenstein D.J., Loeb A., 1995a, ApJ, 439, 520
Eisenstein D.J., Loeb A., 1995b, ApJ, 443, 11

Eke V.R., Cole S., Frenk C.S., 1996, MNRAS, 282, 263
Ellis R.S., Colless M., Broadhurst T., Heyl J., Glazebrook K., 1996, MNRAS, 280, 235
Ellis, G.F.R. 1971, in General Relativity and Cosmology, ed. R.K.Sachs (New York: Academic Press)
Ellis, J.R., 1986, Phil.Trans.R.soc.Lond.A 320
Epstein R.I., 1983, MNRAS, 205, 207
Epstein R.I., 1984, ApJ, 281, 545
Ernst M.H., 1986, in Fractals in Physics, eds. L. Pietronero, E. Tosatti (Elsevier Science Publisher)
Evrard A.E., 1989, ApJ, 341, L71
Evrard A.E., 1990, ApJ, 363, 349
Evrard A.E., 1994, in Durret F., Mazure A., Tran Thanh Van J. eds., Clusters of Galaxies. Editions Frontieres, Gif-sur-Yvette
Evrard A.E., Summers F.J., Davis M., 1994, ApJ, 422, 11
Fadda D., Girardi M., Giuricin G., Mardirossian F., Mezzetti M., 1996, ApJ, 473, 670
Fang, L.Z., Li, S.X., Xiang, S.P., 1984, Astron. Astrophys 140, 77
Fenk, C.S., White, S.D.M., Davis, M., 1983, Ap.J, 271, 417
Finzi, A., 1963, MNRAS, 127, 21
Fort B., Mellier Y., 1994, A&A Rev., 5, 239
Frenk, C.S., White, S.D.M., Efstathiou, G., 1988, Ap.J. 327, 507
Frenk, C.S., White, S.D.M., Efstathiou, G., Davis, M., 1986
Friedmann, A., 1924, Z.Phys, 10, 377 e Z.Phys 1924, 21, 326.
Fry, J.N, Ap.J, 1982, 262, 424
Fugikita M., Kawasaki M., 1994, MNRAS, 269, 563
Gamow, G., 1946, Phys.Rev. 70, 527.
Gardner J.P., Katz N., Hernquist L., Weinberg D.H., 1997, ApJ, 484, 31
Gelato S., Governato F., 1996, in Persic M., Salucci P. eds., Dark Matter 1996. Pasp Conf. Ser.
Gelb J.M., Bertschinger E., 1994, ApJ, 436, 467
Girardi M., Biviano A., Giuricin G., Mardirossian F., Mezzetti M., 1993, ApJ, 404, 38
Giuricin G., Gondolo P., Mardirossian F., Mezzetti M., Ramella M., 1988, A&A, 199, 85
Giuricin G., Mardirossian F., Mezzetti M., 1982, ApJ, 255, 361
Giuricin G., Mardirossian F., Mezzetti M., Monaco P., 1993, ApJ, 407, 22
Gnedin N.Y., Hui L., 1996, ApJ, 472, L73
Gott J.R. III, Turner E.L., 1977, ApJ, 216, 357
Gouda N., Nagashima M., 1997, MNRAS, 287, 515
Gouda, N., sasaki, M., 1986:RiFP-preprint (Kyoto)
Governato F., Babul A., Quinn T, Tozzi P., Baugh C., Katz N., Lake G., 1999, MNRAS 307, 949
Governato F., Tozzi P., Cavaliere A., 1996, ApJ, 458, 18
Gunn, J.E., Gott, J.R., 1972, Ap.J. 176, 1
Gurbatov, S.N., Saichev, A.I., Shandarin, S.F., 1985, Sov.Phys.Dokl. 30, 921.
Guth, A.H., Pi, S.Y., 1982, Phys.Rev.Lett. 49, 1110.
Haehnelt M.G., 1993, MNRAS, 265, 727
Haehnelt M.G., 1995, in Cold Gas at High Redshift, eds. Bremer et al., (see also preprint astro-ph/9512024)
Haehnelt M.G., Rees M.J., 1993, MNRAS, 263, 168
Hanami H., 1993, ApJ, 415, 42
Harrison, R., 1970, Phys.Rev. D 1, 2726
Hawking, S.W., Phys.Lett B 115, 295.
Henriksen R.N., Lachièze-Rey M., 1990, MNRAS, 245, 255
Henry J.P., Arnaud K.A., 1991, ApJ, 372, 410
Henry, J.P., Briel, U.G., 1992, Astron.Astrophys. 259, L 14.
Hoffman Y., 1988, ApJ, 329, 8
Hoffmann, Y., Shandarin, J., 1985, Ap.J., 297, 16
Holtzman, J., Primack, J., 1993, Ap.J. 405, 428
Hoyle F., 1949, in IAU and International Union of Theorethicaland Applied Mechanics Symposium, p. 195
Hucra J.P., Geller M.J., 1982, ApJ, 257, 423
Hui L., Gnedin N.Y., Zhang Y., 1997, ApJ, 486, 599
Ikeuchi S., Murikama I., Rees M.J., 1988, MNRAS, 236, 21P
Jain B., Bertschinger E., 1994, ApJ, 431, 495

Jeans, J.H., 1902, Phil.Trans.R.Soc. 199 A, 49.
Jedamzik K., 1995, ApJ, 448, 1
Jelley, N.A., 1986, Phil. Trans. R. soc. London. A, 320, 487
Jenkins A., Frenk C.S., White S.D.M., Colberg J.M., Cole S., Evrard A.E., Couchman H.P.M., Yoshida N., 2001, MNRAS 321, 372
Jing Y.P., Mo H.J., Borner G., Fang L.Z., 1995, MNRAS, 276, 417
Jones C., Forman W., 1991, in Fabian A.C. ed., Clusters and Superclusters of galaxies.Kluwer Ac. Pub., Dordrecht
Juskievicz, R., Sonoda, D.H.,Barrow, J.D., 1984, MNRAS 209, 139
Kaiser N., 1984, ApJ, 284, L9
Kaiser N., 1991, ApJ, 383, 104
Kaiser N., 1996, in Schramm D. ed., Generation of Large-Scale Cosmological Structures. In press
Kaiser, N., Efstathiou, G., Ellis, R., Frenk, C., Lawrence, A., Rowan-Robinson, M., sanders W., 1991, MNRAS 251, 1.
Kandrup, , 1980, Phys. Rep. 63, n 1, 1
Kashlinsky A., 1987, ApJ, 317, 19
Kashlinsky A., 1993, ApJ, 406, L1
Katz N., 1992, ApJ, 391, 502
Katz N., Quinn T., Bertschinger E., Gelb J.M., 1994, MNRAS, 270, L71
Katz N., Quinn T., Gelb J.M., 1993, MNRAS, 265, 689
Katz N., Weinberg D.H., Hernquist L., 1996, ApJS, 105, 19
Kauffmann G., Guideroni B., White S.D.M., 1994, MNRAS, 267, 981
Kauffmann G., White S.D.M., 1993, MNRAS, 261, 921
Kauffmann G., White S.D.M., Guideroni B., 1993, MNRAS, 264, 201
Kibble, T.W.B., 1976, J. Phys A 9, 1387
Kibble, T.W.B., Turok, N.G., 1986, Phil.Trans.R.Soc.Lond. A 320, 565
Kitayama T., Suto Y., 1996a, MNRAS, 280, 638
Kitayama T., Suto Y., 1996b, ApJ, 469, 480
Klypin A., Borgani S., Holtzman J., Primack J., 1995, ApJ, 444, 1
Klypin A., Holtzman J., Primack J., Regös E., 1993, ApJ, 416, 1
Klypin A., Rhee G., 1994, ApJ, 428, 399
Klypin, A.A., Shandarin, S.F., 1983, MNRAS 204,891
Kofman L., Pogosyan D., 1995, ApJ, 442, 30
Kofman L., Pogosyan D., Shandarin S., Melott A., 1992, ApJ, 393, 437
Kofman L.A., Gnedin N.Y., Bahcall N.A., 1993, ApJ, 413, 1
Kolb, E.W., Turner, M.S., 1990, The Early Universe (Addison-Wesley)
Kontorovich V.M., Kats A.V., Krivitsky D.S., 1992, Sov. Phys. JETP Lett., 55, 1
Lacey C., Cole S., 1993, MNRAS, 262, 627
Lacey C., Cole S., 1994, MNRAS, 271, 676
Lacey C., Silk J., 1991, ApJ, 381, 14
Lachièze-Rey M., 1993a, ApJ, 407, 1
Lachièze-Rey M., 1993b, ApJ, 408, 403
Lahav O., Lilje P.B., Primack J.R., Rees M.J., 1991, MNRAS, 251, 128
Lanzetta K.M., Bowen D.B., Tytler D., Webb J.K., 1995, ApJ, 442, 538
Lawrence A., 1987, PASP, 99, 309
Layzer, D., 1954, AJ 59, 170
Lee, B.W., Weimberg, S., 1977, Phys.Rev.Lett, 39, 165
Liddle A.R., Lyth D.H., Schaefer R.K., Shafi Q., Viana P.T.P., 1995, MNRAS, 281, 531(preprint astro-ph/9511057)
Liddle, A.R., Lyth, D.H.,1993, Phys. Rep. 231, n 1, 2
Lilje P.B., 1990, ApJ, 351, 1
Lilje P.B., 1992, ApJ, 386, L33
Limber D.N., Mathews W.G., 1960, ApJ, 132, 286
Limber D.N., Mathews W.G., 1960, ApJ, 132, 286
Linde, A., 1983, Phys.Lett B 129, 177.
Loeb A., 1993, ApJ, 403, 542
Loh, E., Spillar, E.J., 1986, Ap.J 307 L1
Lokas E.L., Juszkiewicz R., Bouchet F.R., Hivon E., 1996, ApJ, 467, L1
Lubin L.M., Cen R., Bahcall N.A., Ostriker, J.P., 1996, ApJ, 460, 10

Lucchin F., 1989, in Flin P., Duerbeck H.W., eds., Morphological Cosmology. Springer Verlag, Berlin
Lucchin F., Matarrese S., 1988, ApJ, 330, 535
Lucchin, F., Matarrese, S., 1988, Ap.J, 330, 21
Lynden-Bell D., 1967, MNRAS, 136, 101
Lynds R., 1971, ApJ, 168, L87
Lynds R., 1971, ApJ, 168, L87
Lyubimov ,V.A, Novikov, E.G., Nozik, V.Z., Tretyakov, E.G., Kosik, V.S., 1980, Phys.Lett. B, 94, 266
Ma C., Bertschinger E., 1994, ApJ, 434, L5
Makino N., Suto S., 1993, ApJ, 405, 1
Manrique A., Salvador-Solé E., 1995, ApJ, 453, 6
Manrique A., Salvador-Solé E., 1996, ApJ, 467, 504
Martínez-González E., Sanz J.L., 1988a, ApJ, 324, 653
Martínez-González E., Sanz J.L., 1988b, ApJ, 332, 89
Matarrese S., 1996, in Bonometto S., Primack J., Provenzale A., eds., Dark Matter in the Universe, (see also preprint astro-ph/9601172)
Matarrese S., Coles P., Lucchin F., Moscardini L., 1997, MNRAS, 286, 115
Matarrese S., Lucchin F., Moscardini L., Saez D., 1992, MNRAS, 259, 437
Matarrese S., Pantano O., Saez D., 1993, Phys. Rev. D 47, 1311
Matarrese S., Pantano O., Saez D., 1994, Phys. Rev. Lett. 72, 320
Materne J., 1978, A&A, 63, 401
Matteucci F., 1996, Fund. Cosm. Phys., 17, 283
Mazure A., et al., 1996, A&A, 310, 31
Melott A.L., Buchert T., Weiß A.G., 1995, A&A, 294, 345
Melott A.L., Pellman T., Shandarin S.F., 1994, MNRAS, 269, 626
Menci N., Colafrancesco S., Biferale L., 1993, J. Phys., 3, 1105
Menci N., Valdarnini R., 1995, ApJ, 445, 1019
Merritt D., Gebhardt K., 1994, in Durret F., Mazure A., Tran Thanh Van J. eds., Clusters of Galaxies. Editions Frontieres, Gif-sur-Yvette
Meylan G. (ed.), 1995, QSO Absorption Lines. Springer, Berlin
Milgrom, M., 1983, Ap.J, 270, 365
Mo H.J., Miralda-Escudé J., 1994, ApJ, 430, L25
Mo H.J., Miralda-Escudé J., Rees M.J., 1993, MNRAS, 264, 705
Mo H.J., White S.D.M., 1996, MNRAS 282, 347
Monaco P., 1994, in Durret F., Mazure A., Tran Thanh Van J. eds., Clusters of Galaxies. Editions Frontieres, Gif-sur-Yvette
Monaco P., 1995, ApJ, 447, 23
Monaco P., 1997a, MNRAS 287, 753
Monaco P., 1997b, MNRAS 290, 439
Monaco P., 1998, Fund. Cosm. Phys. 19, 153
Monaco P., Giuricin G., Mardirossian F., Mezzetti M., 1994, ApJ, 436, 576
Moutarde F., Alimi J.M., Bouchet F.R., Pellat R., Ramani A., 1991, ApJ, 382, 377
Mukhanov, V.F., Feldman, H.A., Branderberger, R.H., 1992, Phys.Rep. 215, 203
Nagashima M., Totani T., Gouda N., & Yoshii Y. 2001, ApJ 557, 505
Narayan R., White S.D.M., 1988, MNRAS, 231, 97P
Navarro J.F., 1996, in Persic M., Salucci P. eds., Dark Matter 1996. Pasp Conf. Ser., in press
Navarro J.F., Frenk C.S., White S.D.M., 1995a, MNRAS, 275, 56
Navarro J.F., Frenk C.S., White S.D.M., 1995b, MNRAS, 275, 720
Navarro J.F., Frenk C.S., White S.D.M., 1996, ApJ, 462, 563
Newman W.I., Wasserman I., 1990, ApJ, 354, 411
Nusser A., Dekel A., 1990, ApJ, 362, 14
Nusser A., Silk J., 1993, ApJ, 411, L1
Occhionero F., Scaramella R., 1988, A&A, 204, 3
Oort, J., H., 1932, Bull.Astr.Insts.Neth., 6, 249
Ostriker J.P., Cen R., 1996, ApJ, 464, 27
Oukbir J., Blanchard A., 1992, A&A, 262, L21
Padmanabhan T., 1993, Structure Formation in the Universe. Cambridge University Press, Cambridge

Peacock J.A., Heavens A.F., 1985, MNRAS, 217, 805
Peacock J.A., Heavens A.F., 1990, MNRAS, 243, 133
Peccei-Quinn, H.R., 1977, Phys.Rev.Lett, 38, 1440
Peebles P.J.E., 1969, ApJ, 155, 393
Peebles P.J.E., 1990, ApJ, 365, 27
Peebles P.J.E., 1993, Principles of Physical Cosmology. Princeton University Press, Princeton
Peebles P.J.E., Daly R.A., Juszkiewicz R., 1989, ApJ, 347, 563
Peebles, P.J.E. 1980, The Large Scale Structure of the Universe (Princeton: Princeton Univ. Press)
Peebles, P.J.E., 1971, Physical cosmology, Princeton University Press, Princeton.
Peebles, P.J.E., 1980, The large scale structure of the universe, priceton University Press, Princeton.
Peebles, P.J.E., 1982b, Ap.J, Lett. 263, L1
Pei Y.C., 1995, ApJ, 438, 623
Pen U., 1997, ApJ 490, 127 (see also preprint astro-ph/9610147)
Persic M., Salucci P., 1995, ApJS, 99, 501
Persic M., Salucci P., 1996, in Persic M., Salucci P. eds., Dark Matter 1996. Pasp Conf. Ser.
Persic M., Salucci P., Stel F., 1996, MNRAS, 281, 27
Pietronero L., Montuori M., Sylos-Labini F., 1996, in Turok N. ed.,
Pietronero, L., 1987, Physica 144 A, 257 (North-Holland amsterdam)
Pisani A., Giuricin G., Mardirossian F., Mezzetti M., 1992, ApJ, 389, 68
Porciani C., Ferrini F., Lucchin F., Matarrese S., 1996, MNRAS, 281, 311
Press W., Schecter P., 1974, ApJ 187, 425
Press W.H., Flannery B.P., Teukolsky S.A., Vetterling W.T., 1992, Numerical Recipes in Fortran. Cambridge University Press, Cambridge
Press W.H., Schechter P., 1974, ApJ, 187, 425
Press W.H., Teukolsky S.A., 1990, Computers in Physics Jan/Feb, 1990, 92
Rauch M., Haehnelt M.G., Steinmetz M., 1997, ApJ, 481, 601
Rees M.J., 1984, ARA&A, 22, 471
Rees M.J., 1986, MNRAS, 218, 25P
Rees M.J., Ostriker J.P., 1977, MNRAS, 179, 541
Rees, M.J., 1985, MNRAS, 213, 75p
Richstone D., Loeb A., Turner E.L., 1992, ApJ, 393, 477
Risken H., 1989, The Fokker-Planck Equation. Springer Verlag, Berlin
Rodrigues D.D.C., Thomas P.A., 1996, MNRAS, 282, 631
Rowan-Robinson, M., 1985, "The cosmological distance ladder", W.M.Freeman, San Francisco.
Rubin V.C., Burstein D., Ford W.K.Jr, Thonnard N., 1985, ApJ, 289, 81
Rubin V.C., Ford W.K.Jr, Thonnard N., 1980, ApJ, 238, 471
Ryden B.S., 1988, ApJ 329, 589
Ryden, B.S., 1988, Ap.J 333, 78
Sahni V., Coles P., 1996, Phys. Rep., (see preprint astro-ph/9505005)
Sahni V., Shandarin S.F., 1996. MNRAS, 282, 641
Salopek, D.S., Bond, J.R., Bardeen, J.M., 1989, Phys.Rev. D40,1753
Sanders, R.H., , Astron.Astrophys, 136, L21
Sarazin C.L., 1986, Rev. Mod. Phys., 58, 1
Sargent W.L.W., Young P.J., Boksenberg A., Tytler D., 1980, ApJS, 42, 41
Sasaki S., 1994, PASJ, 46, 427
Schaeffer R., Silk J., 1985, ApJ, 292, 319
Schaeffer R., Silk J., 1988a, ApJ, 332, 1
Schaeffer R., Silk J., 1988b, ApJ, 333, 509
Schechter P.L., 1976, ApJ, 203, 297
Sciama, D., 1990, MNRAS 244, 1
Sciama, D.W., 1984, Proc.R.Soc.Lond. A 394, 1.
Shaefer, R.K., Shafi, Q., 1992, Nature 359, 199
Shafi, Q, Stecker, F.W., 1984, Phys.Rev.Lett. 53, 1292
Shandarin S.F., Doroshkevich A.G., Zel'dovich Ya.B., 1983, Sov. Phys. Usp., 26, 46
Shandarin S.F., Zel'dovich Ya.B., 1989, Rev. Mod. Phys., 61, 185

Shaviv N.J., Shaviv G., 1993, ApJ, 412, L25
Shaviv N.J., Shaviv G., 1995, ApJ, 448, 514
Sheth R. K., Mo H. J., Tormen G., 2001, MNRAS 323, 1 (SMT)
Sheth R. K., Tormen G., 1999, MNRAS 308, 119
Sheth R. K., Tormen G., 2002, MNRAS 329, 61 (ST)
Sheth R.K., 1995, MNRAS, 276, 796
Sheth R.K., 1996, MNRAS, 261, 1277
Sheth R.K., Lemson G., 1999a, MNRAS 304, 767
Sheth R.K., Lemson G., 1999b, MNRAS 305, 946
Sikivie, P., 1984, University of Florida, preprint n UFTP-85-104
Sikivie, P., 1985, Phys.Rev. D 32, 2988-2991.
Silk J., 1977, ApJ, 211, 638
Silk J., 1978, ApJ, 220, 390
Silk J., White S.D., 1978, ApJ, 223, L59
Silk, J., 1968, Ap.J 151, 459.
Silk, J., Ap.J 297,1
Smith, S., 1936, Ap.J, 83, 23
Smoluchowski M., 1916, Phys. Z., 17, 557
Starobinsky,A.A., 1982, Phys.Lett. B 117, 175.
Steidel C., Dickinson M., Meyer D., Adelberger K., Sembach K., 1997, ApJ, 480, 568
Steinmetz M., 1996, in Bonometto S., Primack J., Provenzale A., eds., Dark Matter in the Universe, (see also preprint astro-ph/9512013)
Sunyaev R.A., Zel'dovich Ya.B., 1970, Astrophys. Space Sci., 7, 3
Suto, Y., Sato, K., Kodama, H., 1985: Prog.Theor.Phys. 73, 1151
Taylor, A.N., Rowan-Robinson, M., 1992, Nature 359, 396
Tegmark M., Silk J., Rees M.J., Blanchard A., Abel T., Palla F., 1997, ApJ, 474, 1
Thomas P.A., Couchman H.M.P., 1992, MNRAS, 257, 11
Tormen G., Bouchet F.R., White S.D.M., 1997, MNRAS, 286, 865
Tozzi P., Governato F., 1998, "The Young Universe: Galaxy Formation and Evolution at Intermediate and High Redshift". Edited by S. D'Odorico, A. Fontana, and E. Giallongo. ASP Conference Series; Vol. 146; 1998, p.461
Tully R.B., 1987, ApJ, 321, 280
Turner, M.S., 1991, Physica scripta. vol T36, 167
Ueda H., Itoh M., Suto Y., 1993, ApJ, 408, 3
Umemura M., Loeb A., Turner E.L., 1993, ApJ, 419, 459
Valdarnini, R., Bonometto, S.A., 1985, Astron. Astrophys 146, 235
van Albada, T.S., Sancisi, R., Phil.Trans.R.Lond. A 320, 447.
van de Weygaert R., Babul A., 1994, ApJ, 425, L59
Vergassola M., Dubrulle B., Frisch U., Noullez A., 1994, A&A, 289, 325
Viana P.T.P., Liddle A.R., 1996, MNRAS, 281, 323
Vilenkin, A., 1981, Phys.Rev.Lett. 46, 1169, 1496[E]
Weiß A.G., Gottlöber S., Buchert T., 1996, MNRAS, 278, 953
Weinberg S., 1972, Gravitation and Cosmology. Wiley, New York
Weinberg, S., 1978, Phys.Rev.Lett. 40, 223
West M.J., 1994, in Durret F., Mazure A., Tran Thanh Van J. eds., Clusters of Galaxies. Editions Frontieres, Gif-sur-Yvette
West M.J., Jones C., Forman W., 1995, ApJ, 451, L5
West, M.J., Dekel, A., Oemler, A. Jr., 1987, Ap.J 316, 1.
Weyl, H., 1923, Z.Phys., 24, 230.
White M., 2002, ApJS 143, 241
White S.D.M., 1984, ApJ, 286, 38
White S.D.M., Efstathiou G., Frenk C.S., 1993, MNRAS, 262, 1023
White S.D.M., Frenk C.S., 1991, ApJ, 379, 52
White S.D.M., Rees M.J., 1978, MNRAS, 183, 341
White S.D.M., Silk J., 1979, ApJ 231, 1
White, D.M., Frenk, C.S., Davis, M., Efstathiou, G., 1987, Ap.J 313, 505
White, S.D.M., davis, M., Frenk, C.S., 1984, MNRAS 209, 27

Wilczec, F., 1978, Phys.Rev.Lett 40,279
Williams B.G., Heavens A.F., Peacock J.A., Shandarin S.F., 1991, MNRAS, 250, 458
Yahagi H., Nagashima M., Yoshii Y., 2004, ApJ, 605, 709
Yano T., Nagashima M., Gouda N., 1996, ApJ, 466, 1
Yi I., 1996, ApJ, 473, 645
Zabludoff A.I., Geller M.J., Hucra J.P., Vogeley M.S., 1993, AJ, 106, 1273
Zaritsky D., Smith R., Frenk C.S., White S.D.M., 199
Zaritsky D., Smith R., Frenk C.S., White S.D.M., 1993, ApJ, 405, 464
Zel'dovich Ya.B., 1970, A&A, 5, 84
Zel'dovich Ya.B., 1972, MNRAS, 160, 1P
Zel'dovich, Ya. B., 1980, MNRAS, 192, 663
Zel'dovich, Ya.B. 1970, Astrofizika 6, 319 (transl.: 1973, Astrophysics 6, 164)
Zhan Y., 1990, ApJ, 355, 387
Zwichy, F., 1933, Helvetica Physica Acta, 6, 110